



City Research Online

City, University of London Institutional Repository

Citation: Valani, Y.P. (2011). On the partition function for the three-dimensional Ising model. (Unpublished Doctoral thesis, City University London)

This is the accepted version of the paper.

This version of the publication may differ from the final published version.

Permanent repository link: <https://openaccess.city.ac.uk/id/eprint/7793/>

Link to published version:

Copyright: City Research Online aims to make research outputs of City, University of London available to a wider audience. Copyright and Moral Rights remain with the author(s) and/or copyright holders. URLs from City Research Online may be freely distributed and linked to.

Reuse: Copies of full items can be used for personal research or study, educational, or not-for-profit purposes without prior permission or charge. Provided that the authors, title and full bibliographic details are credited, a hyperlink and/or URL is given for the original metadata page and the content is not changed in any way.

On the partition function for the three-dimensional Ising model

Yogendra P. Valani

A thesis submitted for the degree of
Doctor of Philosophy of City University London

City University London,
School of Engineering and Mathematical Sciences,
Northampton Square,
London EC1V 0HB,
United Kingdom

August 2011

The candidate confirms that the work submitted is his own and that appropriate credit has been given where reference has been made to the work of others. This copy has been supplied on the understanding that it is copyright material and that no quotation from the thesis may be published without proper acknowledgement.

Contents

Table of Contents	ii
List of Figures	v
List of Tables	viii
Dedication	ix
Dedication	x
Acknowledgements	xi
Abstract	xii
1 Introduction	1
1.1 Physics background	1
1.1.1 Statistical Mechanics	2
1.1.2 Partition functions	2
1.1.3 Observables	3
1.1.4 Potts models	5
1.2 Known results	6
1.2.1 Two-dimensional Ising model	6
1.2.2 Perturbation expansions	7
1.2.3 Duality	10
1.2.4 Monte-Carlo methods	14
1.2.5 Existing exact finite lattice results	16
1.3 Physical interpretation of results	16
1.4 Universality	17
2 Computational Method	18
2.1 Potts models on graphs	18
2.2 Partition vectors and transfer matrices	20
2.2.1 Transfer matrices	23
2.2.2 Geometry and Crystal lattices	25
2.2.3 Eigenvalues of the transfer matrix	26
2.3 Zeros of the partition function	28
2.3.1 Specific heat	28

2.3.2	Eigenvalues and the zeros distribution	29
2.4	Correlation functions	31
3	Potts model partition functions: Exact Results	34
3.1	On phase transitions in 3d Ising model	37
3.2	Validating our interpretation of results	42
3.2.1	Checking dependence on boundary conditions	45
3.2.2	Checking dependence on size	52
3.3	Further analysis: Specific heat	54
3.4	Eigenvalue analysis	60
3.5	Q -state: 2d Potts models ($Q > 2$)	62
3.6	Q -state: 3d Potts models ($Q > 2$)	64
4	Discussion	68
A	Onsager’s Exact Solution proof	70
A.1	Notations and background maths	70
A.1.1	Matrix algebra	70
A.1.2	Clifford algebra	71
A.2	Rotational matrices	73
A.2.1	Rotations in $2n$ -dimensions	73
A.2.2	Rotational matrices and Clifford algebra	73
A.2.3	Product of rotational matrices	75
A.2.4	Eigenvalues of W	77
A.3	Formulation	78
A.3.1	Local transfer matrices	78
A.3.2	Local transfer matrices and gamma matrices	81
A.3.3	Rotational and transfer matrices	82
A.3.4	Eigenvalues of $S(W)$	85
A.3.5	The indeterminate solution	85
A.3.6	Thermodynamic limit solution	86
B	Code	87
B.1	Hamiltonian symmetries	87
B.2	Transfer matrix symmetries	89
B.2.1	Spin configurations	91
B.3	Large numbers, memory	91
C	Checking results	93
D	Finding Zeros	96

List of Figures

1.1	Specific heat of the two dimensional Ising model	7
1.2	Showing the low temperature expansion for part of a 2d lattice. Full circles denote spins pointing up, and open circles are spins pointing down.	8
1.3	Showing the high temperature expansion for part of a 2d lattice. Full circles denote spins pointing up, and open circles are spins pointing down.	9
1.4	Dual triangular and honeycomb lattice	11
1.5	A graph \mathcal{G} (black vertices and solid lines) representing a 4×4 lattice, and its dual lattice (white vertices and dashed lines).	11
1.6	An example of a mapping between graph $\mathcal{G}' \subset \mathcal{G}$ (black vertices and solid lines) and a dual of \mathcal{G} , $\mathcal{D}' \subset \mathcal{D}$ (white vertices and dashed lines).	13
1.7	Various zeros of a 2d Potts model with $Q = 2$ fixed on graphs \mathcal{G} and \mathcal{D} from Figure 1.5. The solid cross represents the unit axis of the complex temperature plane.	15
2.1	A planar realisation of an undirected graph \mathcal{G}	19
2.2	Shows set $V \subseteq V_{\mathcal{G}}$	20
2.3	Graphs \mathcal{G} and \mathcal{G}'	22
2.4	The resultant graph $\mathcal{G}\mathcal{G}'$, obtained by combining \mathcal{G} and \mathcal{G}' (from Figure 2.3) over V	22
2.5	A graphical example of Lemma 2.2.4	22
2.6	Representing incoming and outgoing spins using \mathcal{I} and \mathcal{E} respectively	23
2.7	Binding graphs, and spin categories	24
2.8	Showing d -dimensional lattices. The grey spin in each figure, represents a typical bulk spin and its nearest neighbour interactions (red edges).	25
2.9	Examples of d -dimensional transfer matrix lattice layers. Incoming (outgoing) spins are modelled by grey (white) vertices	26
2.10	The zeros of $\text{Tr}(\mathcal{T}^{100})$ (red dots) and the zeros of $B(x)$ (blue crosses).	31
2.11	A 2×3 lattice, with sites labelled a and b . The white site is a fixed spin.	33
2.12	A plot of $\langle \mathcal{O}_a \mathcal{O}_b \rangle_s$ against β for the Ising model on a 2×3 lattice.	33
3.1	Evidence of a critical point in 3d Ising model?	35
3.2	The zero distribution for a 10×10 (self dual) lattice.	36
3.3	Zeros of Z in x for the $N_x \times N_x$ Ising model with self-dual boundary conditions.	38

3.4	With reference to Figure 3.3: (a) overlays the zeros distributions close to \mathfrak{F} in the first quadrant; (b) overlays the corresponding specific heat curves.	39
3.5	With reference to Figure 3.1: (a) overlays the zeros distributions close to \mathfrak{F} in the first quadrant; (b) overlays the corresponding specific heat curves.	41
3.6	Graphs of $\tanh(\beta N_i)$, where $N_1 < N_2 < N_3$	42
3.7	Boundary interactions	43
3.8	Zeros of the partition function Z in x for the 14×14 Ising model with various boundary conditions.	45
3.9	Zeros of Z in x for the $N_x \times N'_y$ Ising model with fixed open/periodic boundary conditions.	46
3.10	Zeros of Z in x for the $5 \times 5 \times N'_z$ Ising model.	47
3.11	A configuration of the Ising model on a 3×4 lattice.	48
3.12	Control boundary conditions I	49
3.13	Control boundary conditions II	50
3.14	Control boundary conditions III	51
3.15	Showing the zeros of $Z = x^N + 1$, for various N	52
3.16	Control:lattice size I	53
3.17	Control lattice size II.	54
3.18	With reference to Figure 3.8: (a) overlays the zeros distributions close to \mathfrak{F} in the first quadrant; (b) overlays the corresponding specific heat curves.	55
3.19	Overlay and specific heat of Figure 3.12	56
3.20	Overlay and specific heat of Figure 3.16	56
3.21	Overlay and specific heat of Figure 3.14	57
3.22	Overlay and specific heat of Figure 3.17	57
3.23	An overlay of zero distributions of large lattices close to \mathfrak{F} , along with their corresponding specific heat curves.	58
3.24	A look at the $5 \times 5 \times N_z$ on various axis.	59
3.25	Zeros of the partition function Z for the $10 \times N_y$ Ising model, $N_y = \{10', 20', 50', 99'\}$	60
3.26	Zeros of the partition function Z in $x = e^\beta$	61
3.27	The zeros of the partition functions in Z in $x = e^\beta$ for various $Q = 3$ -state 2d Potts models	62
3.28	The zeros of the partition functions in Z in $x = e^\beta$ for various $(Q > 2)$ -state 2d Potts model	63
3.29	The zeros of the partition functions in Z in $x = e^\beta$ for $(Q = 3)$ -state models on various 3d lattices.	65
3.30	The zeros of the partition functions in Z in $x = e^\beta$ for $(Q = 3)$ -state models on a $3 \times 4 \times 10'$ lattice with various boundary conditions.	66
3.31	The zeros of the partition functions in Z in $x = e^\beta$ for various $(Q > 2)$ -state models on various 3d lattices.	67

A.1	Adding a sequence of horizontal and vertical bonds to a lattice	79
B.1	Showing two possible routes that an extra layer is added to the $4 \times 4 \times L$ lattice (1) . The resultant is a $4 \times 4 \times (L + 1)$ lattice (2)	88
B.2	The spins on a layer of $4 \times 4 \times L$ lattice are organised into columns and the sets labelled V_1, \dots, V_4	90
B.3	Examples of local transfer matrices	90
B.4	A transfer matrix used in the code	90
C.1	3×4 lattice, showing various states of the system	94

List of Tables

3.1	Table of Potts model partition functions, for exact finite lattice presented in this chapter.	37
4.1	Extrapolating the critical point, using various curve fitting techniques.	68
E.1	Exact partition function for Ising model on a $5 \times 5 \times 10'$ lattice	97

॥ सा विद्या या विमुक्तये ॥



भगवान् स्वामीनारायण नी कृपा थी अने परम पूज्य प्रमुख स्वामी महाराज ना आशीर्वाद थी

for my daughter, Priyena

Acknowledgement

I would like to express immense thanks to my primary supervisor, Prof. Paul Martin. This research and thesis would not be possible without him. I am very grateful to have had such a friendly and helpful supervisor. Thank you for all your advice, support, patience and encouragement. For all supervisions (in person, on the phone, via email, skype, and the web forum, etc...), and for the day long supervisions. I would also like to extend my thanks to Paul's family, Paula, Laura and Hannah Martin, for their hospitality during my visits to Leeds.

To my wife Selina, who I met in the first year of my research, I would like to thank for all her support and encouragement throughout. For the endless hours you have spent listening to me. For picking me up, every time I want to give up, and for never letting me give up. I don't know how I would have come this far without you. I am eternally grateful for all the sacrifices you have had to make, especially over the last 6 months.

To all my wonderful family and friends who have supported and believed in me, thank you for being there. I am very fortunate to have a close network of friends who have always been there. For the times when I have had enough and needed some time out, my friends have always been there.

Thank you to my examiners Prof. Uwe Grimm and Prof. Joe Chuang for many useful comments and corrections. I also like to extend my thanks to staff at City University for all their help. Thanks to Dr. Anton Cox my second supervisor. A big thank you to Dr. Maud De Visscher for proofreading and organising funding for my supervisions in Leeds. Also thanks to the IT dept. at City University, in particular Chris Marshall, Jim Hooker, and Ferdie Carty. I would like to thank course officers Sujatha Alexandra and Choy Man, for sorting out countless problems.

There have been a few times during the research, that due to financial difficulties I would not have been able to complete my research. I am indebted to my parents; my wife; siblings Ramnik Valani and Khyati Savani; Jeegar Jagani; Nimesh Depala; Manish and Diptiben Depala, for making it possible for me to continue.

Thanks to Zoe Gumm for proofreading and organising a write-up plan. For many useful physics discussions I am grateful to E. Levi, A. Cavaglia, C. Zhang, E. Banjo. Thanks to M. Patel and J. Jagani for the insightful discussion on statistics and Monte-Carlo techniques.

Finally, a very special thanks to my parents, Pravin and Vasanti Valani, for all their support throughout the entire course of my studies.

Abstract

Our aim is to investigate the critical behaviour of lattice spin models such as the three-dimensional Ising model in the thermodynamic limit. The exact partition functions (typically summed over the order of 10^{75} states) for finite simple cubic Ising lattices are computed using a transfer matrix approach. Q -state Potts model partition functions on two- and three-dimensional lattices are also computed and analysed. Our results are analysed as distributions of zeros of the partition function in the complex-temperature plane. We then look at sequences of such distributions for sequences of lattices approaching the thermodynamic limit. For a controlled comparison, we show how a sequence of zero distributions for finite 2d Ising lattices tends to Onsager's thermodynamic solution. Via such comparisons, we find evidence to suggest, for example, a thermodynamic limit singular point in the behaviour of the specific heat of the 3d Ising model.

Chapter 1

Introduction

1.1 Physics background

This thesis is a study of the analytic properties of certain models of co-operative phenomena (cf. [102, 89, 57]). A physical system exhibits a co-operative phenomenon if there is a coherent relationship between its microscopic constituents leading to macroscopic properties.

A ferromagnet [79, §7.3] is an example of such a system, as there is a coherent relationship between its magnetic dipoles leading to a bulk magnetisation [49].

[1.1] To compare macroscopic properties of a physical system we categorise the system state into *phases* [7]. For example, at low (high) temperature a ferromagnet is said to be in a ferromagnetic (paramagnetic) phase, if it has (does not have) a bulk magnetisation. We can move from one phase to another by adjusting its temperature T (the mechanism for this will be discussed later). We shall only focus on systems (such as the ferromagnet) where phase changes only occur at a definite point. The point at which the phases co-exist is known as the *critical point*. At the critical point the system is said to be undergoing a *phase transition* [89, 27].

Physical experiments on a system can tell us what its critical point is. For example, a well known critical point is the Curie temperature T_c (where $T_c = 1043K$ for iron [11, §1.1]), at which *spontaneous magnetisation* [5] vanishes (cf. Baxter (1982) [9, §1.1]). See Binney et al (1992) [11, §1.6] and references therein for several other examples.

[1.2] The Curie temperature categorises a ferromagnet as being in: the disordered (paramagnetic) phase when $T > T_c$; the ordered (ferromagnetic) phase when $T < T_c$; and a phase transition when $T = T_c$.

We describe this transition (known as the *order/disorder transition*) as follows [37]. In the ferromagnetic phase, magnetic dipoles are not randomly orientated but are aligned parallel (even in the absence of an external field) to give a net magnetisation. This is known as spontaneous magnetisation. Here we denote the net magnetisation by M . As T is increased¹ (ie. by adding heat energy to the system) the orientation of one or more dipoles may fluctuate and become unaligned

¹We ignore any dynamical questions (such as the changes in kinetic energy) that may arise.

from the ordered state. As a result M will decrease. Then at $T = T_c$ we see that M suddenly drops to zero, and remains zero for all $T > T_c$. The magnet has changed to the paramagnetic phase.

We use *statistical mechanics* to investigate phenomena such as the Curie point phase transition.

1.1.1 Statistical Mechanics

Classic mechanical theory does well in following a particle through a force field [7]. It even extends to a many-body system [53, §11]. However, there are typically 6×10^{23} (Avogadro's number) particles [13] in a real world system. Using Newtonian mechanics on this scale would be impossible computationally. On the other hand, thermodynamics [16, 40] is a theory used to observe data for systems on a macroscopic scale. This theory gives results on a macroscopic level, and yet fails to answer how transitions occur between phases [91].

[1.3] *Statistical mechanics* [9, 40, 44, 67, 69] is a theory that attempts to “bridge” the gap between microscopic entities and macroscopic observables. It attempts to predict the macroscopic behaviour of a physical system (or process), by analysing its microscopic components.

In this thesis, we focus on *equilibrium statistical mechanics* [44]. When the state of the system is independent of time we say the system is in *equilibrium* [20]. As an example, consider a hot cup of coffee in a room. As the coffee cools it is not in equilibrium. However when it is at room temperature, the coffee will have the same temperature regardless of whether we observe it over a few minutes or over a few hours. Here we say the system is in equilibrium.

As real world systems/phenomena are far too complex to accurately investigate mathematically, a simplistic model that extracts only the essential features is employed [50]. The aim of this model is to predict the results of an unobserved (but suitably nearby) regime. In this thesis, we shall use a Potts model [83] (Section 1.1.4). See Baxter (1982) [9] for examples of other statistical mechanics models.

In the next section we introduce a function that relates macroscopic observables and microscopic states.

1.1.2 Partition functions

In statistical mechanics, the *partition function* Z , is a function that relates the temperature (a thermodynamic quantity) of a system to its microscopic states. There are several types of partition functions, each associated with a type of statistical ensemble (or a type of free energy) [13]. Here we study the *canonical ensemble*, a system in which heat is exchanged in an environment where temperature, volume and the number of particles is fixed.

At time instance t , the energy of a system will depend on the position and velocity of all atoms in the system. Instead of trying to determine each individual molecule's position and velocity at any t , all possible instances are calculated. These are known as microscopic states. Further, we use Ω as the set of all possible microstates.

Definition 1.1.1. *The partition function is then defined as*

$$Z(T) = \sum_{\sigma \in \Omega} e^{-H(\sigma)/k_B T} \quad (1.1.1)$$

where T is the absolute temperature and k_B is Boltzmann's constant ($k_B \approx 1.3807 \times 10^{-23} \text{J/K}$).

Note it is convenient to let

$$\beta = 1/k_B T. \quad (1.1.2)$$

The energy function H , is tailored to fit the desired phenomenon, where

$$H : \Omega \rightarrow \mathbb{R} \quad (1.1.3)$$

associates a real energy value to each state. This function is generally referred to as the Hamiltonian.

The Hamiltonian is explicitly defined in Sections 1.1.4 and 1.2.1, for the Potts model and Ising model respectively. For these models, we assume that only the orientation of magnetic dipole pairs contribute to the energy of the system, whilst all other dynamic components of the system are fixed. Quite simply H depends on nearest neighbour interactions and the relative orientation of the atoms. Any kinetic energy due to orientation variation is enclosed in β and considered negligible.

In the next section, we see that the partition function is merely a normalising constant (cf. [44, §1.3]). However, it contains all the information we need to work out particular thermodynamical properties of a system. That is, thermodynamic quantities such as internal energy, specific heat, and spontaneous magnetisation can be calculated from the log derivatives of the partition function.

1.1.3 Observables

An *observable*, denoted \mathcal{O} , is a measurable property of a physical system. The general idea is to observe the value of the property over repeated experiments, identify certain regularities and then express the observable as a theoretical law. The law is then used to predict future (nearby) observable events.

At any time instance, the probability of finding the system in state σ , at temperature β is

$$P(\sigma) = \frac{\exp(\beta H(\sigma))}{Z}; \quad (1.1.4)$$

recall Definition 1.1.1 for the definition of the variables β, H and Z . An *expectation value* is a thermal average

$$\langle \mathcal{O} \rangle := \frac{\sum_{\sigma \in \Omega} \mathcal{O}(\sigma) e^{\beta H(\sigma)}}{Z}. \quad (1.1.5)$$

The *variance* is a measure of how volatile the system is around the expectation, and is given by

$$\langle \mathcal{O}^2 \rangle - \langle \mathcal{O} \rangle^2. \quad (1.1.6)$$

The Helmholtz free energy F (c.f [16]) of a system, which may be obtained from the partition function, is of the form

$$F = -k_B T \ln Z. \quad (1.1.7)$$

Many thermodynamic quantities (such as the internal energy, specific heat, and spontaneous magnetisation [52]) can then be calculated from suitable derivatives of Equation (1.1.7). Note, we shall use partial derivatives as F will depend on several variables.

The specific heat C_V is defined in terms of the heat Q required to change the temperature by δT of a mass m . It is simply expressed as $Q = mC_V\delta T$, where C_V depends on the material being heated. For an infinitesimal temperature change dT and a corresponding quantity of heat dQ , we then have

$$dQ = mC_V dT. \quad (1.1.8)$$

The specific heat can now be written as

$$C_V = \frac{1}{m} \frac{dQ}{dT}. \quad (1.1.9)$$

For our studies on phase transitions, we are not concerned with the specific heat of any material in particular, but with the changes in C_V , at certain changes in T .

The internal energy $\langle H \rangle$ of a system can now be derived from the log derivative of the partition function. That is

$$\begin{aligned} \frac{\partial \ln(Z)}{\partial \beta} &= \frac{\partial}{\partial \beta} \ln \left(\sum_{\Omega} e^{\beta H} \right) \\ &= \frac{\sum_{\Omega} H e^{\beta H}}{\sum_{\Omega} e^{\beta H}} \\ &= \langle H \rangle. \end{aligned} \quad (1.1.10)$$

The specific heat C_V is given by the second log differential of the partition function as follows:

$$\begin{aligned} C_V &= \frac{\partial^2 \ln(Z)}{\partial \beta^2} \\ &= \frac{\partial}{\partial \beta} \left(\frac{\partial \ln(Z)}{\partial \beta} \right) \\ &= \frac{\partial}{\partial \beta} \left(\frac{\sum_{\Omega} H e^{\beta H}}{\sum_{\Omega} e^{\beta H}} \right) \\ &= \frac{(\sum_{\Omega} e^{\beta H}) \cdot (\sum_{\Omega} H^2 e^{\beta H}) - (\sum_{\Omega} H e^{\beta H})^2}{(\sum_{\Omega} e^{\beta H})^2} \\ &= \left(\frac{\sum_{\Omega} H^2 e^{\beta H}}{\sum_{\Omega} e^{\beta H}} \right) - \left(\frac{\sum_{\Omega} H e^{\beta H}}{\sum_{\Omega} e^{\beta H}} \right)^2 \\ &= \langle H^2 \rangle - \langle H \rangle^2 \end{aligned} \quad (1.1.11)$$

We refer the reader to Huang (1987) [40], for the further derivations of observables such as pressure, spontaneous magnetisation, and entropy.

1.1.4 Potts models

[1.4] In this thesis, we shall only model the atomic structure of *crystalline* ferromagnets [71]. A crystalline solid is essentially a solid in which atoms are physically spaced in a regular three dimensional array. That is, we may think of a magnet as a set of magnetic dipoles residing on the sites of a *crystal lattice* [33], that are able to exchange energy between themselves.

Our objective is to study interacting systems such as a ferromagnet and investigate its critical behaviour. A “lattice spin system” is used to model specific aspects of a magnet’s behaviour under certain conditions [50] (ie. it may aid our understanding of certain co-operate phenomena such as the Curie point phase transitions).

The orientation of a magnetic dipole can be modelled by a variable known as a “spin”. We place a spin on each site of the lattice. The set of interacting spins on a lattice is known as a *lattice spin system* [50]. Note that interactions tend only to be significant for nearest neighbour spins; anything further away and the interaction energy tends to be negligible.

[1.5] The *Potts model* [83] is regarded as a model of a lattice spin system. Consider a lattice \mathcal{L} with N sites. Associate a spin variable to each site on \mathcal{L} , where each spin can take Q values, say $1, 2, \dots, Q$. Physically this could represent the orientation of a magnetic dipole sitting on a crystal lattice. As dipole interactions tend to be short range, we restrict the model’s Hamiltonian H to include only spin-to-spin nearest neighbour interactions.

Define Ω as the set of all possible spin states. Each element of Ω assigns a state (from Q possibilities) to each spin. Specifically, if there are N spins, then there are Q^N possible states of the system in total (ie. $Q^N = |\Omega|$).

The Hamiltonian (see (1.1.3)) is now explicitly defined as

$$H(\sigma) = -\epsilon \sum_{\langle ij \rangle} \delta_{\sigma_i \sigma_j}, \quad (1.1.12)$$

where: $\sigma \in \Omega$ is the state of the system; σ_i is the value of the spin on site i of the lattice; ϵ is the interaction energy between nearest neighbour spins; the summation is over all nearest neighbour spins (denoted $\langle ij \rangle$); and

$$\delta_{\sigma_i \sigma_j} = \begin{cases} 1, & \text{if } \sigma_i = \sigma_j \\ 0, & \text{if } \sigma_i \neq \sigma_j \end{cases} \quad (1.1.13)$$

The partition function for the Q -state Potts model is then defined as

$$Z = \sum_{\sigma \in \Omega} e^{-\beta H(\sigma)}, \quad (1.1.14)$$

where Ω is the set of all possible spin configurations and $\beta = 1/k_B T$. Specifically T is the temperature, and k_B is Boltzmann’s constant.

The Potts model has helped enhance our understanding of the general theory of critical phenomena [29, 99, 100], and it can be applied to model a wide range of physical systems (cf. [49]). In the next section, we introduce the Ising model, which is a special case of the Potts model.

1.2 Known results

1.2.1 Two-dimensional Ising model

The Potts model is a generalisation of a simple model of ferromagnetism called the *Ising model* [55]. The Ising model is the $Q = 2$ -state Potts Model. One of the most important discoveries in the field of statistical mechanics is Onsager’s solution [78] of the 2d Ising model in a zero magnetic field. Onsager’s solution is too complex to interpret for the context of this thesis. Instead we use a simplification of his result, as derived by Martin [61, §2]. The proof of the solution is presented in Appendix A.

Many models in statistical mechanics can be regarded as a special case of the general Ising model (cf. [9]). The Ising model is a mathematical model of a physical ferromagnetic substance. The Hamiltonian for the Ising model is

$$H(\sigma) = -\epsilon \sum_{\langle ij \rangle} \sigma_i \sigma_j - \mu \sum_{i=1}^N \sigma_i, \quad (1.2.1)$$

where: constants ϵ and μ are the interaction energy and external magnetic fields respectively; σ_i is a spin on a site i of a lattice with N sites; and the sum is over all nearest neighbours $\langle ij \rangle$. Note each σ_i only takes values ± 1 , which are usually referred to as “up”, “down” states.

In his PhD Thesis [41] Ernest Ising solved the one dimensional Ising model and found that it is not capable of modelling a phase transition. He also assumed that this was true in the case of higher dimensions [42]. In 1936, Peierls [82] put forward a simple argument that the two dimensional Ising model is indeed capable of exhibiting a phase transition. This led to an influx of further study in the field [15],

[1.6] Peierls considered the two dimensional Ising model [70] at zero temperature in thermal equilibrium. At low temperature the majority of spins are aligned, that is they hold the same value, and the model is said to be in an ordered phase. At high temperature the majority of spins are not aligned, and the model is said to be in a disordered phase. Suppose we increase (decrease) the temperature of the model in the ordered (disordered) phase. Then a few spins may gain (lose) energy and flip (align). However, overall, we would still consider the model to be in an ordered (disordered) state.

Now as we continue to increase (decrease) the temperature, so many spins will have flipped (aligned) that the model is now be considered to have changed phase and is considered mostly disordered (ordered). However, there must exist some temperature at which the model is considered to be both states. This point is known the critical temperature T_c of the Ising model.

With appropriate boundary conditions the solution of the 2d Ising model in a zero magnetic field on a $n \times m$ square lattice may be written in the terms of the product

$$Z_{mn} = \prod_{r=1}^m \prod_{s=1}^n \left\{ 1 - \frac{1}{2} K \left(\cos \frac{2\pi r}{m} + \cos \frac{2\pi s}{n} \right) \right\}, \quad (1.2.2)$$

where

$$K = \frac{\exp(-2\beta) \{1 - \exp(-4\beta)\}}{\{1 + \exp(-4\beta)\}^2} \quad (1.2.3)$$

The specific heat C_V , for Onsager's exact solution near the critical temperature $\beta_c = \sqrt{2} + 1$ is [40].

$$\frac{1}{k_B} C_V \approx \frac{8\beta_c^2}{\pi} \left[-\log \left| 1 - \frac{\beta}{\beta_c} \right| + \log \left| \frac{1}{2\beta_c} \right| - \left(1 + \frac{\pi}{4} \right) \right] \quad (1.2.4)$$

A plot of Equation (1.2.4) is shown in Figure 1.1.

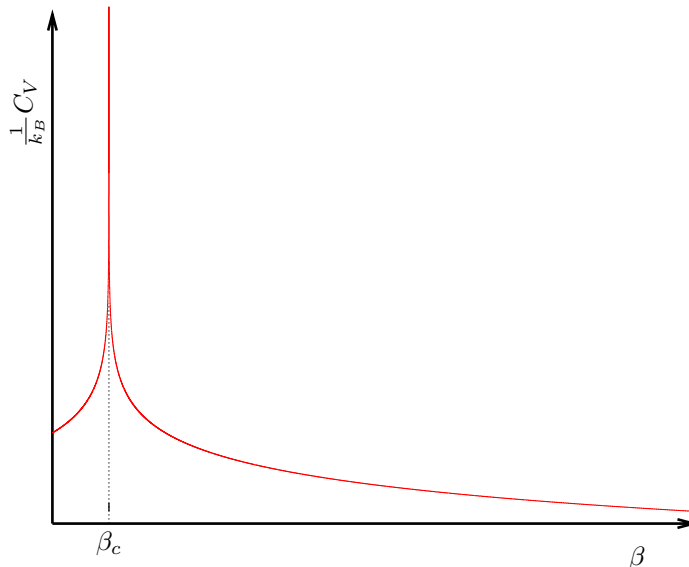


Figure 1.1: Specific heat of the two dimensional Ising model

1.2.2 Perturbation expansions

Perturbation expansion is a mathematical method used to approximate the solution of a problem that cannot be solved exactly [50, 9]. In the absence of exact solutions to problems such as the Potts model, we can find certain terms of the partition function and estimate certain expectation values. For instance, Guttman and Enting [35] found a series for the free energy of the $Q = 3$ -state Potts model to around 40 terms.

Kramers and Wannier [51] used duality (discussed in detail in the next section) and perturbation expansion to find the exact critical temperature of the 2d Ising model. Here we use their method to explain perturbation expansions. We focus on the 2d square lattice, but the method can be applied to any multi-dimensional lattice.

Recall, the partition function $Z(T)$ (1.1.1), and the Ising model Hamiltonian H (1.2.1). Note, with reference to Equation (1.2.1), we fix $M = 0$, $\epsilon = 1$ and then expand the R.H.S..

Consider the model at low temperature K , on a 2d lattice with N sites. Suppose all spins are pointing in the same direction. That is, either all up or all down (see Figure 1.2(a) for example). Then, with periodic boundary conditions, we have $H = -2N$, and the largest term in the series is $2e^{2NK}$ (cf. Appendix C for further details).

Now if we flip any spin on the lattice (see Figure 1.2(b) for example), then four of the interactions change from -1 to +1. There are $2N$ possible states where one spin points down and the rest are

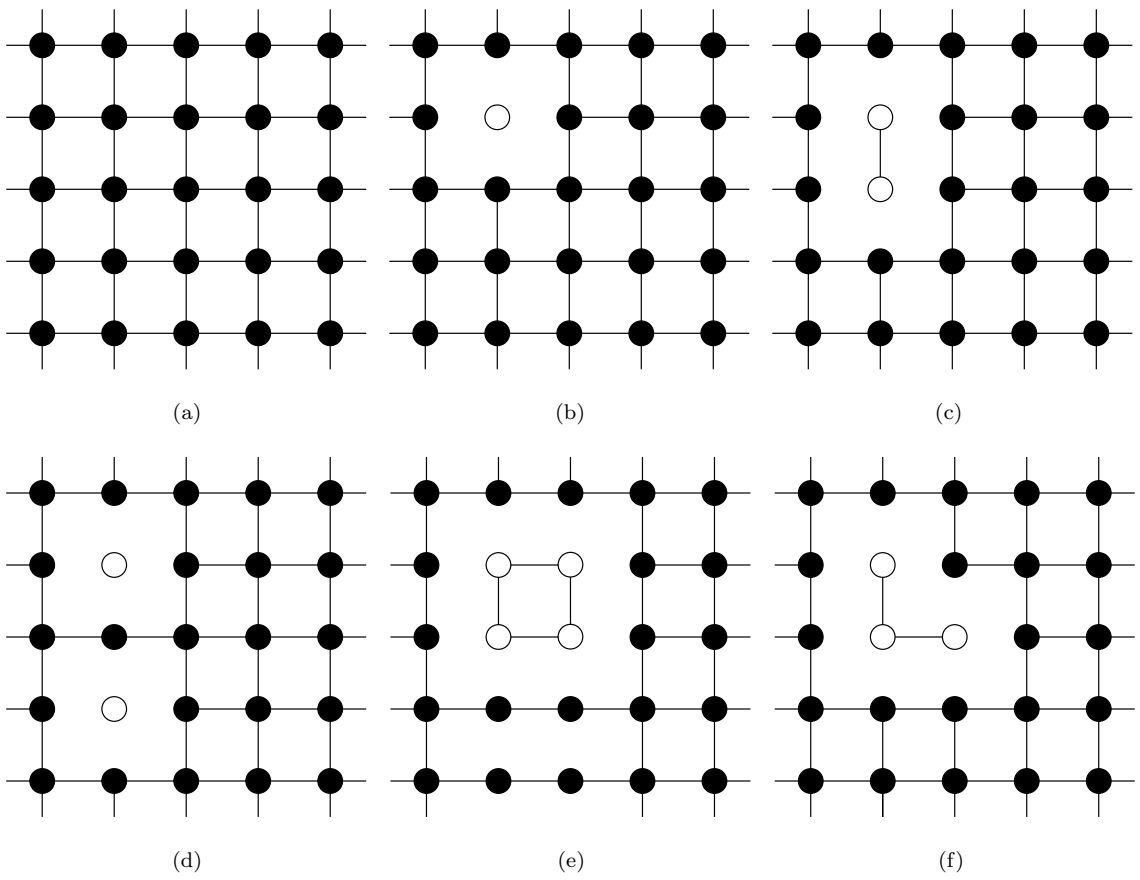


Figure 1.2: Showing the low temperature expansion for part of a 2d lattice. Full circles denote spins pointing up, and open circles are spins pointing down.

up (or vice versa). Thus the next term is $2Ne^{(2N-8)K}$.

The next term has $4N$ states when two adjacent spins are down and the rest are up (or vice versa), see Figure 1.2(c). The change in the Hamiltonian from all up (or all down) is -12 .

Figures 1.2(d)-(f), all have the same Hamiltonian value. This is a combination of: two non-adjacent spins (Figure 1.2(d)); four adjacent spins forming a square (Figure 1.2(e)); or any three adjacent spins (Figure 1.2(f)).

The partition function for the K expansion is

$$Z(K) = 2e^{2NK} + 2Ne^{(2N-8)K} + 4Ne^{(2N-12)K} + N(N-5)e^{(2N-16)K} + \dots \quad (1.2.5)$$

$$= 2e^{2NK} (1 + Ne^{-8K} + 2Ne^{-12K} + \frac{1}{2}N(N-5)e^{-16K} + \dots) \quad (1.2.6)$$

$$= 2e^{2NK} P(e^{-2K}), \quad (1.2.7)$$

where P is a polynomial.

In a similar manner, we now consider the expansion at high temperature K^* . This time every spin is pointing in the opposite direction to its nearest neighbours, see Figure 1.3(a). The leading term in this case is $2e^{-2NK^*}$. Then in a similar manner to the low temperature expansion, by changing suitable spins we find the next few terms, Figure 1.3(b)-(f).

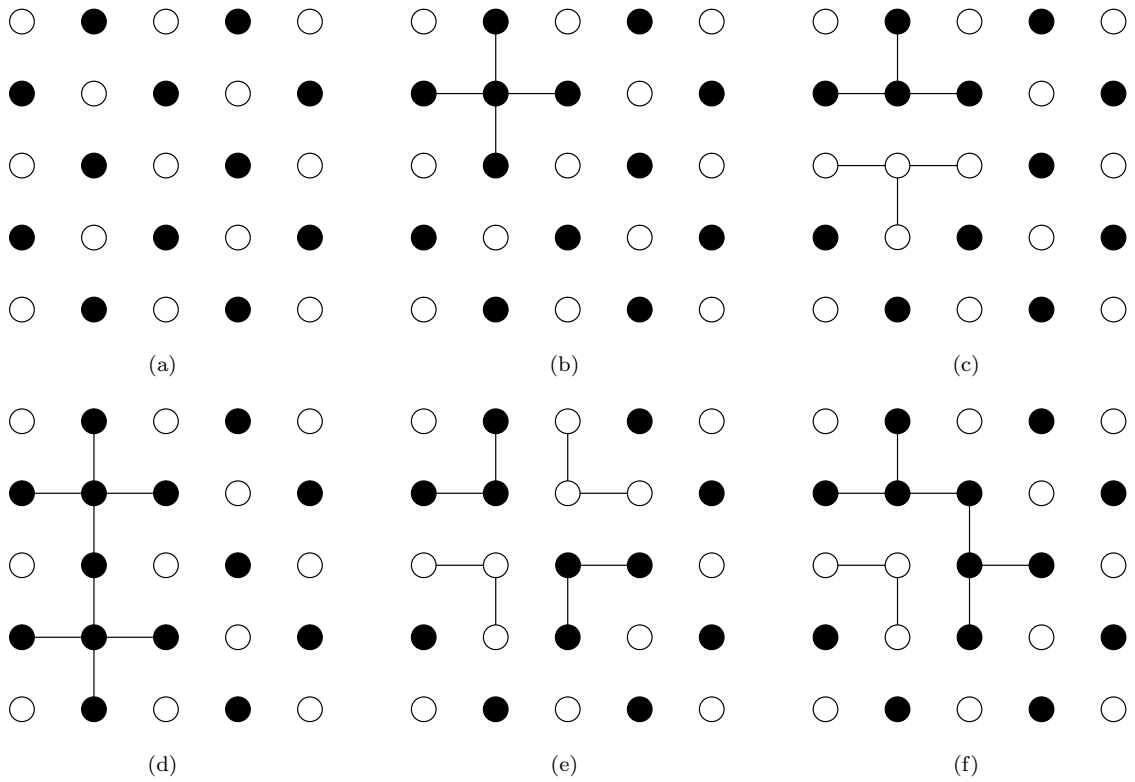


Figure 1.3: Showing the high temperature expansion for part of a 2d lattice. Full circles denote spins pointing up, and open circles are spins pointing down.

The partition function for the K^* expansion is

$$Z(K^*) = 2e^{-2NK^*} (1 + Ne^{8K^*} + 2Ne^{12K^*} + \frac{1}{2}N(N-5)e^{16K^*} + \dots) \quad (1.2.8)$$

Note this series does not converge. However, we can write $Z(K^*)$ in terms of \tanh . That is, as $\sigma_i\sigma_j = \pm 1$, then we can use the identity

$$\exp(\beta\sigma_i\sigma_j) = \cosh(\beta) + \sigma_i\sigma_j \sinh(\beta) = \cosh(\beta)(1 + \sigma_i\sigma_j \tanh(\beta)), \quad (1.2.9)$$

to write $Z(K^*)$ as

$$Z(K^*) = 2^N \cosh(K^*)^{2N} (1 + N \tanh(K^*)^4 + 2N \tanh(K^*)^6 + \dots) \quad (1.2.10)$$

$$= 2^N \cosh(K^*)^{2N} P(\tanh(K^*)). \quad (1.2.11)$$

Note, the derivation of this expansion is explained in the next section (specifically, Equation (1.2.24)). But for now, the graphical explanation of the low-temperature and high-temperature expansions should make the correspondence between the two clear, ie. $P(e^{-2K}) = P(\tanh K^*)$ [50]. To justify this relationship, suppose we let

$$e^{-2K} = \tanh(K^*). \quad (1.2.12)$$

Then, we write Equation (1.2.7) as

$$\begin{aligned}
Z(K) &= 2 \tanh(K^*)^{-N} P(\tanh(K^*)) && \text{(using (1.2.12))} \\
&= 2 \tanh(K^*)^{-N} [2^{-N} \cosh(K^*)^{-2N} Z(K^*)] && \text{(by Equation (1.2.11))} \\
&= 2 (2 \sinh(K^*) \cosh(K^*))^{-N} Z(K^*) \\
&= 2 \sinh(2K^*)^{-N} Z(K^*) && \text{(1.2.13)}
\end{aligned}$$

[1.7] The *free energy density* f (cf. [64]), is

$$f = -k_B T \lim_{N \rightarrow \infty} \frac{1}{N} \ln(Z),$$

where N is the number of spins. By Peierls argument (paragraph [1.6]) there exists a temperature β_c , where $K = K^* = \beta_c$ and

$$-k_B T \lim_{N \rightarrow \infty} \left(\frac{1}{N} \ln Z(K) \right) = -k_B T \lim_{N \rightarrow \infty} \left(\frac{1}{N} \ln Z(K^*) \right) + kT \ln(\sinh(2\beta_c)).$$

Thus, the critical temperature of the 2d Ising model is when

$$\sinh(2\beta_c) = 1,$$

thus

$$\beta_c = \frac{1}{2} \ln(1 + \sqrt{2}).$$

1.2.3 Duality

We can use duality to pass information we know about one model to its “dual” model (as we shall see later). This is quite a powerful tool, as we show that certain properties of a model, that may not manifest too easily on one may do so on its dual [9, 74]. For example, Figure 1.4 is a planar representation of a triangular lattice and its dual honeycomb lattice. (See Baxter [9, §6, §12] for a detailed example of this duality transformation.)

Duality transformations can be generalised to d -dimensional simple hypercubic lattices [36]. For example, Savit [86] shows that the 3d Ising model is dual to a lattice gauge model. See Martin [60] for an example of this duality transformation.

Kramers and Wannier [51] showed that the 2d Ising model is *self-dual*. That is, the 2d Ising model can be expressed as another 2d Ising model. They used duality to determine the critical temperature for the 2d Ising model in a zero magnetic field (detailed in Section 1.2.2).

2d Ising model duality

Here we demonstrate how duality works for the 2d $Q = 2$ (Ising) Potts model. To begin, we recall some graph notation [25]. Let \mathcal{G} be a planar graph. We define a dual graph $\mathcal{D}(\mathcal{G})$, of a plane-embedded graph \mathcal{G} . We can then rewrite the partition function Z , on a lattice \mathcal{L} , from Equation (1.1.14) in a form that allows us to write a duality transformation between the partition functions on \mathcal{G} and $\mathcal{D}(\mathcal{G})$ (formally regarded as lattices in the obvious way).

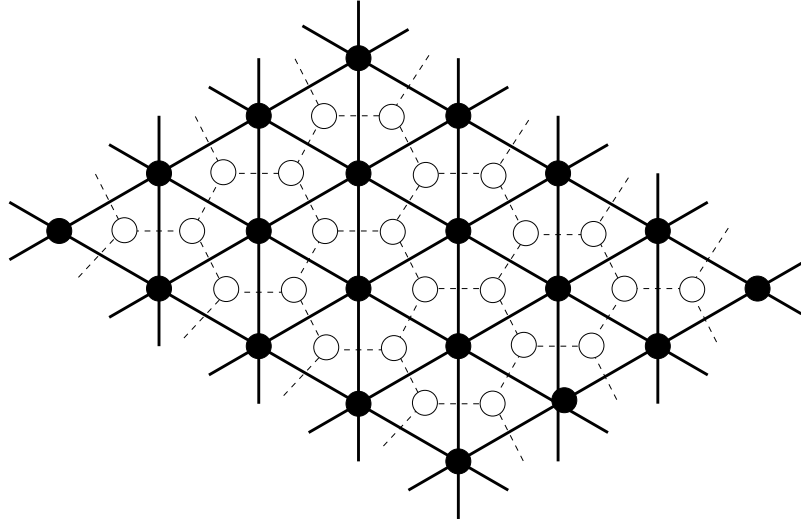


Figure 1.4: A section of a triangular lattice (black vertices and solid lines) and its dual honeycomb lattice (white vertices and dashed lines).

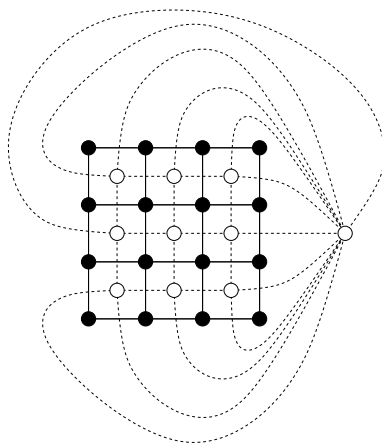


Figure 1.5: A graph \mathcal{G} (black vertices and solid lines) representing a 4×4 lattice, and its dual lattice (white vertices and dashed lines).

Recall a graph $\mathcal{G} = \mathcal{G}(V_{\mathcal{G}}, E_{\mathcal{G}})$, with $V_{\mathcal{G}}$ the set of vertices of \mathcal{G} , $E_{\mathcal{G}}$ the set of edges of \mathcal{G} . Suppose \mathcal{G} is plane-embedded, and let $F_{\mathcal{G}}$ be the set of faces of \mathcal{G} in this embedding. A face is a region bounded by edges, and the set includes the outer infinite region. Note by Euler's formula that

$$|V_{\mathcal{G}}| - |E_{\mathcal{G}}| + |F_{\mathcal{G}}| = 2. \quad (1.2.14)$$

Let \mathcal{D} be the dual graph of \mathcal{G} (for example, see Figure 1.5). That is, in the centre of each face of \mathcal{G} , we place a vertex of \mathcal{D} . And for each edge in \mathcal{G} that separates two faces we draw an edge of \mathcal{D} , whose vertices are the vertices of \mathcal{D} that lie in the faces it separates. Also add a vertex of \mathcal{D} outside \mathcal{G} , that connect all edges on the boundary of \mathcal{G} . Note, \mathcal{G} and \mathcal{D} are not isomorphic to each other in general, thus implying that $Z_{\mathcal{D}} \neq Z_{\mathcal{G}}$. Also note

$$|E_{\mathcal{G}}| = |E_{\mathcal{D}}|, \quad |V_{\mathcal{G}}| = |F_{\mathcal{D}}|, \quad \text{and} \quad |F_{\mathcal{G}}| = |V_{\mathcal{D}}|. \quad (1.2.15)$$

We now show how the partition function described in Equation (1.1.1) can be formulated in terms of \mathcal{G} and its sub-graphs. Let \mathcal{G}' be an *edge sub-graph* of \mathcal{G} , written $\mathcal{G}' \subseteq \mathcal{G}$. That is: $V_{\mathcal{G}} = V_{\mathcal{G}'}$, and $E_{\mathcal{G}'} \subseteq E_{\mathcal{G}}$.

Let $x = e^\beta$ and $v = x - 1$, then

$$\exp(\beta\delta_{\sigma_i, \sigma_j}) = 1 + v\delta_{\sigma_i, \sigma_j} \quad (1.2.16)$$

so the Q -state Potts partition function $Z_{\mathcal{G}}$ (Equation (1.1.14)), is rewritten as

$$Z_{\mathcal{G}} = \sum_{\sigma \in \Omega} \prod_{\langle ij \rangle \in E_{\mathcal{G}}} (1 + v\delta_{\sigma_i, \sigma_j}), \quad (1.2.17)$$

where $\langle ij \rangle$ represent the nearest neighbour interactions. Note each factor of the product corresponds to an interaction (bond).

If we multiply out the product of Equation (1.2.17), then the terms of this expansion can be represented by the edge sub-graphs $\mathcal{G}' \subseteq \mathcal{G}$. The edge sets of \mathcal{G}' correspond to the v factors in the terms. After carrying out spin configuration summation, we can write the partition function in the ‘dichromatic polynomial’ [97] form (see e.g. [8])

$$Z_{\mathcal{G}} = \sum_{\mathcal{G}' \subseteq \mathcal{G}} v^{|E_{\mathcal{G}'}|} Q^{|C_{\mathcal{G}'}|}, \quad (1.2.18)$$

where $|C_{\mathcal{G}'}|$ is the number of connected clusters in \mathcal{G}' , including isolated vertices.

Now we fix $Q = 2$. Suppose we rewrite the factor $\exp(\beta\delta_{\sigma_i, \sigma_j})$ from the partition function, not as in Equation (1.2.17) but as

$$(1 + (x - 1)\delta_{\sigma_i, \sigma_j}) = \left(\frac{x + 1}{2} + \frac{(x - 1)}{2}(2\delta_{\sigma_i, \sigma_j} - 1) \right). \quad (1.2.19)$$

Then Equation (1.2.17) can be written as

$$Z_{\mathcal{G}} = \sum_{\sigma \in \Omega} \prod_{\langle ij \rangle \in E_{\mathcal{G}}} \left(\frac{x + 1}{2} + \frac{(x - 1)}{2}(2\delta_{\sigma_i, \sigma_j} - 1) \right). \quad (1.2.20)$$

By factoring out the largest term of the product we have

$$Z_{\mathcal{G}} = \left(\frac{x + 1}{2} \right)^{|E_{\mathcal{G}}|} \sum_{\sigma \in \Omega} \prod_{\langle ij \rangle \in E_{\mathcal{G}}} \left(1 + \frac{(x - 1)}{x + 1}(2\delta_{\sigma_i, \sigma_j} - 1) \right), \quad (1.2.21)$$

$$= \left(\frac{x + 1}{2} \right)^{|E_{\mathcal{G}}|} \sum_{\sigma \in \Omega} \sum_{\mathcal{G}' \subseteq \mathcal{G}} \prod_{\langle ij \rangle \in E_{\mathcal{G}'}} \left(\frac{x - 1}{x + 1} \right) (2\delta_{\sigma_i, \sigma_j} - 1), \quad (1.2.22)$$

$$= \left(\frac{x + 1}{2} \right)^{|E_{\mathcal{G}}|} \sum_{\sigma \in \Omega} \sum_{\mathcal{G}' \subseteq \mathcal{G}} \left(\frac{x - 1}{x + 1} \right)^{|E_{\mathcal{G}'|} \prod_{\langle ij \rangle \in E_{\mathcal{G}'}} (2\delta_{\sigma_i, \sigma_j} - 1). \quad (1.2.23)$$

As an example consider the lattice consisting of a single square, and \mathcal{G}' , a single edge. Here we have

$$\begin{aligned} \sum_{\sigma \in \Omega} \prod_{\langle ij \rangle \in E_{\mathcal{G}'}} (2\delta_{\sigma_i, \sigma_j} - 1) &= \sum_{\sigma \in \Omega} (2\delta_{\sigma_1, \sigma_2} - 1) = \sum_{\sigma \in \Omega} 2\delta_{\sigma_1, \sigma_2} - \sum_{\sigma \in \Omega} 1 \\ &= 2 \sum_{\sigma \in \Omega} \delta_{\sigma_1, \sigma_2} - \sum_{\sigma \in \Omega} 1 = 2 \cdot 2^{N-1} - 2^N = 0 \end{aligned}$$

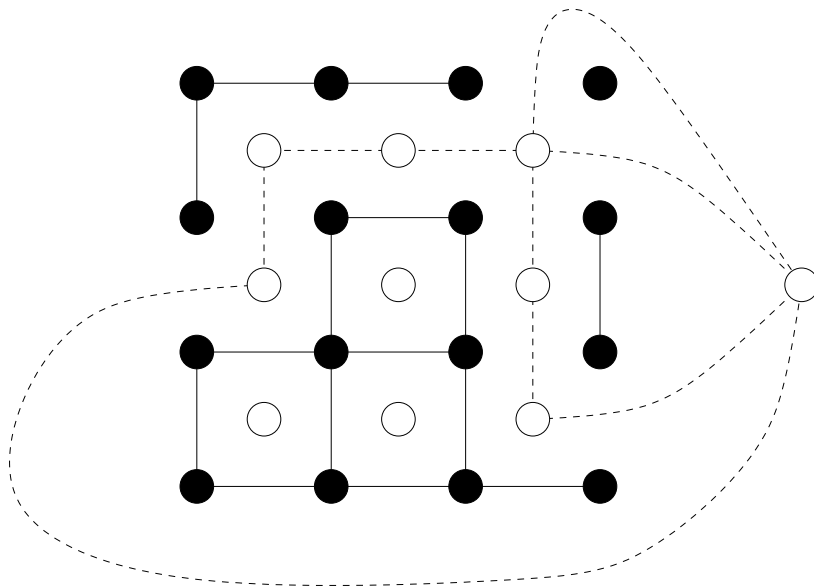


Figure 1.6: An example of a mapping between graph $\mathcal{G}' \subset \mathcal{G}$ (black vertices and solid lines) and a dual of \mathcal{G} , $\mathcal{D}' \subset \mathcal{D}$ (white vertices and dashed lines).

In fact, the sum is zero whenever the graph \mathcal{G}' describes a ‘non-even covering’ of \mathcal{G} . An *even covering* is a sub-graph \mathcal{G}' such that every vertex has an even number of edges.

One sees that if \mathcal{G}' describes an even covering of \mathcal{G} , then the sum is always 2^N . Thus we have:

$$Z_{\mathcal{G}} = 2^N \left(\frac{x+1}{2} \right)^{|E_{\mathcal{G}}|} \sum_{\text{even coverings } \mathcal{G}'} \left(\frac{x-1}{x+1} \right)^{|E_{\mathcal{G}'|} \quad (1.2.24)$$

We now show a formulation of duality for the $Q = 2$ (Ising) Potts model in two dimensions.

Let \mathcal{D} be the dual graph of \mathcal{G} . Suppose for any $\mathcal{G}' \subseteq \mathcal{G}$, we introduce an edge sub-graph $\mathcal{D}' \subseteq \mathcal{D}$ such that $E_{\mathcal{D}'}$ is the complement set of $E_{\mathcal{G}'}$ (see Figure 1.6 for example). By construction the connected components of \mathcal{D}' form “islands” around clusters of \mathcal{G}' .

For the $Q = 2$ model, we can write the partition function explicitly in terms of the islands

$$Z_{\mathcal{D}} = 2x^E \sum_{\text{Islands } H} \left(x^{-l(H)} \right), \quad (1.2.25)$$

where $l(H)$ is the length of an island H and $E = |E_{\mathcal{D}}|$.

There is a bijection between the islands of \mathcal{D} and the coverings of \mathcal{G} that takes sub-graphs onto identical, but shifted sub-graphs.

Note that if \mathcal{G} is self-dual, then the partition function is ‘almost’ invariant under the transformations [64]

$$x^{-1} \leftrightarrow \frac{x-1}{x+1}. \quad (1.2.26)$$

(cf. (1.2.12) and (1.2.26).) Further, for the Q -state Potts model the duality relation is (see Martin [62])

$$x \rightarrow \frac{x+(Q-1)}{x-1} \quad (1.2.27)$$

The square lattice is almost self-dual, in the sense that in the square lattice is taken to another square lattice up to boundary effects. (cf. Figure 1.5 with the self-dual lattice in Chen et al. (1996) [19], Figure 1).

The invariance property of the model is then called self-duality. In this sense, self-duality for the square lattice model holds true ‘up to boundary effects’.

[1.8] More generally, and more precisely, let P be a polynomial in $\frac{1}{x}$, such that Equation (1.2.25) is written as

$$Z_{\mathcal{D}} = 2x^E P\left(\frac{1}{x}\right) \quad (1.2.28)$$

Then

$$2^N \left(\frac{x+1}{2}\right)^E P\left(\frac{x-1}{x+1}\right) = Z_{\mathcal{G}}. \quad (1.2.29)$$

(Compare with Equation (1.2.13)).

Example 1.1. Fix $Q = 2$, using \mathcal{G} and \mathcal{D} from Figure 1.5, then by Equation (1.2.24) we have

$$\begin{aligned} Z_{\mathcal{G}} = & 2 + 8x^2 + 32x^3 + 72x^4 + 224x^5 + 584x^6 + 1216x^7 + 2638x^8 + 4928x^9 + \\ & + 7344x^{10} + 9984x^{11} + 11472x^{12} + 9984x^{13} + 7344x^{14} + 4928x^{15} + \\ & + 2638x^{16} + 1216x^{17} + 584x^{18} + 224x^{19} + 72x^{20} + 32x^{21} + 8x^{22} + 2x^{24}, \end{aligned} \quad (1.2.30)$$

and by Equation (1.2.25)

$$Z_{\mathcal{D}} = 2x^4 + 8x^6 + 138x^8 + 232x^{10} + 316x^{12} + 184x^{14} + 100x^{16} + 24x^{18} + 18x^{20} + 2x^{24}. \quad (1.2.31)$$

The zeros of Equations (1.2.30) and (1.2.31) are plotted in Figures 1.7(a) and 1.7(b) respectively. The zeros are invariant in the dashed grey circle shown. Plotting the zeros in the same plane (Figure 1.7(c)), highlights the invariance property. Figure 1.7(d), displays the distribution of zeros for $P(x^{-1}) + P\left(\frac{x+1}{x-1}\right)$.

We shall use this duality relation to validate our results in Chapter 3, and discuss the importance of the dashed grey circle.

1.2.4 Monte-Carlo methods

One of the most popular methods used in approximating observables is using a *Monte-Carlo method* [52]. There are quite a few different types of Monte-Carlo algorithms, but the overall concept is the same. Here we describe a Monte-Carlo algorithm known as the Metropolis algorithm [72]. We shall discuss some of the advantages and disadvantages of Monte-Carlo methods.

In general, the Metropolis algorithm uses a manageable sized sample of configurations. From this sample, we can approximate observable data. The algorithm works by considering suitable changes in energy δE between states. The algorithm is as follows [52]:

1. Choose an initial state.
2. Choose a random site i .

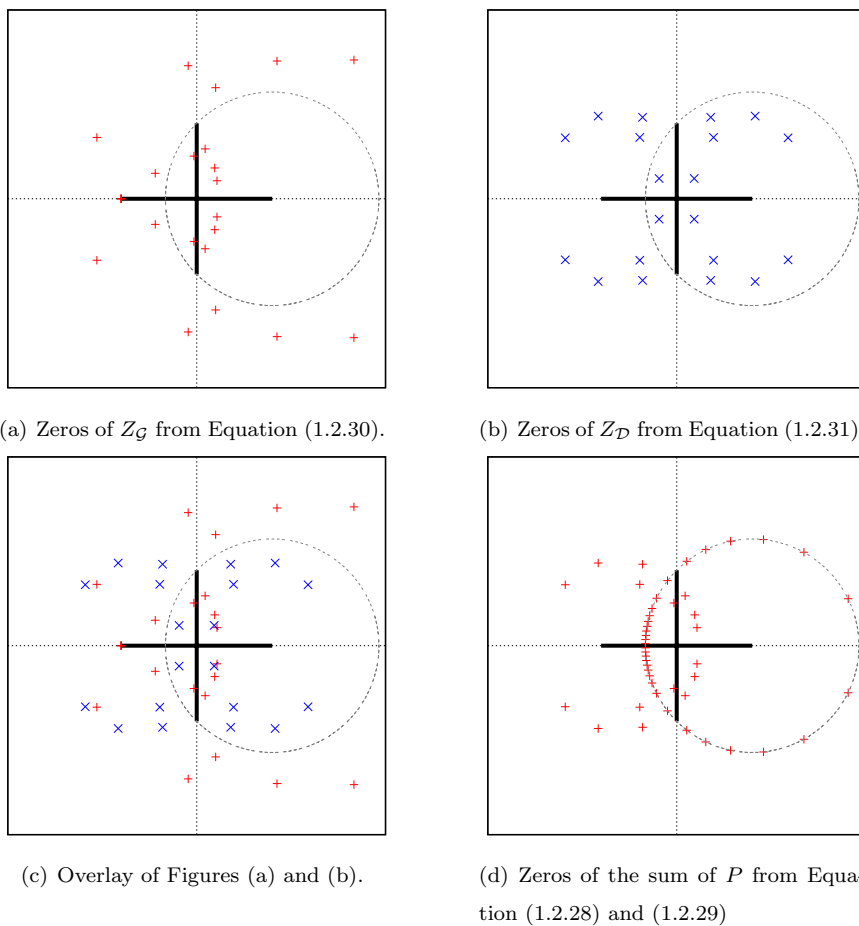


Figure 1.7: Various zeros of a 2d Potts model with $Q = 2$ fixed on graphs \mathcal{G} and \mathcal{D} from Figure 1.5. The solid cross represents the unit axis of the complex temperature plane.

3. Calculate the change in energy δE , if the spin at site i is changed/flipped.
4. Generate a random number r , in the interval $[0, 1]$.
5. If $r < \exp(-\delta E/k_B T)$, change/flip the spin.
6. Iterate from step 2.

Thermal averages from this sample can then be calculated.

An estimate of the critical point β_c for the 3d Ising model, on a simple cubic lattice (by Talapov and Blöte (1996) [92]) is

$$\beta_c = J/k_B T_c = 0.2216544, \quad (1.2.32)$$

with a claimed standard deviation of 3×10^{-7} . A Monte-Carlo algorithm was used to compute this result. It was checked against the exact solution of the 2d Ising model.

The advantages of using the Monte-Carlo method, lie within the advantages of sampling techniques. When analytic techniques fail, the Monte-Carlo method can be used to give an insight into the behaviour of the system. Due to the limitations of computer speed and memory, for large systems with an extremely large number of configurations, approximating may be the only way to find the partition function.

How true or fair are all possible configurations being represented by our sample of configurations? The results obtained using Monte-Carlo methods are exposed to statistical error. That is because we are looking at a sample of the population (ie. all possible states/configurations of the system). However, the accuracy of the system (reducing the magnitude of the statistical errors) may be increased simply by increasing the sample size (including more states). This does require further processor time. Also questions arise on how many computations are carried out for the sample to be accurate and in thermodynamic equilibrium (for example, how many iterations should we carry out; what the size of the sample should be; etc...).

1.2.5 Existing exact finite lattice results

In this section, we discuss some published Q -state Potts model results on finite 2d and 3d lattices.

In 1982, Pearson [81], found the exact partition function for the 3d Ising model on $4 \times 4 \times 4$ simple cubic lattice. He obtained his result by identifying symmetries that significantly reduced the number of configurations to be enumerated from 2^{64} to 2^{32} .

In 1990, Bhanot and Sastry [10] calculated the partition function for a $4 \times 5 \times 5$ lattice. To compute this result they used the Connection Machine, a “massively” parallel computer. Using the Connection machine, they were able to enumerate the states of the partition function using 2^{20} processors.

For the $Q > 2$ state Potts model on 2d and 3d lattice see Martin [61, 66, 63, 64]. Martin has used a transfer matrix approach (§2.2.1) to obtain his results. In his paper we also find some interesting anisotropic [64] 2d Potts model results, such as the 5 and 6-state models on a 6×7 lattice.

1.3 Physical interpretation of results

Our focus of study is on phase transitions, and what happens to a material as the critical temperature is approached. Phase transitions manifest as singularities in our results [64, §1.4.2]. Phase transitions are classified by where the lowest derivative of the free energy is discontinuous (cf. [39]). For example, we say it is a first order phase transition if the first derivative is discontinuous. Divergence in the specific heat (§1.1.3) is a signal of a second-order phase transition.

In statistical mechanics, we use correlation functions to measure how spins at various points on the lattice interact. In our systems, correlation functions contain important information about physical phase transitions [40]. Close to the critical temperature the *spin-spin correlation length* diverges [50, §II.A], and this can be interpreted as a signal for a second-order phase transition.

The zeros of the partition function are a powerful tool used for studying phase transitions and critical phenomena in finite-size systems [32]. In 1965 Fisher [30] considered the Ising model as a polynomial (in the variable $e^{2\beta}$), and studied the behaviour of its zero distribution. He showed that, in the *thermodynamic limit* (cf. Blundell [13, §1.2]), phase transitions occur where the distribution of zeros cut the real axis. By studying a suitable sequence of zero distributions, any

such stabilising features that may occur can be interpreted as an indication of what may happen in the thermodynamic limit.

1.4 Universality

Recall, a critical point of a system is a time-independent property of where phase transition occur. It separates the system into phases. *Order parameters* [49, 64] describe the phase a system is in. The average magnetisation of a ferromagnet and the density of a liquid-gas material are examples of order parameters [69]. *Critical exponents* describe the behaviour of order parameters near a transition².

According to the *universality* hypothesis, the critical behaviour of a system depends on properties such as the dimension of space and the symmetries of the system [9, 34, 69]. That is

“If we could solve a model with the same dimensionality and symmetry as a real system, universality asserts that we should obtain the exact critical components of the real system.” – Baxter (1982) [9].

Each system is assigned to a *universality class* [52]. Systems that have the same set of critical exponents belong to the same universality class. For example, universality puts a liquid-gas transition and Ising magnet transition into the same class [69, §8.1.3]. Also according to universality the gas-liquid phase transition of carbon dioxide, the gas-solid phase transition of xenon and the phase transition of the 3d Ising model should be in the same class [9].

In the following chapter, we present a method for finding the critical temperature of the 3d Ising model. First we describe a method to compute partition functions for the Q -state Potts model, and then study the specific heat order parameter. We present our results in the form of zeros distributions and specific heat plots in Chapter 3.

²See Wu (1982) [99], Mattis (2008) [67] for a table of critical exponents for the Q -state Potts model.

Chapter 2

Computational Method

For Potts models on lattices of any significant size, to calculate the partition function by a brute-force enumeration of states is not feasible. For this reason, technical tools such as *transfer matrices* are now introduced [9, §7.2].

In order to introduce transfer matrix formalism we start by recalling the necessary mathematical machinery and notations in a slightly more general setting. We have in part followed the analysis by Martin (1991) [64] in this chapter.

2.1 Potts models on graphs

Basic notations for spin configurations

For Q a natural number, define the set $\underline{Q} = \{1, 2, \dots, Q\}$. For us, then, Q -state Potts spin variables can be considered to take values from \underline{Q} .

For S, T sets we write $\text{hom}(S, T)$ for the set of all maps from S to T [45, §1.6].

If a set S indexes the spins in a given Potts model (for example, the set of physical locations might serve this purpose) we shall write Σ_S for the set of spins.

The set of all spin configurations of some set Σ_S of Q -state Potts spins is thus

$$\Omega_S := \text{hom}(\Sigma_S, \underline{Q})$$

Note that mathematically this is the same as $\text{hom}(S, \underline{Q})$.

Let A be some finite set of symbols [28]. A string over A is a finite sequence of symbols drawn from that set. Let A^k denote the set of all strings over A of length k .

Example 2.1. Fix $Q = 2$, then $\underline{Q}^3 = \{111, 211, 121, 221, 112, 212, 122, 222\}$.

Apply a total order R on set S , and write σ_i for the i th spin in this order. We can then write Ω_S as a set of strings. That is, for each $f \in \Omega_S$ we may encode it as an element of $\underline{Q}^{|\Sigma_S|}$ by

$$f(\sigma_i) = x_i \tag{2.1.1}$$

where x_i is the i th symbol of string $x \in \underline{Q}^{|\Sigma_S|}$. Also note that $|\Omega_S| = Q^{|\Sigma_S|}$.

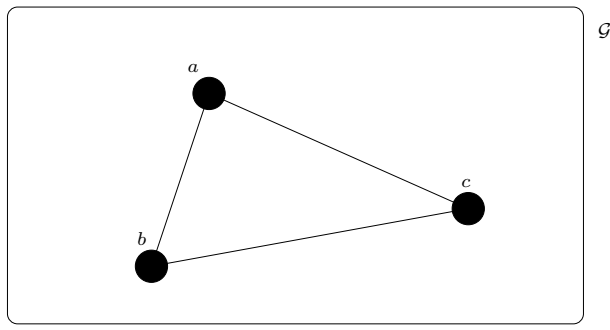


Figure 2.1: A planar realisation of an undirected graph \mathcal{G} .

Similarly we can think of each $f \in \Omega_S$ as a $|\Sigma_S|$ -tuple vector: the i th element of f is $f(\sigma_i)$.

Example 2.2. For $Q = 2$ fixed, we have the set \underline{Q}^3 . Let $S = \{1, a, 3\}$. Assume that a total order relation R , orders the elements of S as $a < 1 < 3$. Also let $\Sigma_S = \{\sigma_1, \sigma_a, \sigma_3\}$. Then for $712 \in \underline{Q}^3$, the corresponding function $f \in \Omega_S$ is

$$f(\sigma_1) = 1, \quad f(\sigma_a) = 7 \quad \text{and} \quad f(\sigma_3) = 2. \quad (2.1.2)$$

This is also written as vector $(f(\sigma_a), f(\sigma_1), f(\sigma_3))$, which evaluates to $(7, 1, 2)$.

Graphs as Potts model ‘lattices’

Recall [25, §1.1] that a simple undirected graph $\mathcal{G} = \mathcal{G}(V_{\mathcal{G}}, E_{\mathcal{G}})$ is a set of vertices $V_{\mathcal{G}}$ together with a set of edges $E_{\mathcal{G}}$, which are unordered pairs from $V_{\mathcal{G}}$.

Example 2.3. Figure 2.1 encodes a graph \mathcal{G} , with three arbitrarily labelled vertices a, b and c . That is $V_{\mathcal{G}} = \{a, b, c\}$, $E_{\mathcal{G}} = \{\{a, b\}, \{a, c\}, \{b, c\}\}$.

A lattice spin system [50] is modelled here as a Potts model on a simple undirected graph $\mathcal{G}(V_{\mathcal{G}}, E_{\mathcal{G}})$ [101]. A vertex $i \in V_{\mathcal{G}}$ represents a physical site on the lattice, on which resides a spin σ_i ; and the set of edges $E_{\mathcal{G}}$ represents the bond or nearest neighbour interactions between spins.

For each choice of graph \mathcal{G} and natural number Q we have the Potts model Hamiltonian (cf. Section 1.1.4):

$$H_{\mathcal{G}} : \Omega_{V_{\mathcal{G}}} \rightarrow \mathbb{R} \\ H_{\mathcal{G}}(f) = \sum_{\{i,j\} \in E_{\mathcal{G}}} \delta_{f(\sigma_i), f(\sigma_j)}. \quad (2.1.3)$$

Where $\delta_{a,b}$ is the *Kronecker delta*, that returns a value of 1 if $a = b$, and 0 otherwise. We shall write $H_{\mathcal{G}}$ as just H , when the dependence on \mathcal{G} is clear.

Example 2.4. Using \mathcal{G} from Example 2.3 with $V_{\mathcal{G}}$ totally ordered in the natural way and configuration $(1, 2, 2) \in \Omega_{V_{\mathcal{G}}}$, the Hamiltonian value is

$$H((1, 2, 2)) = \delta_{1,2} + \delta_{1,2} + \delta_{2,2} = 1 \quad (2.1.4)$$

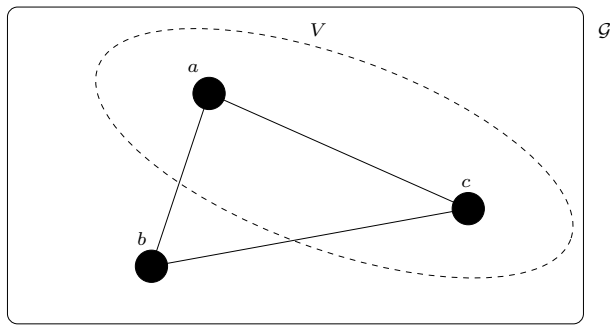


Figure 2.2: Shows set $V \subseteq V_G$.

The notion of Potts partition function Z [40] can then be regarded as a map from the set of graphs \mathcal{G} to the set of polynomials Z_G in $\exp(\beta)$. That is (cf. Equation (1.1.1)):

$$Z_G = \sum_{\sigma \in \Omega_{V_G}} \exp \beta H_G(\sigma). \quad (2.1.5)$$

Here physically $\beta = -1/k_B T$ (k_B is Boltzmann's constant, T the temperature). For the remainder of this section let $x = \exp(\beta)$.

Example 2.5. Using \mathcal{G} from Example 2.3, and fixing $Q = 2$, then $Z_G = 2e^{3\beta} + 6e^\beta$.

2.2 Partition vectors and transfer matrices

In this section. *Partition vectors* [64, §2.1] will be explained. A specialisation to transfer matrix formulation is then made in Section 2.2.1.

Let $V \subseteq V_G$ for any graph \mathcal{G} . For Q -state Potts model configuration $c \in \Omega_V$, we define $\Omega_{V_G}^V|_c$ as the set of spin configurations where the spins associated to V are fixed to c . Note $\Omega_{V_G}^V|_c \subset \Omega_{V_G}$.

Example 2.6. Let $V_G = \{a, b, c\}$ and $V = \{a, c\}$ (see Figure 2.2). Fix $Q = 2$. Take the natural order on V_G , and the natural order by restriction of this order on V , then

$$\Omega_{V_G} = \{(1, 1, 1), (2, 1, 1), (1, 2, 1), (2, 2, 1), (1, 1, 2), (2, 1, 2), (1, 2, 2), (2, 2, 2)\}, \quad (2.2.1)$$

and $\Omega_V = \{(1, 1), (2, 1), (1, 2), (2, 2)\}$. Then for configuration $(1, 1) \in \Omega_V$, we have

$$\Omega_{V_G}^V|_{(1,1)} = \{(1, 1, 1), (1, 2, 1)\}. \quad (2.2.2)$$

The partition function with the configuration of spins in subset V fixed to configuration c ($c \in \Omega_V$) is

$$Z_G^V|_c := \sum_{\sigma \in \Omega_{V_G}^V|_c} \exp(\beta H(\sigma)). \quad (2.2.3)$$

Definition 2.2.1. The partition vector Z_G^V is a vector indexed by Ω_V .

The c -th component of Z_G^V ($c \in \Omega_V$) is $Z_G^V|_c$. Note

$$Z_G = \sum_{c \in \Omega_V} Z_G^V|_c. \quad (2.2.4)$$

Example 2.7. Consider graph \mathcal{G} in Figure 2.2, where the subset of vertices $V = \{a, c\}$ is indicated.

Fix $Q = 2$. We have $\Sigma_V = \{\sigma_a, \sigma_c\}$, and

$$Z_{\mathcal{G}}^V = (Z_{\mathcal{G}}^V|_{(1,1)}, Z_{\mathcal{G}}^V|_{(1,2)}, Z_{\mathcal{G}}^V|_{(2,1)}, Z_{\mathcal{G}}^V|_{(2,2)}) \quad (2.2.5)$$

$$= (x^3 + x, 2x, 2x, x^3 + x). \quad (2.2.6)$$

Note, summing up the entries of $Z_{\mathcal{G}}^V$ give $Z_{\mathcal{G}}$ from Example 2.5.

[2.1] We now formulate a method for combining the partition vectors for two Potts models on graphs to make a Potts model partition function for a larger graph. We refer to this as *binding*. To do this, first we must define the union operator of two graphs (cf. [94] for several variations on combining graphs).

Definition 2.2.2. For the union $\mathcal{G} \cup \mathcal{G}'$ of graphs \mathcal{G} and \mathcal{G}' , we have:

$$V_{\mathcal{G} \cup \mathcal{G}'} = V_{\mathcal{G}} \cup V_{\mathcal{G}'}, \quad \text{and} \quad E_{\mathcal{G} \cup \mathcal{G}'} = E_{\mathcal{G}} \cup E_{\mathcal{G}'}$$

Theorem 2.2.3 (Chapman-Kolmogorov [80]). Let \mathcal{G} and \mathcal{G}' be graphs such that $E_{\mathcal{G}} \cap E_{\mathcal{G}'} = \emptyset$.

Let $\mathcal{G}\mathcal{G}'$ denote $\mathcal{G} \cup \mathcal{G}'$ and $V = V_{\mathcal{G}} \cap V_{\mathcal{G}'}$. Then

$$Z_{\mathcal{G}\mathcal{G}'} = \sum_{c \in \Omega_V} (Z_{\mathcal{G}}^V|_c)(Z_{\mathcal{G}'}^V|_c) = Z_{\mathcal{G}}^V \cdot Z_{\mathcal{G}'}^V \quad (2.2.7)$$

Proof. Recall Equation (2.1.5). For graph $\mathcal{G}\mathcal{G}' = \mathcal{G} \cup \mathcal{G}'$, we have

$$Z_{\mathcal{G}\mathcal{G}'} = \sum_{\sigma \in \Omega_{V_{\mathcal{G}\mathcal{G}'}}} e^{\beta H_{\mathcal{G}\mathcal{G}'}(\sigma)} \quad (2.2.8)$$

Providing $E_{\mathcal{G}} \cap E_{\mathcal{G}'} = \emptyset$, then

$$H_{\mathcal{G}\mathcal{G}'}(\sigma) = H_{\mathcal{G}}(\sigma) + H_{\mathcal{G}'}(\sigma). \quad (2.2.9)$$

for every configuration $\sigma \in \Omega_{V_{\mathcal{G}\mathcal{G}'}}$. Thus

$$Z_{\mathcal{G}\mathcal{G}'} = \sum_{\sigma \in \Omega_{V_{\mathcal{G}\mathcal{G}'}}} \left(e^{\beta H_{\mathcal{G}}(\sigma)} \right) \left(e^{\beta H_{\mathcal{G}'}(\sigma)} \right) \quad (2.2.10)$$

Now if $V = V_{\mathcal{G}} \cap V_{\mathcal{G}'}$ then

$$Z_{\mathcal{G}\mathcal{G}'} = \sum_{c \in \Omega_V} \left(\sum_{\sigma \in \Omega_{V_{\mathcal{G}}|_c}} e^{\beta H_{\mathcal{G}}(\sigma)} \right) \left(\sum_{\sigma' \in \Omega_{V_{\mathcal{G}'|_c}}} e^{\beta H_{\mathcal{G}'}(\sigma')} \right) \quad (2.2.11)$$

$$= \sum_{c \in \Omega_V} (Z_{\mathcal{G}}^V|_c)(Z_{\mathcal{G}'}^V|_c) \quad (2.2.12)$$

□

The second identity in Equation (2.2.7) is an equivalent statement by Definition 2.2.1.

Example 2.8. Fix $Q = 2$. For graphs \mathcal{G} and \mathcal{G}' , see Figure 2.3. The partition vector $Z_{\mathcal{G}}^V$ is

$$(Z_{\mathcal{G}}^V|_{(1)}, Z_{\mathcal{G}}^V|_{(2)}) = (x^3 + 3x, x^3 + 3x). \quad (2.2.13)$$

Also

$$Z_{\mathcal{G}'}^V = (x^2 + 2x + 1, x^2 + 2x + 1) \quad (2.2.14)$$

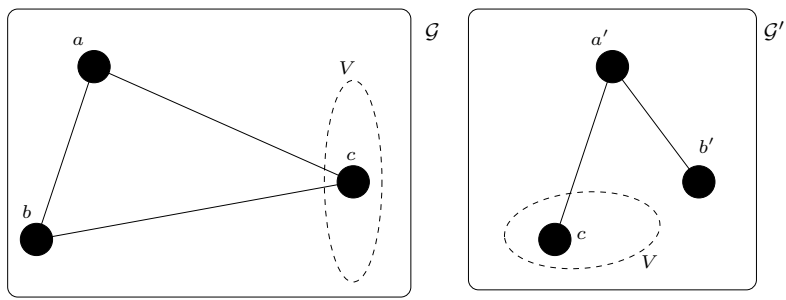


Figure 2.3: Graphs \mathcal{G} and \mathcal{G}'

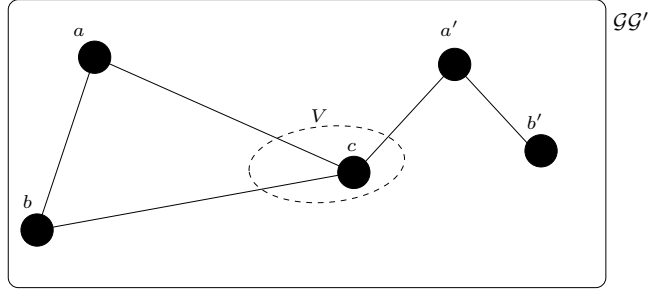


Figure 2.4: The resultant graph $\mathcal{G}\mathcal{G}'$, obtained by combining \mathcal{G} and \mathcal{G}' (from Figure 2.3) over V .

Then for graph $\mathcal{G}\mathcal{G}' = \mathcal{G} \cup \mathcal{G}'$ (Figure 2.4), $V_{\mathcal{G}\mathcal{G}'} = \{a, a', b, b', c\}$, $V = \{c\}$, and

$$\begin{aligned}
 Z_{\mathcal{G}\mathcal{G}'} &= (Z_{\mathcal{G}}^V|_1 \cdot Z_{\mathcal{G}'}^V|_1) + (Z_{\mathcal{G}}^V|_2 \cdot Z_{\mathcal{G}'}^V|_2) \\
 &= (x^3 + 3x)(x^2 + 2x + 1) + (x^3 + 3x)(x^2 + 2x + 1) \\
 &= 2x^5 + 4x^4 + 8x^3 + 12x^2 + 6x
 \end{aligned} \tag{2.2.15}$$

A mild generalisation of Theorem 2.2.3 is as follows.

Notation: For sets V and V' let $V \setminus V'$ denote the set of all elements in V that are not in V' .

Lemma 2.2.4. *Let \mathcal{G} and \mathcal{G}' be graphs such that $E_{\mathcal{G}} \cap E_{\mathcal{G}'} = \emptyset$. Let $\mathcal{G}\mathcal{G}' = \mathcal{G} \cup \mathcal{G}'$ and $V = V_{\mathcal{G}} \cap V_{\mathcal{G}'}$ and $V' \subseteq V_{\mathcal{G}\mathcal{G}'}$. Then*

$$Z_{\mathcal{G}\mathcal{G}'}^{V'}|_{c'} = \sum_{c \in \Omega_{V \setminus V'}} (Z_{\mathcal{G}}^V|_{c'})(Z_{\mathcal{G}'}^V|_{c'}). \tag{2.2.16}$$

Here c' is the configuration associated to V' and then to V .

The proof of Lemma 2.2.4 is similar to the proof of Theorem 2.2.3 (cf. Chapman-kolmogorov

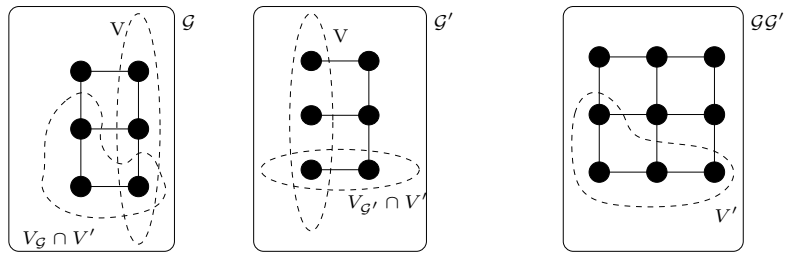


Figure 2.5: A graphical example of Lemma 2.2.4

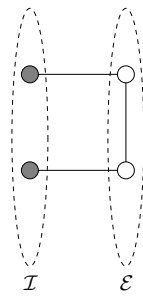


Figure 2.6: Representing incoming and outgoing spins using \mathcal{I} and \mathcal{E} respectively

equation [80]). Figure 2.5 is a graphical representation of Lemma 2.2.4. The next section shows how Lemma 2.2.4 implies matrix multiplication can be used to combine partition vectors.

2.2.1 Transfer matrices

In this section we show that the partition function (Equation (2.1.5)) is for certain very regular graphs \mathcal{G} the trace of the N th power of a certain matrix. We call this matrix the *transfer matrix* [88, 12, 9, 6, 65, 85, 23]. A computational feature of using transfer matrices is that we may compute $Z_{\mathcal{G}}$ by repeatedly binding smaller systems together.

Recall the partition vector $Z_{\mathcal{G}}^V$. Let $\mathcal{E} \subset V$. We call $\Sigma_{\mathcal{E}}$ the set of *outgoing* spins. Let $\mathcal{I} \subset V$ such that $V = \mathcal{E} \cup \mathcal{I}$. Call $\Sigma_{\mathcal{I}}$ the set of *incoming* spins. $Z_{\mathcal{G}}^V$ is now trivially reorganised as a matrix, denoted \mathcal{T} . The rows and columns of \mathcal{T} are indexed by $\Omega_{\mathcal{I}}$ and $\Omega_{\mathcal{E}}$ respectively. The element in the i -th row, j -th column is

$$\mathcal{T}_{ij} = Z_{\mathcal{G}}^{\mathcal{I}, \mathcal{E}}|_{i,j}, \quad (2.2.17)$$

where $i \in \Omega_{\mathcal{I}}$ and $j \in \Omega_{\mathcal{E}}$. Indeed for any collection of subsets $V_i \subset V$ such that $V = \cup_i V_i$ we define $Z_{\mathcal{G}}^{V_1, V_2, \dots}|_{c_1, c_2, \dots}$ in the obvious way — leading to what might be called a *partition tensor* [64, 46].

Example 2.9. Fix $Q = 2$. Let the graph in Figure 2.6 model a spin system. The incoming and outgoing vertex (spin) sets have been labelled \mathcal{I} and \mathcal{E} respectively. Then

$$\mathcal{T} = \begin{pmatrix} x^3 & x & x & x \\ x^2 & x^2 & 1 & x^2 \\ x^2 & 1 & x^2 & x^2 \\ x & x & x & x^3 \end{pmatrix} \quad (2.2.18)$$

Let $\mathcal{T}_{\mathcal{G}}$ and $\mathcal{T}_{\mathcal{G}'}$ be transfer matrices associated to graphs \mathcal{G} and \mathcal{G}' respectively, with $\mathcal{I}_{\mathcal{G}}, \mathcal{E}_{\mathcal{G}}$ and $\mathcal{I}_{\mathcal{G}'}, \mathcal{E}_{\mathcal{G}'}$ being the index sets to the incoming and outgoing spins for $\mathcal{T}_{\mathcal{G}}$ and $\mathcal{T}_{\mathcal{G}'}$ respectively.

If $\mathcal{E}_{\mathcal{G}} = \mathcal{I}_{\mathcal{G}'}$, and $E_{\mathcal{G}} \cap E_{\mathcal{G}'} = \emptyset$ then by Lemma 2.2.4, we have the matrix product

$$\mathcal{T}_{\mathcal{G}\mathcal{G}'} = \mathcal{T}_{\mathcal{G}}\mathcal{T}_{\mathcal{G}'}. \quad (2.2.19)$$

Note $\mathcal{I}_{\mathcal{G}\mathcal{G}'} = \mathcal{I}_{\mathcal{G}}$ and $\mathcal{E}_{\mathcal{G}\mathcal{G}'} = \mathcal{E}_{\mathcal{G}'}$.

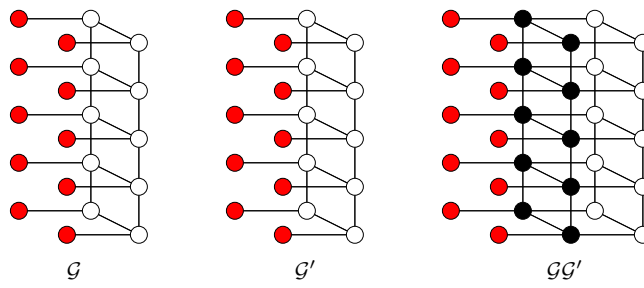


Figure 2.7: Spin systems modelled by graphs \mathcal{G} and \mathcal{G}' and $\mathcal{G}\mathcal{G}'$, where \mathcal{G} and \mathcal{G}' are connected to form $\mathcal{G}\mathcal{G}'$. The red, white, and black vertices model incoming, outgoing, and internal spins respectively.

After matrix multiplication, any further binding with $\mathcal{T}_{\mathcal{G}\mathcal{G}'}$ is restricted to incoming and outgoing spins of $\mathcal{G}\mathcal{G}'$. The set $\mathcal{E}_{\mathcal{G}} \cap \mathcal{I}_{\mathcal{G}'}$ becomes the set of *internal* vertices of $\mathcal{G}\mathcal{G}'$. That is, the spin configuration information of these vertices is summed over, such that no further binding from these vertices is possible. We shall often refer to these spins as internal spins.

For an example of such graphs see Figure 2.7. Here we model incoming, outgoing, and internal spins in each graph using red, white and black vertices respectively.

The partition function for a suitable large regular graph (such as a crystal structure cf. §2.2.2) can then be calculated by iteratively multiplying suitably smaller manageable transfer matrices. To do this, we introduce *isomorphisms* between graphs.

Definition 2.2.5. *Two graphs \mathcal{G} and \mathcal{G}' are said to be isomorphic [18] if there is a one-to-one mapping $\phi : V_{\mathcal{G}} \rightarrow V_{\mathcal{G}'}$ such that if and only if $\{a, b\} \in E_{\mathcal{G}}$ then $\{\phi(a), \phi(b)\} \in E_{\mathcal{G}'}$.*

For instance, suppose \mathcal{G} is isomorphic (in the strong sense) to \mathcal{G}' , and $|\mathcal{E}_{\mathcal{G}}| = |\mathcal{I}_{\mathcal{G}}| = |\mathcal{E}_{\mathcal{G}'}| = |\mathcal{I}_{\mathcal{G}'}|$ then we can take $\mathcal{T}_{\mathcal{G}} = \mathcal{T}_{\mathcal{G}'}$. It then follows that

$$\mathcal{T}_{\mathcal{G}\mathcal{G}'} = \mathcal{T}_{\mathcal{G}}\mathcal{T}_{\mathcal{G}'} = (\mathcal{T}_{\mathcal{G}})^2. \quad (2.2.20)$$

Let $\mathcal{G}(L)$ be the graph union of L isomorphic graphs \mathcal{G} . The partition function is given by

$$Z_{\mathcal{G}(L)} = \sum_{s \in \Omega_{\mathcal{I}_{\mathcal{G}(L)}}} \left(\sum_{t \in \Omega_{\mathcal{E}_{\mathcal{G}(L)}}} (\mathcal{T}_{\mathcal{G}}^L|_{st}) \right) \quad (2.2.21)$$

where $\mathcal{I}_{\mathcal{G}(L)}$ is the incoming spin set for $\mathcal{G}(L)$ (ie. $\mathcal{I}_{\mathcal{G}}$ for the first \mathcal{G} in $\mathcal{G}(L)$); and $\mathcal{E}_{\mathcal{G}(L)}$ is the outgoing spin set for $\mathcal{G}(L)$ (ie. $\mathcal{E}_{\mathcal{G}}$ for the last \mathcal{G} in $\mathcal{G}(L)$). Note that if \mathcal{D} is the column vector with $\mathcal{D}_i = 1$ for all configurations in $\Omega_{\mathcal{I}_{\mathcal{G}}}$ then

$$Z_{\mathcal{G}(L)} = \mathcal{D}^T \mathcal{T}^L \mathcal{D}. \quad (2.2.22)$$

To obtain periodic boundary condition (Section 2.2.2) we identify the incoming and outgoing spins of $(\mathcal{T}_{\mathcal{G}})^L$. To do this, we sum over the states where incoming and outgoing configurations are equal. Specifically

$$Z_{\mathcal{G}(L)} = \text{Tr}(\mathcal{T}_{\mathcal{G}}^L). \quad (2.2.23)$$

2.2.2 Geometry and Crystal lattices

This section is on graphs as regular crystal lattices [71] embedded in Euclidean space [31, 36].

Potts Model in d -dimension

We ‘place’ spins in \mathbb{R}^d so as to form a d -dimensional *lattice* modelling a physical crystal lattice. Let \mathcal{L}^d denote the d -dimensional hypercubic lattice. Here, we define $\mathcal{L} = \mathcal{L}^d$ as a finite set of regularly spaced sites embedded in the Euclidean space \mathbb{R}^d of the form $\{\{1, \dots, N_1\} \times \{1, \dots, N_2\} \times \dots \times \{1, \dots, N_d\} | N_i \in \mathbb{N}\}$. On each site resides a spin. Figure 2.8, the sub-figures depict examples of d -dimensional lattices. We draw lines between nearest-neighbour sites to represent corresponding interactions between spins.

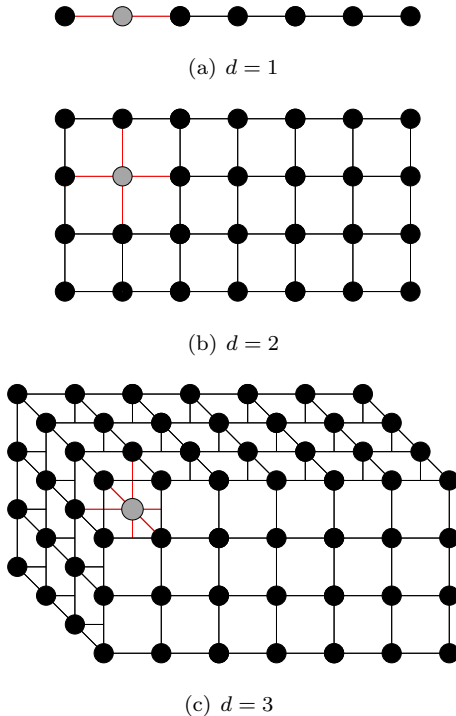


Figure 2.8: Showing d -dimensional lattices. The grey spin in each figure, represents a typical bulk spin and its nearest neighbour interactions (red edges).

Layer transfer matrix

Our d -dimensional lattice can be built up by a set of $(d - 1)$ -dimensional sub-lattices. We shall call these *layers* of a lattice. Note, in the case of $d = 1$, a layer is just a single point.

In $d = 3$ we shall use the notation $N_x \times N_y \times N_z$, ($N_x, N_y, N_z \in \mathbb{N}$) to represent \mathcal{L} with N_z layers. Each layer has N_y columns each containing N_x sites. The total number of sites is $N_x N_y N_z$.

For the Q -state Potts model on \mathcal{L} , the i th layer interacts only with the $i - 1$ th and $i + 1$ th layers.

Now suppose we wanted to calculate a Q -state Potts model partition function on a lattice $N_x \times N_y \times N_z$. We could use a transfer matrix \mathcal{T} that is indexed by the spin configuration of two

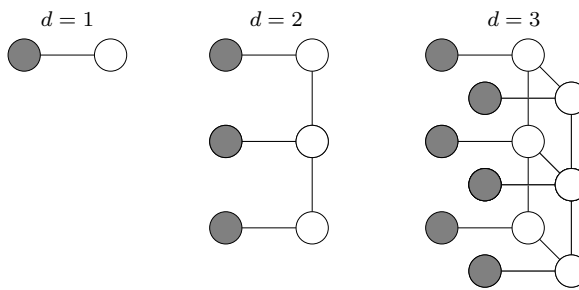


Figure 2.9: Examples of d -dimensional transfer matrix lattice layers. Incoming (outgoing) spins are modelled by grey (white) vertices

layers. We shall refer to this as the “layer transfer matrix”. Note \mathcal{T} is a $Q^{N_x N_y} \times Q^{N_x N_y}$ matrix. Figure 2.9 are examples d -dimensional transfer matrix lattice layers.

For the remainder of this Thesis we shall only be concerned with the given regular crystal lattice structure, and graph \mathcal{G} (Section 2.1) shall be regarded as a lattice in the obvious way. Further, we shall refer to the partition function as just Z .

As we have seen, where it can be applied, the transfer matrix formalism speeds up partition function calculations. If in addition, as in crystal lattices, the layer has *symmetry*, then some further speed-ups can be achieved. In Appendix B, we show how to use such symmetries of \mathcal{T} to find \mathcal{T}^L for relatively large \mathcal{T} .

Boundary Conditions

In dimension d , the number n of nearest neighbours to each spin is $n = 2d$ up to boundary effects [21]. A finite-sized lattice (as defined so far) has spins on the boundary of the lattice that have $n < 2d$. We refer to this as the lattice having *open* boundary conditions. The lattices in Figure 2.8, are examples of lattices with open boundary conditions.

An alternative is to introduce an extra interaction between spins on opposite sides of the boundary. In this case all spins on a lattice have the same number of nearest neighbours, and there are exact translation symmetries. We refer to this as applying *periodic* boundary conditions.

2.2.3 Eigenvalues of the transfer matrix

Recall the layer transfer matrix \mathcal{T} , Section 2.2.1, such as in Example 2.9.

For this \mathcal{T} , all entries are monomials in $x = e^\beta$. In particular all entries are positive for real β .

Suppose \mathcal{T} binds layers i and $i + 1$. Then by Theorem 2.2.3, we may write \mathcal{T} as a product of more *local* transfer matrices, say $\mathcal{T}_{i+1}, \mathcal{T}_{i,i+1}$. Specifically \mathcal{T}_{i+1} is restricted to only the interactions on layer $i + 1$, and $\mathcal{T}_{i,i+1}$ is restricted to only the interactions between layers i and $i + 1$.

Example 2.10. For \mathcal{T} in given in Example 2.9 (page 23)

$$\mathcal{T} = \mathcal{T}_{i,i+1}\mathcal{T}_{i+1} = \begin{pmatrix} x^2 & x & x & 1 \\ x & x^2 & 1 & x \\ x & 1 & x^2 & x \\ 1 & x & x & x^2 \end{pmatrix} \begin{pmatrix} x & & & \\ & 1 & & \\ & & 1 & \\ & & & x \end{pmatrix}$$

[2.2] By symmetry of the Hamiltonian, $\mathcal{T}_{i,i+1}$ and \mathcal{T}_{i+1} are Hermitian matrices for real β . Note, they both are real symmetric and \mathcal{T}_{i+1} is also a diagonal matrix. One can then show that \mathcal{T} is similar (in the technical sense) to a real symmetric matrix (and hence Hermitian).

Let $\{\lambda_i\}$ be the set of eigenvalues of \mathcal{T} . Also, for each λ_i , let v'_i and v_i be the corresponding row and column eigenvectors respectively. That is

$$\mathcal{T}v_i = \lambda_i v_i \tag{2.2.24}$$

and

$$v'_i \mathcal{T} = \lambda_i v'_i. \tag{2.2.25}$$

For us let r and w be suitable boundary vectors (such as \mathcal{D}^T and \mathcal{D} from Equation (2.2.22)) such that

$$Z = r\mathcal{T}^N w.$$

Define coefficients a_i and b_i by

$$r = \sum_i a_i v'_i \quad \text{and} \quad w = \sum_i b_i v_i \tag{2.2.26}$$

Note that a_i and b_i are constants, depending only on the fixed boundary conditions r and w .

Then

$$r \mathcal{T}^N w = \left(\sum_i a_i v'_i \right) \mathcal{T}^N \left(\sum_j b_j v_j \right) \tag{2.2.27}$$

$$= \left(\sum_i a_i (\lambda_i^N v'_i) \right) \left(\sum_j b_j v_j \right) \tag{2.2.28}$$

By the similarity of \mathcal{T} to a real symmetric matrix, eigenvectors v'_i and v_j can be chosen to be orthonormal. Thus, by *completeness of the set of eigenvectors* [73], we have

$$\lambda_i^N v'_i v_j = \begin{cases} \lambda_i^N, & j = i \\ 0, & \text{otherwise} \end{cases}, \tag{2.2.29}$$

for all i, j .

Thus Equation (2.2.28) simplifies to

$$r \mathcal{T}^N w = \sum_i (a_i b_i \lambda_i^N) \tag{2.2.30}$$

so

$$Z = r \mathcal{T}^N w = \sum_i K_i \lambda_i^N, \tag{2.2.31}$$

where $K_i = a_i b_i$ for all i .

Theorem 2.2.6 (Perron-Frobenius). ¹ *A finite-dimensional positive matrix has unique eigenvalue that has the largest magnitude of all eigenvalues. Further this eigenvalue is positive and there is an associated eigenvector that is also positive.*

It follows from the theorem that if β is real then \mathcal{T} has a largest eigenvalue.

Let λ_0 denote the largest eigenvalue of \mathcal{T} (for $\beta \in \mathbb{R}$) then Equation (2.2.31) can be expressed in the form

$$Z = \sum_i K_0 \lambda_0^N \frac{K_i}{K_0} \left(\frac{\lambda_i}{\lambda_0} \right)^N \quad (2.2.32)$$

$$= K_0 \lambda_0^N \left(1 + \sum_{i>0} \frac{K_i}{K_0} \left(\frac{\lambda_i}{\lambda_0} \right)^N \right). \quad (2.2.33)$$

For a given real value of β , we have

$$\lim_{N \rightarrow \infty} Z = K_0 \lambda_0^N. \quad (2.2.34)$$

Recall [75] the *free energy density* $f = (1/N) \ln Z$. For us then, in the limit $N \rightarrow \infty$ we have [64, §2.5]

$$f(\beta) = \lim_{N \rightarrow \infty} \left(\frac{\ln(K_0 \lambda_0^N)}{N} \right) = \ln(\lambda_0) \quad (2.2.35)$$

This equation thus connects the physics to the partition function to the largest eigenvalue of \mathcal{T} .

In Section 2.3, we go further and connect the eigenvalues of \mathcal{T} to the *zeros* of the partition function in complex β .

2.3 Zeros of the partition function

In this section we show how the complex zeros of the partition function relate to the eigenvalues of the transfer matrix, and to physics.

We shall discuss the distribution of the zeros and their sensitivity to varying lattice sizes. Also, we show how the distribution of zeros are used to extract information on real physical attributes from our system.

Note the zeros are themselves hard to compute, even given the exact partition function. They are found by using a modified Newton-Raphson technique, see Appendix D.

2.3.1 Specific heat

Recall Section 1.1.3, the specific heat C_V is [96, §19.1] given by

$$C_V/k_B = -\beta^2 \frac{\partial^2 \ln Z}{\partial \beta^2}. \quad (2.3.1)$$

For us, Z is the Q -state Potts model partition function (Equation (2.1.5)).

¹For proof see [76], [64, §2.4]

As Z is a polynomial in $x = e^\beta$, we can write it in terms of its zeros x_i [90]. That is

$$Z = Q \prod_i (e^\beta - x_i). \quad (2.3.2)$$

In statistical mechanics, thermodynamic limit singularities that occur in derivatives of the free energy correspond to phase transitions (cf. [26, 30]). Recall Section 1.1.3, the *Helmholtz free energy* is $F = -k_B T \ln Z$ [16]. So in the Potts model case we have

$$F = -1/\beta \left(\ln Q + \sum_i \ln(e^\beta - x_i) \right). \quad (2.3.3)$$

[2.3] Remark: Here we consider specific heat capacity as an “extensive” variable. It is often useful to consider specific heat by an intensive measure [17]. To do this, we divide C_V by an extensive measure, say the total number of spins on the lattice N . We shall use $c_V := C_V/N$ to differentiate between the two.

Note

$$\frac{\partial \ln Z}{\partial \beta} = \frac{\partial}{\partial \beta} \left(\ln Q + \sum_i \ln(e^\beta - x_i) \right) \quad (2.3.4)$$

$$= e^\beta \sum_i \frac{1}{e^\beta - x_i}. \quad (2.3.5)$$

Thus, we can express Equation (2.3.1) in terms of the partition function zeros as:

$$C_V/k_B\beta^2 = -\frac{\partial^2 \ln Z}{\partial \beta^2} \quad (2.3.6)$$

$$= -\frac{\partial}{\partial \beta} \left(e^\beta \sum_i \frac{1}{e^\beta - x_i} \right) \quad (2.3.7)$$

$$= -\sum_i \left(\frac{e^\beta}{e^\beta - x_i} - \frac{e^{2\beta}}{(e^\beta - x_i)^2} \right) \quad (2.3.8)$$

$$= e^\beta \sum_i \frac{x_i}{(e^\beta - x_i)^2}. \quad (2.3.9)$$

Thus Equation (2.3.9) states complex temperature singularities [68] in the specific heat occur when $e^\beta = x_i$.

As physically meaningful temperatures are real and positive, then β must also be real and positive. For us however, the coefficients of Z are all positive, and therefore the zeros will lie off the real positive x axis [64, §11.1].

[2.4] Only in the thermodynamic limit where the distribution of zeros is continuous, do we find a “critical point”. That is, the singular point at which the zeros cut the real axis. Thus, as the complex roots x_i get closer to the real axis, the more tightly they indicate the position of a phase transition.

2.3.2 Eigenvalues and the zeros distribution

In Section 2.2.3, we showed that the partition function can be approximated numerically for real β via the largest eigenvalue of the transfer matrix. With this in mind we now show how the

distribution of zeros of the partition function in the complex plane is related to the eigenvalues of the transfer matrix.

Recall Equation (2.2.31). Setting $Z = 0$, and letting $K_i = a_i b_i$, we have

$$\sum_i (K_i \lambda_i^N) = 0. \quad (2.3.10)$$

Suppose \mathcal{T} has two jointly largest magnitude eigenvalues at some value of β , or in some small range of β values. (Note that the Perron-Frobenius Theorem 2.2.6 cannot be expected to apply when β is not real.) Denote the two largest magnitude eigenvalues as λ_0 and λ_1 . Then expanding Equation (2.3.10):

$$K_0 \lambda_0^N + K_1 \lambda_1^N + \sum_{i \neq 0,1} K_i \lambda_i^N = 0, \quad (2.3.11)$$

and rearranging, we obtain

$$\frac{K_0 \lambda_0^N}{K_1 \lambda_1^N} = -1 - \sum_{i \neq 0,1} \frac{K_i \lambda_i^N}{K_1 \lambda_1^N}. \quad (2.3.12)$$

Here

$$\lim_{N \rightarrow \infty} \left(\frac{K_0 \lambda_0^N}{K_1 \lambda_1^N} \right) = -1. \quad (2.3.13)$$

Also note

$$\frac{\ln K_0}{N} + \log \lambda_0 = \frac{\ln(-K_1)}{N} + \log \lambda_1$$

so approaching the limit $\log \lambda_0^N \approx \log \lambda_1^N$. Equation (2.3.13) is then

$$\left(\frac{\lambda_0}{\lambda_1} \right) = \sqrt[N]{-1} \quad (2.3.14)$$

Martin [64] block diagonalises a small Q -state Potts model transfer matrix and shows that its eigenvalues take the form

$$\lambda_{\pm} = A(x) \pm \sqrt{B(x)},$$

where $A(x)$, and $B(x)$ are polynomials in $x = \exp(\beta)$. We shall just use this result, and refer the reader to the book for the proof.

We re-express $\lambda_+^N + \lambda_-^N$ using the following identity. For scalars C and D

$$C^N + D^N = \prod_n (C + \exp(2\pi i n/N) D) \quad (2.3.15)$$

where the product is over $n = 1, 2, \dots, N$, if N is odd; and over $n = 1/2, 3/2, \dots, N - 1/2$ for N even [64, §11.2].

The zeros of $\lambda_+^N + \lambda_-^N$ occur only when $|\lambda_+| = |\lambda_-|$ [56]. That is, when

$$e^{i(2\pi n/N)} = \frac{\lambda_+}{\lambda_-}. \quad (2.3.16)$$

By Equation 2.3.15 we see that the zeros of $\lambda_+^N + \lambda_-^N$ lie on the same loci as the zeros of Z_G . Further, the endpoints of these loci are at the zeros of $B(x)$ (where $\lambda_+ = \lambda_-$).

For a finite N , the zeros of Z thus end up indicating the ‘analytic structure’ [3, 95] of the largest eigenvalues for the corresponding \mathcal{T} . (See [54, §4.10] for detailed exposition.)

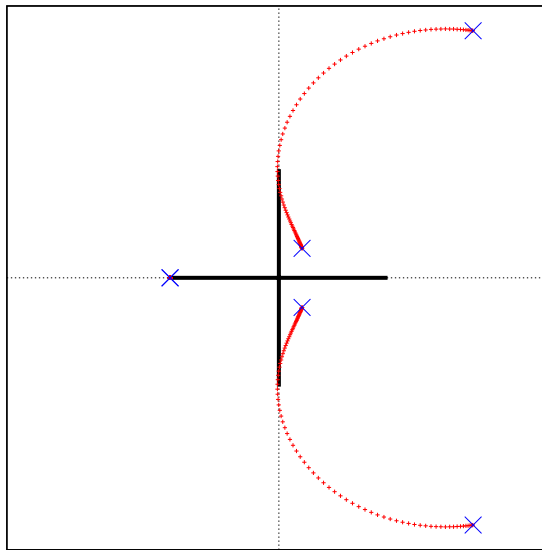


Figure 2.10: The zeros of $\text{Tr}(\mathcal{T}^{100})$ (red dots) and the zeros of $B(x)$ (blue crosses).

Example 2.11. In Example 2.9 (page 23), the transfer matrix \mathcal{T} for $Q = 2$ Potts model on a 2 site wide lattice is given. The eigenvalues for \mathcal{T} are

$$\left\{ e^{2\beta} - 1, \frac{1}{2} \left(e^{3\beta} + e^{2\beta} + e^{\beta} + 1 \pm (e^{\beta} + 1) \sqrt{e^{4\beta} - 4e^{3\beta} + 10e^{2\beta} - 4e^{\beta} + 1} \right), e^{3\beta} - e^{\beta} \right\}$$

Then choose

$$\lambda_{\pm} = \frac{1}{2} \left(e^{3\beta} + e^{2\beta} + e^{\beta} + 1 \pm (e^{\beta} + 1) \sqrt{e^{4\beta} - 4e^{3\beta} + 10e^{2\beta} - 4e^{\beta} + 1} \right)$$

In Figure 2.10 (cf. Fig. 4.4 [54]), we plot the $B(x) = 0$ with blue crosses and use the red points to show the zeros of $Z = \text{Tr}(\mathcal{T}^{100})$. Note, there are two zeros of $B(x) = 0$ at $(-1, 0)$.

This model itself is too small to extract meaningful physics from. See Chapter 3 for many much larger cases; and an analysis of their physical significance.

2.4 Correlation functions

The transfer matrix formalism that we have described allows us, in principle, to compute other physical observables besides those derived from Z , such as correlation functions. At present our computational methodology does not help sufficiently to allow computing correlation functions on the large lattices with which we work. Nonetheless, for completeness we end this Chapter with a brief formal discussion of such physically interesting observables.

Recall (Section 1.1.3) that an observable \mathcal{O} on a lattice system is a map on the set of configurations Ω ,

$$\mathcal{O} : \Omega \rightarrow \mathbb{R} \tag{2.4.1}$$

For example, for a Potts model on a graph \mathcal{G} with $a, b \in V_{\mathcal{G}}$

$$\mathcal{O}_a := \delta_{\sigma_a, 1}$$

An *expectation value* is a *thermal average*

$$\langle \mathcal{O} \rangle := \frac{\sum_{\sigma \in \Omega} \mathcal{O} e^{\beta H(\sigma)}}{Z_{\mathcal{G}}} \quad (2.4.2)$$

Suppose spins σ_a and σ_b , are fixed to state $q \in Q$.

Fix σ_a 's position on the lattice, then we shall observe $\langle \mathcal{O}_a \mathcal{O}_b \rangle$ for various suitable separations d , on the lattice of σ_b from σ_a . (We are assuming here that the lattice, that is the graph \mathcal{G} , is such that the notion of separation makes sense.)

This allows us to study the relation between the distance of spins, and their influence on each other.

At large β (low temperature) there is a high expectation of agreement between spins. This agreement is due to the fact that all spins are mostly aligned at this temperature, and is not dependent on the distance between a and b .

To adjust for this non-correlated agreement we calculate the *subtracted* spin-spin correlation function [64]

$$\langle \mathcal{O}_a \mathcal{O}_b \rangle_s := \langle \mathcal{O}_a \mathcal{O}_b \rangle - \langle \mathcal{O}_a \rangle \langle \mathcal{O}_b \rangle. \quad (2.4.3)$$

At zero temperature, the probability that the Ising model is in a particular frozen state is $1/2$. This is because of the symmetry of the model. To ‘correct’ this we choose a spin on the boundary of the lattice and fix its state to c . Now at low temperature the configuration of the system will be in the frozen state with all spins in state c . Our model models “spontaneous symmetry breaking” [64, §1.4] in this way.

Define diagonal matrix U_a with rows and columns indexed by the same configuration space as \mathcal{T} . Let $(U_a)_{\sigma\sigma} = \delta_{\sigma(a),c}$, for all $\sigma \in \mathbb{N}$.

For boundary vectors r and w , we have [64, §2.6]

$$\langle \mathcal{O}_a \mathcal{O}_b \rangle_s = \frac{r \mathcal{T}^M U_a \mathcal{T}^d U_b \mathcal{T}^{N-M-d} w}{Z} - \frac{r \mathcal{T}^M U_a \mathcal{T}^{N-M} w}{Z} \cdot \frac{r \mathcal{T}^{M+d} U_b \mathcal{T}^{N-M-d} w}{Z} \quad (2.4.4)$$

(where M determines the position of a relative to the left boundary of the lattice).

One finds (see e.g. Kogut [50]) that $\langle \mathcal{O}_a \mathcal{O}_b \rangle_s$ typically decays exponentially with d :

$$\langle \mathcal{O}_a \mathcal{O}_b \rangle_s \sim \exp(-|d|/\xi(\beta)), \quad (2.4.5)$$

The decay length $\xi(\beta)$ is called the *correlation length*. (The correlation length may be expressed in terms of eigenvalues of \mathcal{T} . See [59, §2.6].)

The program used to compute large Potts model partition functions for this work relies highly on symmetry within the transfer matrix. Due to this we cannot compute the correlation function of a system of any real significant size in our exact-calculation framework.

Toy Example

Consider the 2×3 lattice shown in Figure 2.11. Fix $Q = 2$. The white vertex represents a spin with configuration fixed to 1 (symmetry breaking condition). Here \mathcal{T} is indexed in the usual manner (see Section 2.2.1, for example).

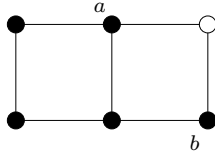


Figure 2.11: A 2×3 lattice, with sites labelled a and b . The white site is a fixed spin.

Sites a and b have been labelled. Then

$$U_a = \begin{pmatrix} 1 & 0 & 0 & 0 \\ 0 & 1 & 0 & 0 \\ 0 & 0 & 0 & 0 \\ 0 & 0 & 0 & 0 \end{pmatrix}, \quad U_b = \begin{pmatrix} 1 & 0 & 0 & 0 \\ 0 & 0 & 0 & 0 \\ 0 & 0 & 1 & 0 \\ 0 & 0 & 0 & 0 \end{pmatrix},$$

For open boundary conditions we define the row vectors $r = (x, 1, 1, x)$ and $w = (1, 1, 0, 0)$.

Then

$$\begin{aligned} Z &= rT^2w = x^7 + 6x^5 + 9x^4 + 9x^3 + 6x^2 + 1, \\ \langle \mathcal{O}_a \rangle &= (rTU_aTw)/Z = (x^7 + 4x^5 + 6x^4 + 3x^3 + 2x^2)/Z, \\ \langle \mathcal{O}_b \rangle &= (rT^2U_bw)/Z = (x^7 + 4x^5 + 6x^4 + 3x^3 + 2x^2)/Z, \\ \langle \mathcal{O}_a\mathcal{O}_b \rangle &= (rTU_aTU_bw)/Z = (x^7 + 3x^5 + 3x^4 + x^2)/Z. \end{aligned}$$

In Figure 2.12, we plot $\langle \mathcal{O}_a\mathcal{O}_b \rangle_s$ for this example. We also mark the critical temperature e^{β_c} of the 2d Ising model [78].

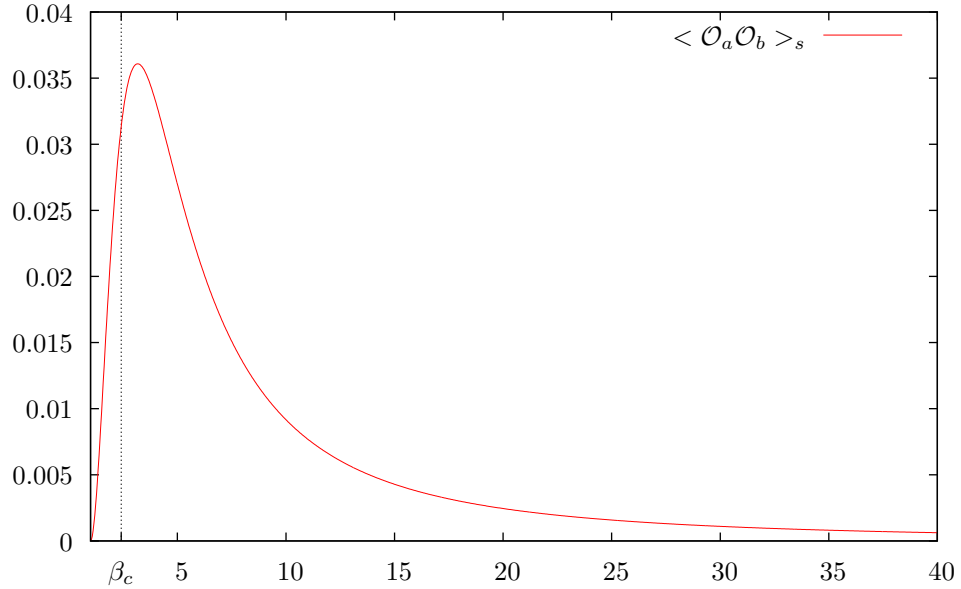
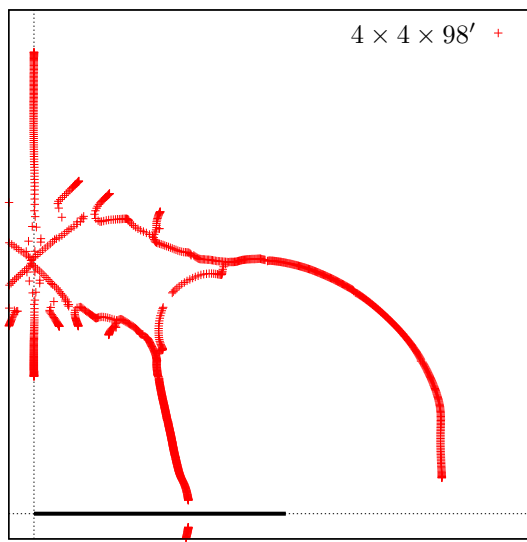


Figure 2.12: A plot of $\langle \mathcal{O}_a\mathcal{O}_b \rangle_s$ against β for the Ising model on a 2×3 lattice.



Chapter 3

Potts model partition functions: Exact Results

In this Chapter, we give our results. A convenient way to present a partition function which is polynomial in e^β is by plotting its zeros in the e^β -Argand plane (see e.g. [30, 81, 60, 64, 19]). Here, then, we give the zeros of the partition function for various lattices, displayed in the e^β -Argand plane and variants thereof. Some specific heat graphs are also presented.

[3.1] Since none of these models, apart from the 2d Ising model [78], is integrable in the thermodynamic limit [9], the main challenge in *interpreting* these results is in extrapolating from our finite lattices to the limit (cf. [58, 66]). We study how varying lattice size and boundary conditions affect the specific heat and zeros by computing, for each model, several variations of each.

The figure above is a zeros distribution for a 3d Ising model. The $4 \times 4 \times 98'$ refers to lattice size (the prime is explained later) and solid line represents the interval $[0, 1]$. How do we interpret this distribution? We start this chapter by introducing the terms and notations used to describe such figures. The 3d Ising model is then discussed. For example, Figure 3.1 shows our results for the 3d Ising model on various lattices. However we are immediately confronted with the need for a means to interpret such results. So together with the 3d model we look at the 2d Ising model, and hence

show how physical phenomena such as phase transitions are manifested in the zero distribution.

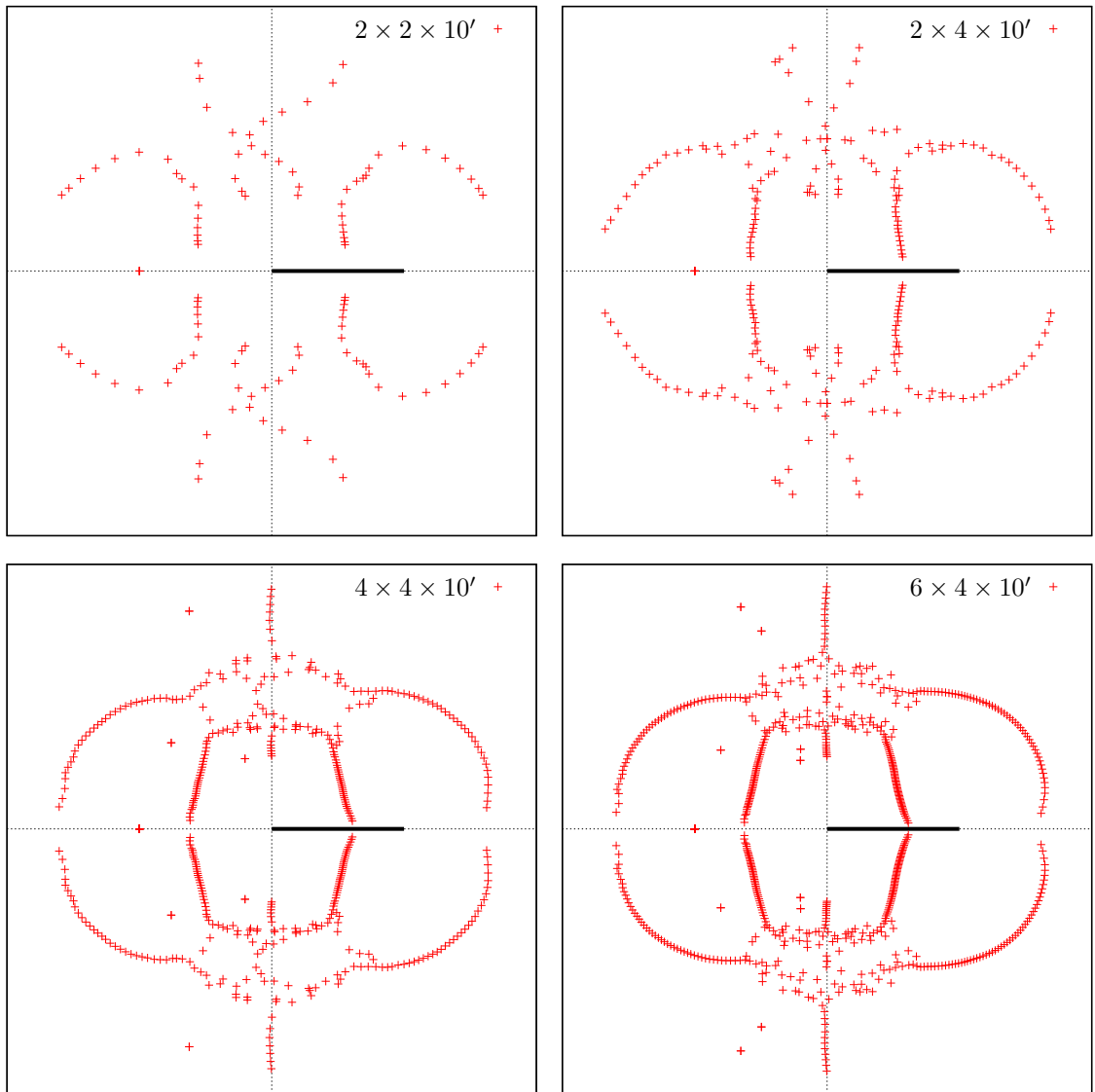


Figure 3.1: Zeros of the partition function Z in $x = e^\beta$ for the $N_x \times N_y \times 10'$ Ising model. The degree of Z in sub-figure: (a) is 116; (b) is 232; (c) is 464; (d) is 696.

We use the following notation for lattice sizes and boundary conditions (BCs):

- $N \times M \times \dots$ means an $N \times M \times \dots$ hypercubic lattice with periodic BCs in every direction.
- A direction with open BCs is indicated as N' .
- $N \times M$ means an $N \times M$ lattice with self dual BCs¹.
- $(N \times M)^*$ means the dual of a $N \times M$ lattice².

So for example $5 \times 5 \times 10'$ means a lattice periodic in the length 5 directions, and with open BCs in the long direction.

Figure 3.2 show the zeros distribution for the 2d Ising model partition on a 10×10 lattice. We use this figure as a visual aid to describing some of the terms used in this chapter. The solid black line in this figure (and all subsequent figures) is the interval $[0, 1]$ in the Argand plane. (Note that for $x = e^\beta$ this region is the anti-ferromagnetic region).

The values of β that have direct physical significance lie in the interval $[0, \infty)$ on the real axis. That is, where temperature is real and positive, either for ferro- or anti-ferromagnetic coupling. The ferromagnetic region is indicated by a green line in the figure. We shall refer to it as \mathfrak{F} .

We find it useful to separate the e^β plane into quadrants. We label the 2nd, 3th, and 4th quadrant as indicated in Figure 3.2. The 1st quadrant is labelled with the lattice size and boundary condition.

Many of the zero distributions presented are grouped together under one figure, like in Figure 3.1. We refer to sub-figures in the order: left to right top to bottom, as (a), (b)... etc. So for example Figure 3.1(c) is the zero distribution for the 3d model on the $4 \times 4 \times 10'$ lattice.

Recall, from Section 2.3, the way in which zero distributions approximate analytic structures (of transfer matrix eigenvalues). With this in mind, we call the linear distributions of zeros sometimes apparent in these plots “arms”, as indicated in Figure 3.2. Note that the rigorous justification for this requires a sequence tending, in a suitable sense, to a limit distribution. Thus the identification of ‘arms’ in any given figure is not an exact science. For example, note the two large ‘arms’ in the 3rd and 4th quadrant are certainly not clear cut. (Although in this case we know that, as part of a sequence, they again approach a linear distribution in their respective quadrants.)

Table 3.1 lists the maximal sizes of the figures in this thesis.

¹See Fig. 1.1 in Chen et al (1996) [19], for an example of a lattice with self-dual boundary conditions.

²See §1.2.3, for an explanation of dual lattices.

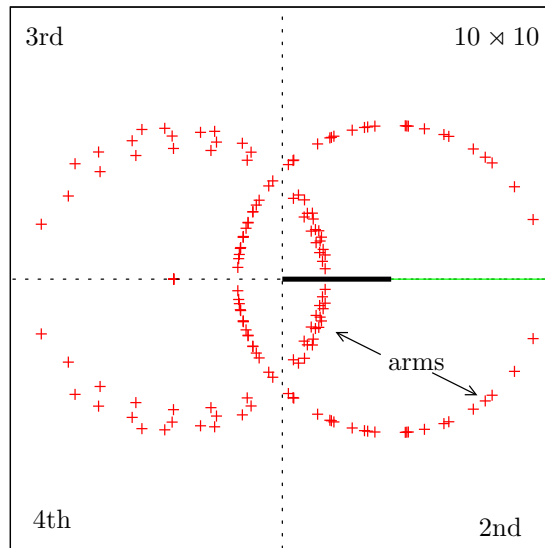


Figure 3.2: The zero distribution for a 10×10 (self dual) lattice.

Q	size: $n \times m \times l$	source	figure	Q	size: $n \times m$	source	figure
2	$4 \times 4 \times 4$	Pearson [81]	3.13(d)	2	18×18	Kaufman [48]	3.3(c)
2	$4 \times 5 \times 5'$	Bhanot [10]	3.16(c)	2	14×14	Kaufman [48]	3.8(c)
2	$4 \times 4 \times 10$	NEW	3.14(d)	2	$10 \times 99'$	Kaufman [48]	3.25(d)
2	$4 \times 6 \times 10'$	NEW	3.1(d)	3	06×09	NEW	3.27(a)
2	$5 \times 5 \times 10'$	NEW	3.10(b)	3	10×12	Martin [66]	3.27(b)
2	$5 \times 5 \times 19'$	NEW	3.10(c)	3	12×16	NEW	3.27(c)
2	$4 \times 4 \times 98'$	NEW	3.26(c)	4	8×8	NEW	3.28(a)
3	$3 \times 3 \times 9'$	Martin [60]	3.29(b)	4	10×16	NEW	3.28(b)
3	$3 \times 4 \times 10'$	NEW	3.30(d)	5	7×7	NEW	3.28(c)
3	$4 \times 4 \times 10'$	NEW	3.29(f)	5	7×9	Martin [64]	3.28(d)
4	$3 \times 4 \times 10'$	NEW	3.31(b)	5	10×16	NEW	3.28(d)
5	$3 \times 3 \times 9'$	NEW	3.31(c)	6	6×6	NEW	3.28(e)
6	$3 \times 3 \times 9'$	NEW	3.31(d)	6	10×10	NEW	3.28(f)

Table 3.1: Table of Potts model partition functions, for exact finite lattice presented in this chapter.

3.1 On phase transitions in 3d Ising model

For the 2d Potts model, an exact solution for $Q = 2$ is well known. For suitable boundary conditions (BCs) (see Appendix for details) it is:

$$Z_{MN}(x) = \prod_{r=1}^M \prod_{s=1}^N \left\{ 1 - \frac{1}{2} K(x) \left(\cos \frac{2\pi r}{M} + \cos \frac{2\pi s}{N} \right) \right\}, \quad (3.1.1)$$

where

$$K(x) = \frac{x^{-2} \{1 - x^{-4}\}}{\{1 + x^{-4}\}^2} \quad (3.1.2)$$

(we review the solution in detail in the appendix, following Onsager's method [78], §A). We compare finite lattice results obtained by our methods to the exact thermodynamic limit solution in order to study the relationship between sequences of finite-size results and limit results. This relationship will be what guides our interpretation of sequences of finite lattice results in the cases where we do not have exact thermodynamic limit solutions. It also gives us a way to study finite size effects in general.

Signals of phase transition: 2d Ising model

The zeros distributions for the 2d Ising model on 5×5 , 10×10 , 18×18 , and $\infty \times \infty$ (thermodynamic limit) are shown in Figure 3.3, respectively. In the limit the zeros form two solid circles as shown in Figure 3.3(d).

In the limit the zeros have perfect 8-fold symmetry: inversion in the unit circle; symmetry by complex conjugation; and sign-reversal symmetry (since it is a function of x^2). Further, the circle on the right does cut the real axis in \mathfrak{F} , at $e^{\beta c} = \sqrt{2} + 1$.

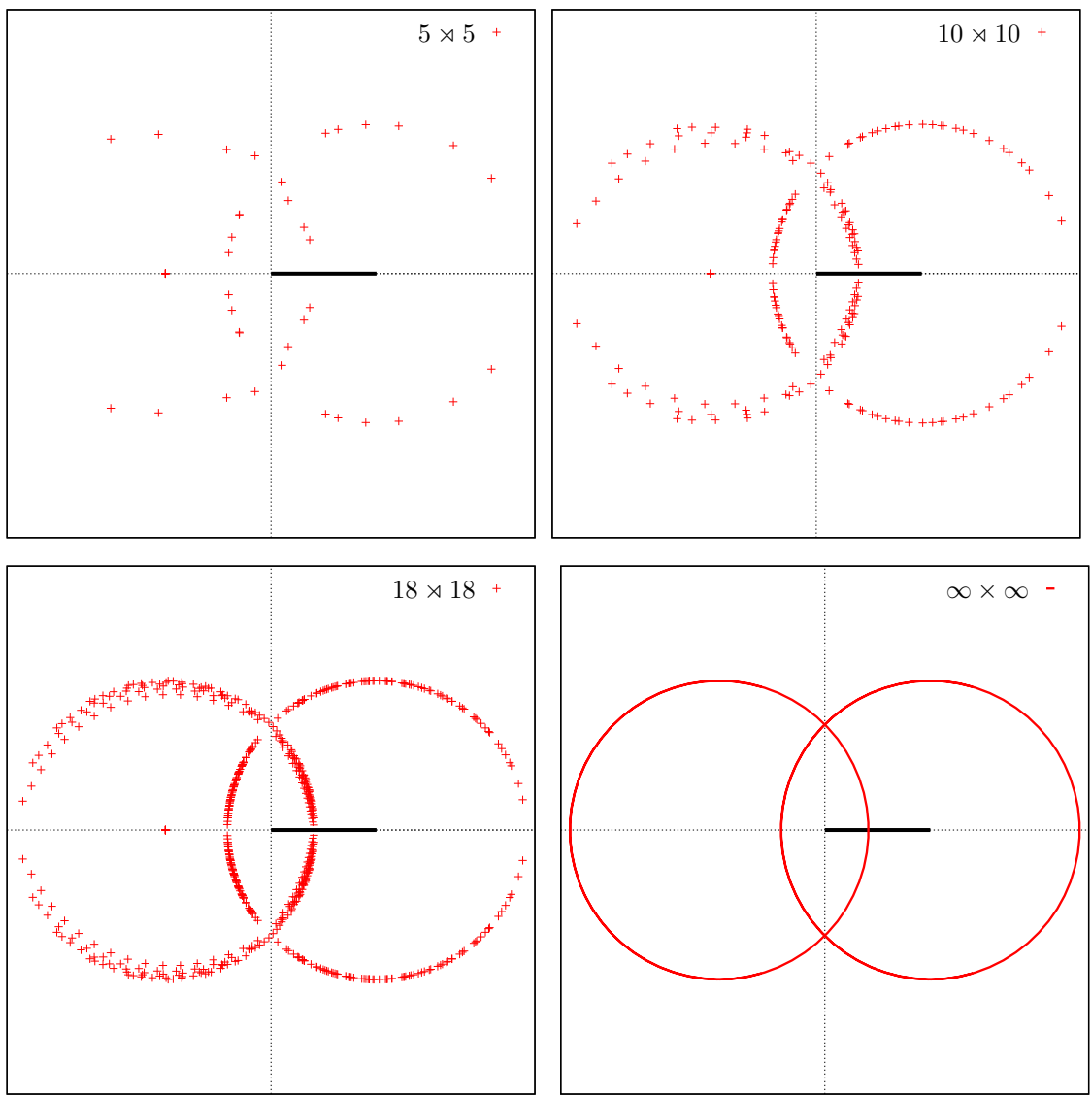


Figure 3.3: Zeros of Z in x for the $N_x \times N_x$ Ising model with self-dual boundary conditions. The degree of Z in sub-figure: (a) is 50; (b) is 200; (c) is 648.

If we view Figures 3.3(a)-(d) as a sequence of figures. Then as the size of the lattice increase, notice the way the zeros start to form two circles like those in Figure 3.3(d).

For now we shall focus on the large arms in the 1st and 2nd quadrant, which are linear enough (as it were) to have ‘endpoints’. Note, for the 2d Ising model, the specific locus is known. However, when we come to study other models, we will not know it in general, or if one even exists.

Notice as the lattice size increases, the endpoints of each arm get closer to \mathfrak{F} . In light of our analysis in Section 2.3, we interpret this behaviour as an indication of a critical point — a thermodynamic limit singular point in the behaviour of the specific heat.

Evidence of ‘Phase transitions’ in the 3d Ising model

A strict real-beta singular point can occur only in the thermodynamic limit. Our models however, are finite-sized. Nonetheless, suppose we view Figure 3.1 in a similar manner to the 2d model.

That is, if we look at the figures as a sequence of figures, we see that as the size of the lattice increases the zeros start to form some sort of structure analogous to the 2d case. Notice, the two large arms in the 1st and 2nd quadrant pinch the real axis. (Note, we shall look at the point they pinch in further detail later in the chapter). Also, the zeros for the $6 \times 4 \times 10'$ lattice show the same 8 fold symmetries are also present.

Recall Section 2.3.1, our signal for a phase transition is a singular point in the specific heat curve. The specific heat curves plots in this chapter are $C_V/k_B\beta^2$ against $\exp(\beta)$ unless stated otherwise. We accompany the plots with an overlay of corresponding zero distributions close to \mathfrak{F} . Recall that Equation (2.3.9) gives a direct relationship between these plots.

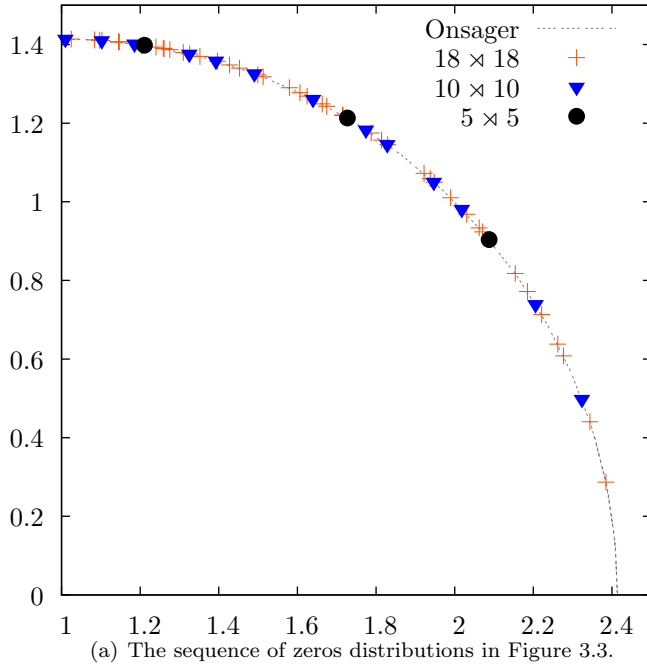


Figure 3.4(a) shows a blow up of the 1st quadrant. Here we overlay the sub-figures of Figure 3.3. The thermodynamic limit solution case is indicated by the thin grey line. The specific heat curves of these models are plotted in 3.4(b) and we have marked the critical point e^{β_c} .

[3.2] For Figure 3.4(b), we compute the part of C_V coming from the high and low temperature ends of the polynomial Z (and the limit Z), to show how they are the same or nearly the same.

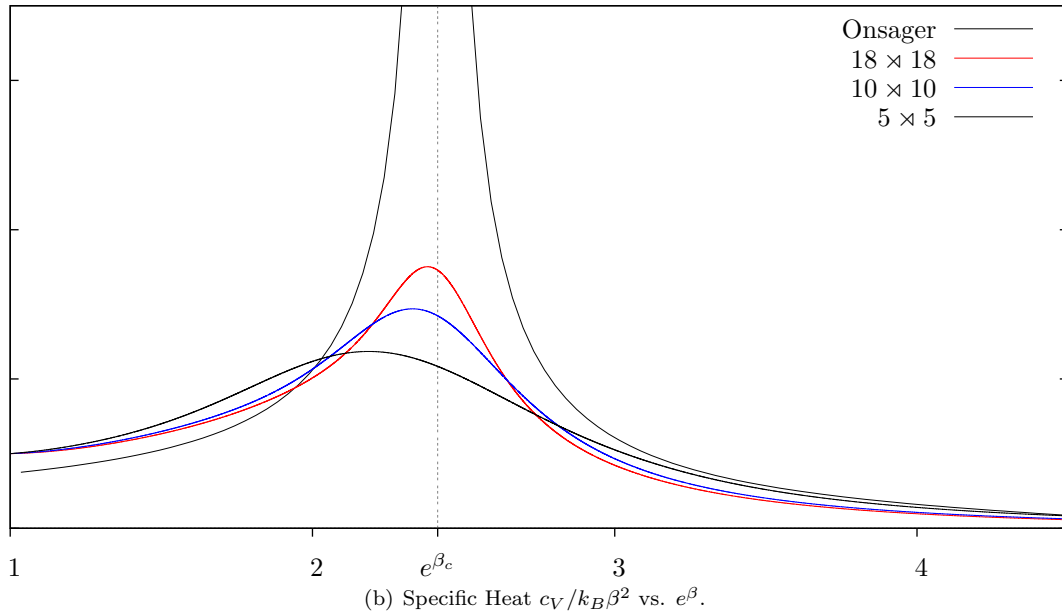


Figure 3.4: With reference to Figure 3.3: (a) overlays the zeros distributions close to \mathfrak{F} in the first quadrant; (b) overlays the corresponding specific heat curves.

A blowup of the zeros of Figure 3.1 in the first quadrant pinching \mathfrak{F} is shown in Figure 3.5(a). For comparison, we also indicate an estimate critical temperature given by $\beta = 0.2216544$ with a claimed standard deviation of 3×10^{-7} , (Talapov and Blöte (1996) [92], using a Monte–Carlo simulation) for the 3d Ising model, as

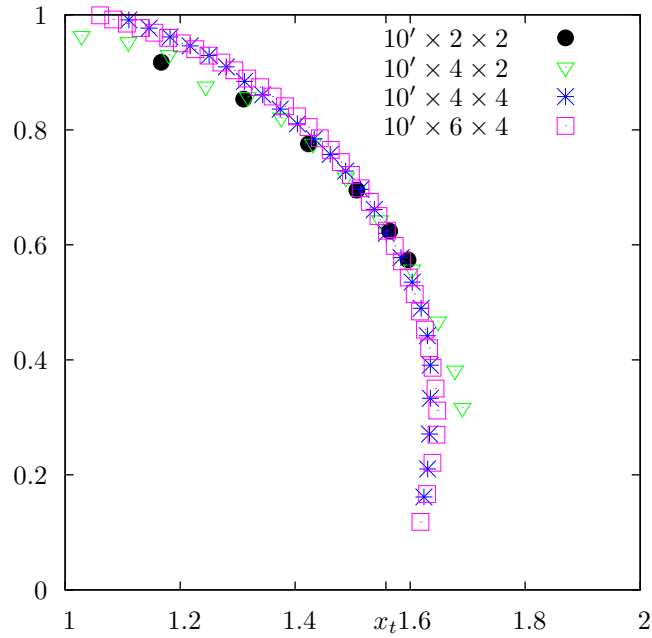
$$e^{2\beta} \approx 1.558 =: x_t. \tag{3.1.3}$$

Note, Talapov and Blöte give β in the Ising model variable. In Equation (3.1.3), we convert this to our Potts model variable, hence $e^{2\beta}$.

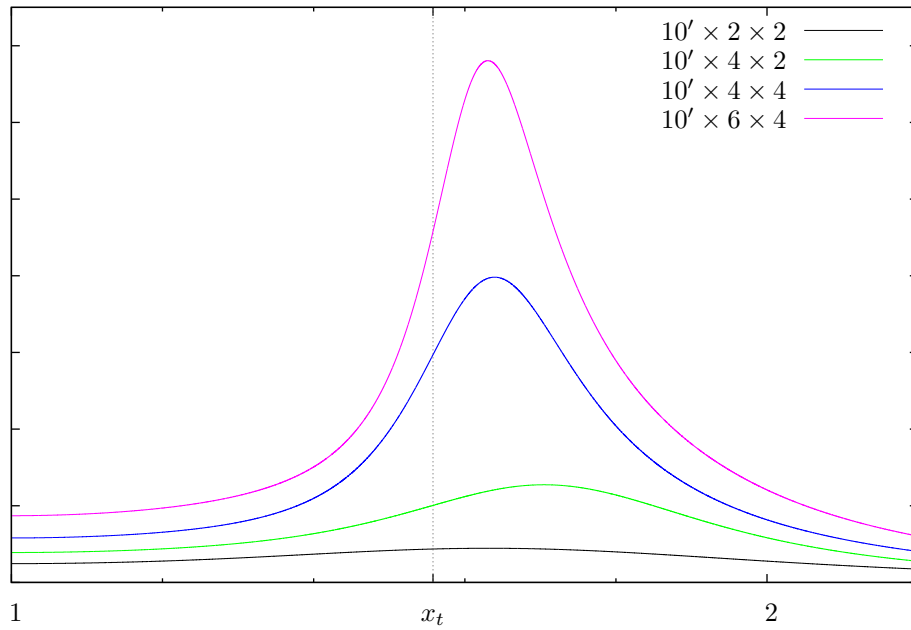
The respective specific heat curves for Figure 3.1 are plotted in Figure 3.5(b). In all further, specific heat plots related to the 3d Ising model, we shall use a dashed vertical line to indicate x_t .

Notice the ‘divergence’ in the specific heat close to the x_t .

[3.3] Comparing the 2d and 3d sequences, we claim that these results are evidence not only that the 3d Ising model is capable of modelling a phase transition, but also that the relevant part of the complex analytic structure of Z is linear, as in the 2d case (cf. the clock model in [64] Figure 11.9 for example).



(a) An overlay in the positive quadrant of the zero distributions in Figure 3.1.



(b) The corresponding specific heat curves.

Figure 3.5: With reference to Figure 3.1: (a) overlays the zeros distributions close to \mathfrak{F} in the first quadrant; (b) overlays the corresponding specific heat curves.

3.2 Validating our interpretation of results

In this thesis, the zeros of the Potts model partition function for finite-sized 2d and 3d lattices are studied. Are our finite-size partition function results credible approximations to thermodynamic limit systems?

Suppose the partition function Z for some toy model on a lattice with N spins is [64, §11.1]

$$Z = x^{2N} + 1. \quad (3.2.1)$$

The free energy density f is written in the form

$$\begin{aligned} f &= N^{-1} \ln(Z) \\ &= N^{-1} \ln(x^{2N} + 1) \\ &= N^{-1} \ln(x^N(x^N + x^{-N})). \end{aligned} \quad (3.2.2)$$

As $x = \exp(\beta)$,

$$\begin{aligned} f &= \frac{1}{N} (\ln(e^{\beta N}) + \ln(e^{\beta N} + e^{-\beta N})) \\ &= \beta + \frac{1}{N} \ln(2 \cosh(\beta N)) \\ &= \beta + \frac{1}{N} \ln(2) + \frac{1}{N} \ln(\cosh(\beta N)). \end{aligned} \quad (3.2.3)$$

The internal energy is

$$\begin{aligned} U &= -\frac{\partial N^{-1} \ln(Z)}{\partial \beta} \\ &= -\left(1 + \frac{1}{N} \frac{N \sinh(\beta N)}{\cosh(\beta N)}\right) \\ &= -1 - \tanh(\beta N) \end{aligned} \quad (3.2.4)$$

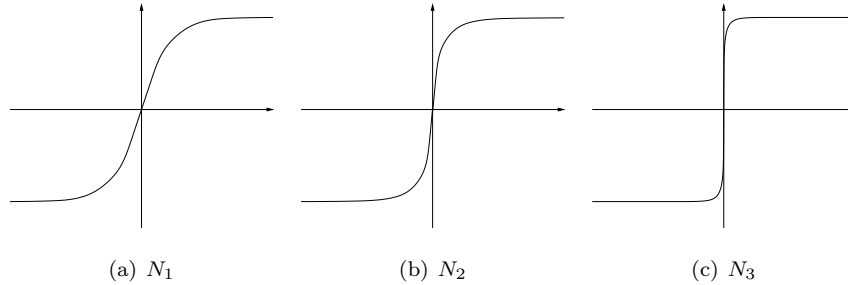


Figure 3.6: Graphs of $\tanh(\beta N_i)$, where $N_1 < N_2 < N_3$

Figure 3.6 shows the tanh graph for various N . Notice at $\beta = 0$, the change in U becomes more and more rapid as N increases. In the limit, U is discontinuous. So even our simple toy model shows signs of displaying a first order phase transition [4] (albeit at zero temperature). See Baxter (1982) [9] for an example of a phase transition (at zero temperature) for the 1d Ising model.

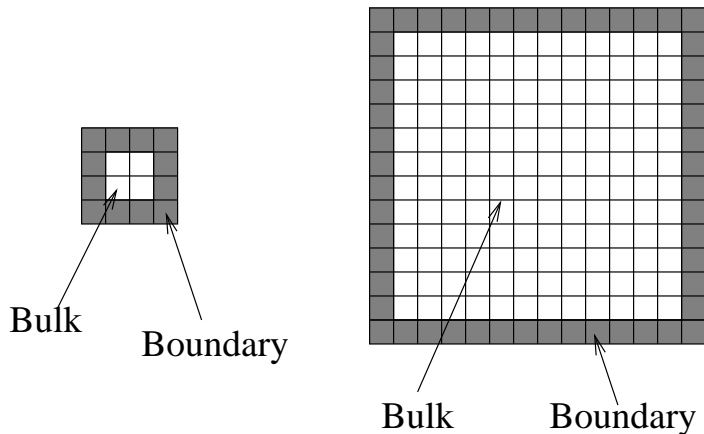


Figure 3.7: A 5×5 , and a 15×15 lattice. The grey shaded area in each figure highlights the number of spins on the boundary and their nearest neighbour interactions. The larger the lattice the smaller the ratio of spins on the boundary to spins in the bulk. In these figures, the ratio is $16 : 9$ spins and $56 : 169$ respectively.

For a thermodynamic system we consider the following finite-size properties [64]:

- (1) **size** - the bulk observables of a physical system are independent of the systems size. For example, consider temperature at which an ice cube and an ice berg melts. Here we find that both will melt at the same temperature. That is, the thermodynamic properties of the system are independent to the size of the system.
- (2) **boundary** - the number of particles close to the boundary of the system are negligible compared to those in the bulk of the system (cf. Figure 3.7). For example, consider an ice cube melting. At certain (non-critical) temperatures, the surface of the ice cube may be a mixture of liquid and ice, but the bulk of the cube may still frozen. However, at the critical temperature, the bulk of the ice cube will also start to melt.

The results in Figure 3.1 and 3.3 are a *sequence* of lattice sizes tending to the thermodynamic *limit*. We now recall (cf. [22]) the formal definition “limit of a sequence”.

Definition 3.2.1 (Limit of a sequence). *Let a_n be an infinite sequence of real numbers (where $n = 0, 1, 2, \dots$). We say a real number A is the limit of a_n as n goes to infinity if, for every real positive number ϵ , there exists an integer δ (which depends on ϵ) such that for all $n > \delta$, $|a_n - A| < \epsilon$.*

The sequence of graphs in Figure 3.6 contains many examples of Definition 3.2.1, that is, a limit for each β value. Suppose each β has a limit, then the plot of all the limits against β is another graph, say the “limit” graph.

Let a_n be the gradient of $\tanh(n\beta)$ at a given β . For example, at $\beta = 0.01$ we have $A = 0$. The *limit* graph in this case is a step function, which has zero gradient everywhere except at $\beta = 0$. This notion of limit graph then generalises the definition (which, as it is, is just for number sequences).

Note, the 1d Potts model and the toy model described above, the sequence has a “natural” order. In 2d and 3d, a natural order is not as clear. Ideally, we would to keep to globally square and cubic lattices dimensions for 2d and 3d respectfully, however this is not always computationally possible.

In Sections 3.2.1 and 3.2.2 we check if: (a) the arms approaching \mathfrak{F} also tend to some sequence; (b) our results are dependent on any boundary or size effects.

3.2.1 Checking dependence on boundary conditions

What is evidence of limit behaviour that can be interpreted from determining the limits of our zeros distribution? We check boundary dependence, by applying various boundary conditions to a fixed size lattice. First we shall investigate the “behaviour” of the zeros distribution for the 2d Ising model under various boundary conditions. Then we carry out parallel checks on the 3d Ising model.

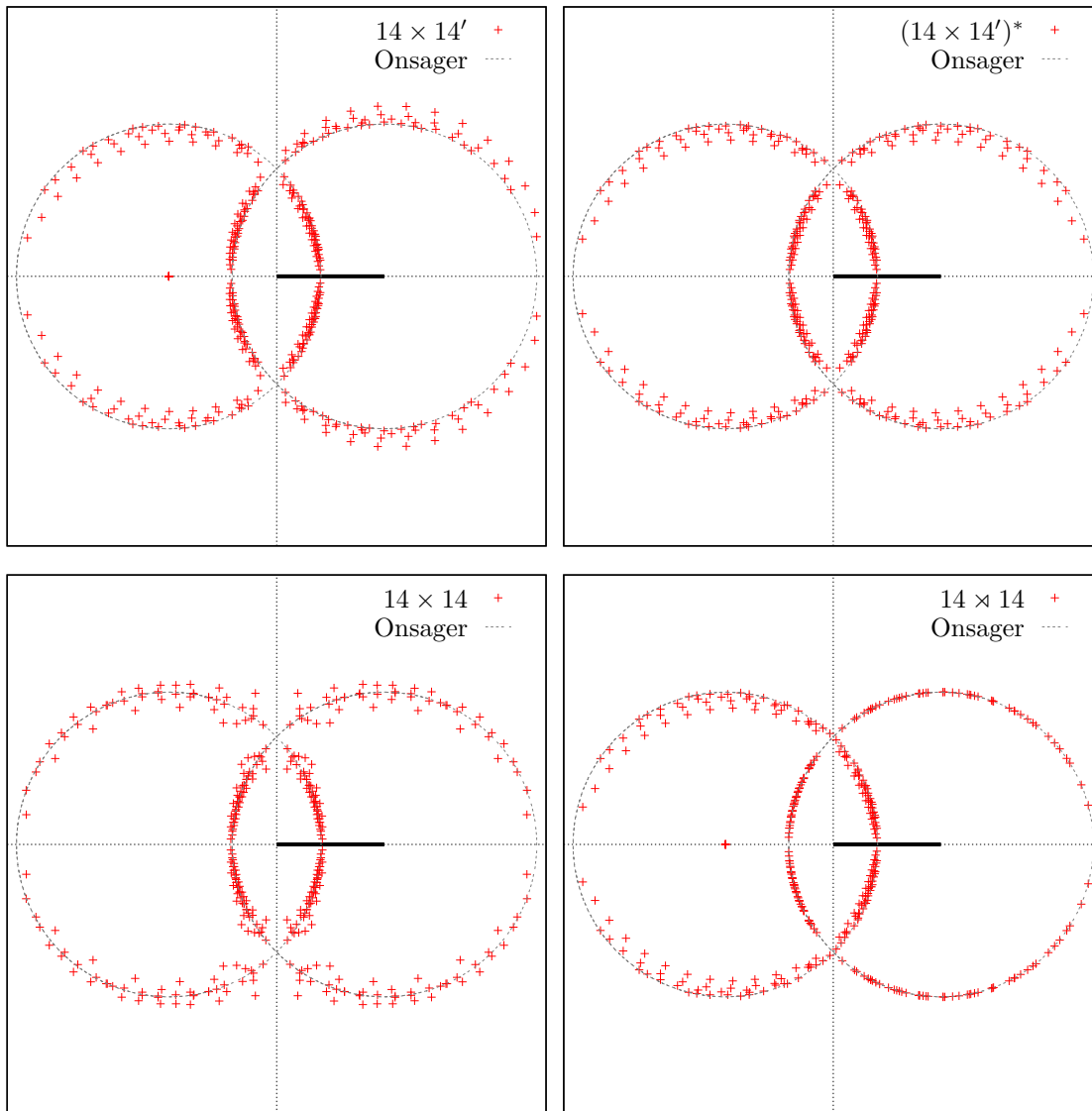


Figure 3.8: Zeros of the partition function Z in x for the 14×14 Ising model with various boundary conditions. The degree of Z in sub-figure: (a) is 378; (b) is 378; (c) is 392; (d) is 392.

Figure 3.8 shows the zero distributions for a model on a 14×14 lattice with various boundary conditions. It is useful to overlay each distribution with Onsager's solution (grey circles). The variation of the position of the zeros in each figure suggests that this model is susceptible to interactions of spins on the boundary.

For a 2d finite-sized model (such as in Figure 3.8), we see that by applying dual boundary

conditions, the zeros (in the positive region) comply better with the thermodynamic limit solution. See Figure 3.8(d) or Chen et al (1996) [19] for example. We can apply such boundary condition because the 2d Ising model is self-dual [50]. The 3d Ising model is not self-dual³, so how else may we interpret the role of boundary conditions in our results?

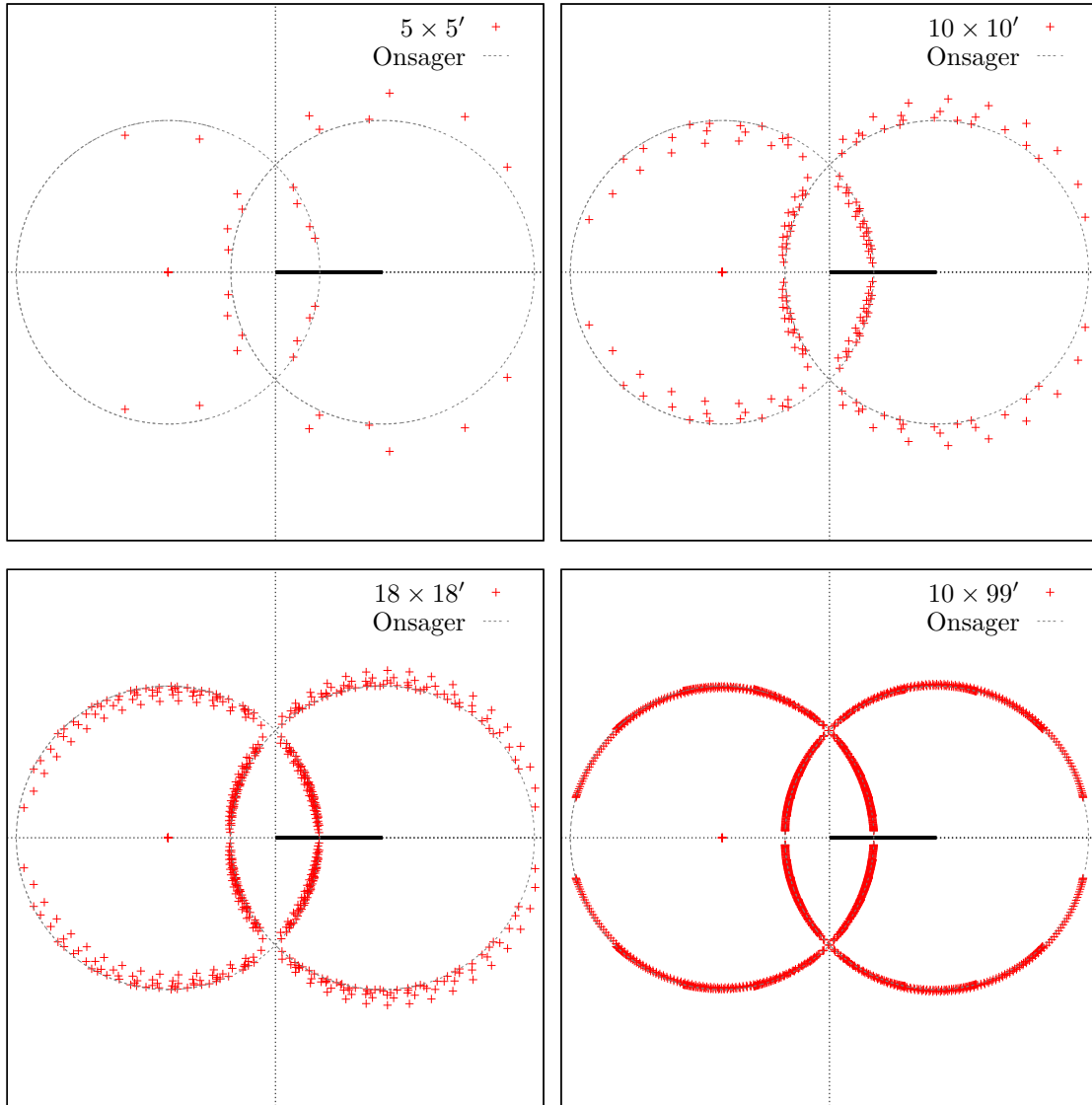


Figure 3.9: Zeros of Z in x for the $N_x \times N'_y$ Ising model with fixed open/periodic boundary conditions. The degree of Z in sub-figure: (a) is 45; (b) is 190; (c) is 630; (d) is 1970. (What effect do boundary conditions have on zero distributions?)

The zeros of the 2d Ising models in Figure 3.9, have boundary conditions that are similar to the ones we have in the 3d Potts model case. ie. a combination of open and periodic boundary conditions. Notice as the lattice size increases the position of zeros comply better to the thermodynamic limit case (also see Figure 3.25). Also note that the endpoints of the $18 \times 18'$ Ising model lie closer to \mathfrak{F} than in the case of the $10 \times 99'$ Ising model.

Recall that the $10 \times 99'$ zeros are a model (in the sense of Section 2.3.2) of the analytic structure

³It is dual to the Ising gauge model, see Savit (1980) [86]

of the largest eigenvalue of the 10-site wide lattice transfer matrix. Whereas the $18 \times 18'$ zeros (while they might be not as good model of the 18 site wide transfer matrix, and is a smaller lattice in terms of number of sites) are a better model of a large square lattice.

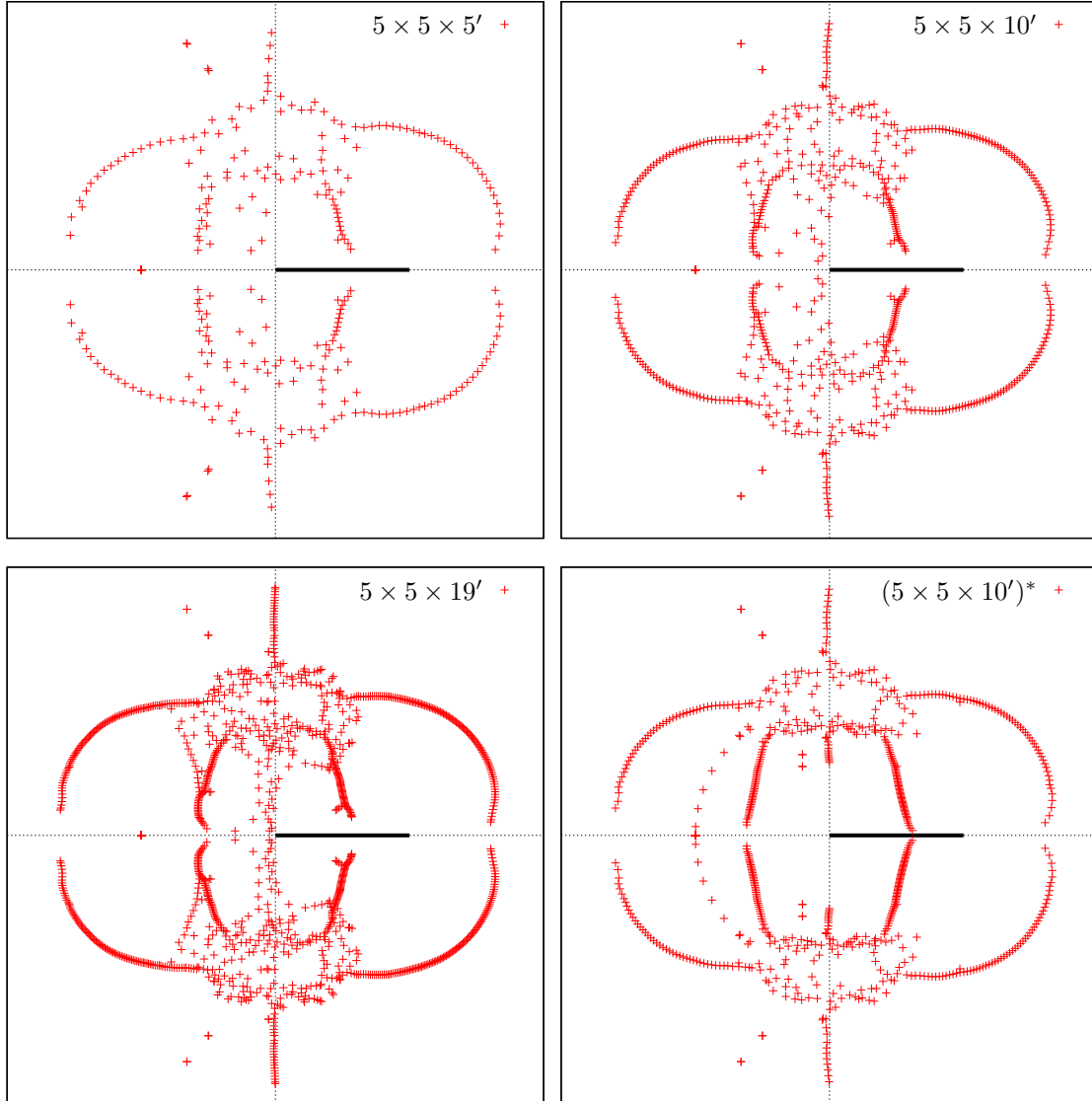


Figure 3.10: Zeros of Z in x for the $5 \times 5 \times N'_z$ Ising model. The degree of Z in sub-figure: (a) is 350; (b) is 725; (c) is 1400 (d) is 725.

Consider the zeros of the 3d Ising model on a $5 \times 5 \times 5'$ lattice (Figure 3.10(a)). In the first quadrant the inversion symmetry in the unit circle is “broken” by what seems to be a zero trailing off the line of zeros approaching the anti-ferromagnetic region. The zeros of the $5 \times 5 \times 10'$ and $5 \times 5 \times 19'$ confirm this, and might even seem to indicate that they are approaching the region at two separate points. However, in comparison, the $6 \times 4 \times 10'$ lattice (Figure 3.1(d)) does not show this effect. So which one is the correct approximation?

[3.4] First, we compare the *ground-state* configurations of the $5 \times 5 \times 10'$ and $6 \times 4 \times 10'$ model at high β (low temperature). That is, a configuration when the Hamiltonian value is a maximum (ie. when all the spins are aligned). For the $5 \times 5 \times 10'$ case it is $2x^{725}$ and for $6 \times 4 \times 10'$ case it

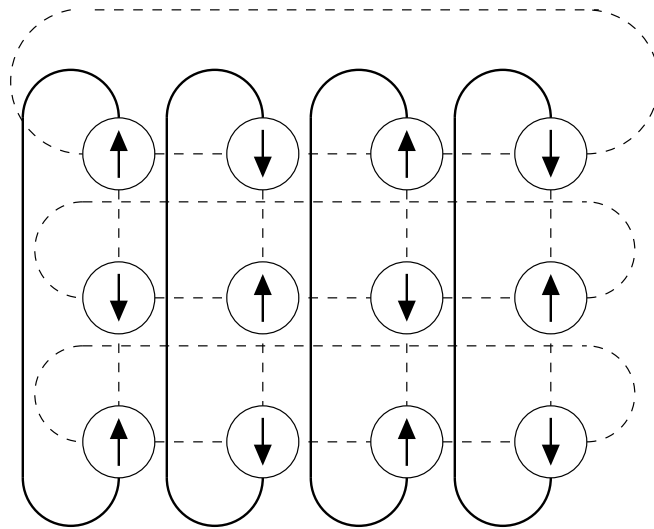


Figure 3.11: A configuration of the Ising model on a 3×4 lattice.

is $2x^{696}$.

At low β (high temperature) the ground-state configuration is the configuration with a minimum Hamiltonian value. The term for the $6 \times 4 \times 10'$ at this ground-state configuration is $2x^0$. Here every spin is in a different state to its nearest neighbour. For the $5 \times 5 \times 10'$ the ground-state is $2470x^{100}$ (see Appendix E). This is because, whenever periodic boundary conditions are applied to a side with an odd number of spins, then it is not possible (for the $Q = 2$ -state model at least) for a configuration to have every spin in a different state to its nearest neighbour. For example, in Figure 3.11 we show a configuration for a $Q = \{\uparrow, \downarrow\}$ -state Potts model on a 3×4 lattice.

The next terms in each model, at high and low temperature are obtained by changing the state of a spin on the boundary. The partition function Z for the $6 \times 4 \times 10'$ model is

$$Z = 2x^{696} + 96x^{691} + \dots + 96x^5 + 2.$$

However, the partition function Z' for the $5 \times 5 \times 10'$ model is

$$Z' = 2x^{725} + 100^{720} + \dots + 126000x^{101} + 2470x^{100}.$$

Note that for Z , the coefficients and the change in energy is the same for a high and low temperature expansion (see Section 1.2.2). This is not the case for Z' , and hence, the inversion in the unit circle symmetry is broken.

Recall in Figure 3.8, by applying self-dual boundary conditions on 2d Ising model, the zeros comply better with the thermodynamic limit solution. The 3d Ising model is not however self-dual. So suppose we manipulate the partition function slightly. That is, we sum together corresponding coefficients of the ferromagnetic and anti-ferromagnetic models. This will then make the coefficients for the high/low temperature expansions the same. Figure 3.10(d) (labelled ' $(5 \times 5 \times 10')^*$ '), shows the distribution for such a manipulation.

Now the zeros are inverted in the unit circle, and we see the distribution has “cleaned up”. The caveat to this is that there is an extra line of zeros that lie on the unit circle in the 3rd and

4th quadrant.

To summarise, the impact of the spins on the boundary depends on the dimension of the lattice. Next, we look at a lattice where N_x is odd and N_y is even. In Figures 3.12 - 3.14 we compare periodic/open boundary conditions on various lattice sizes.

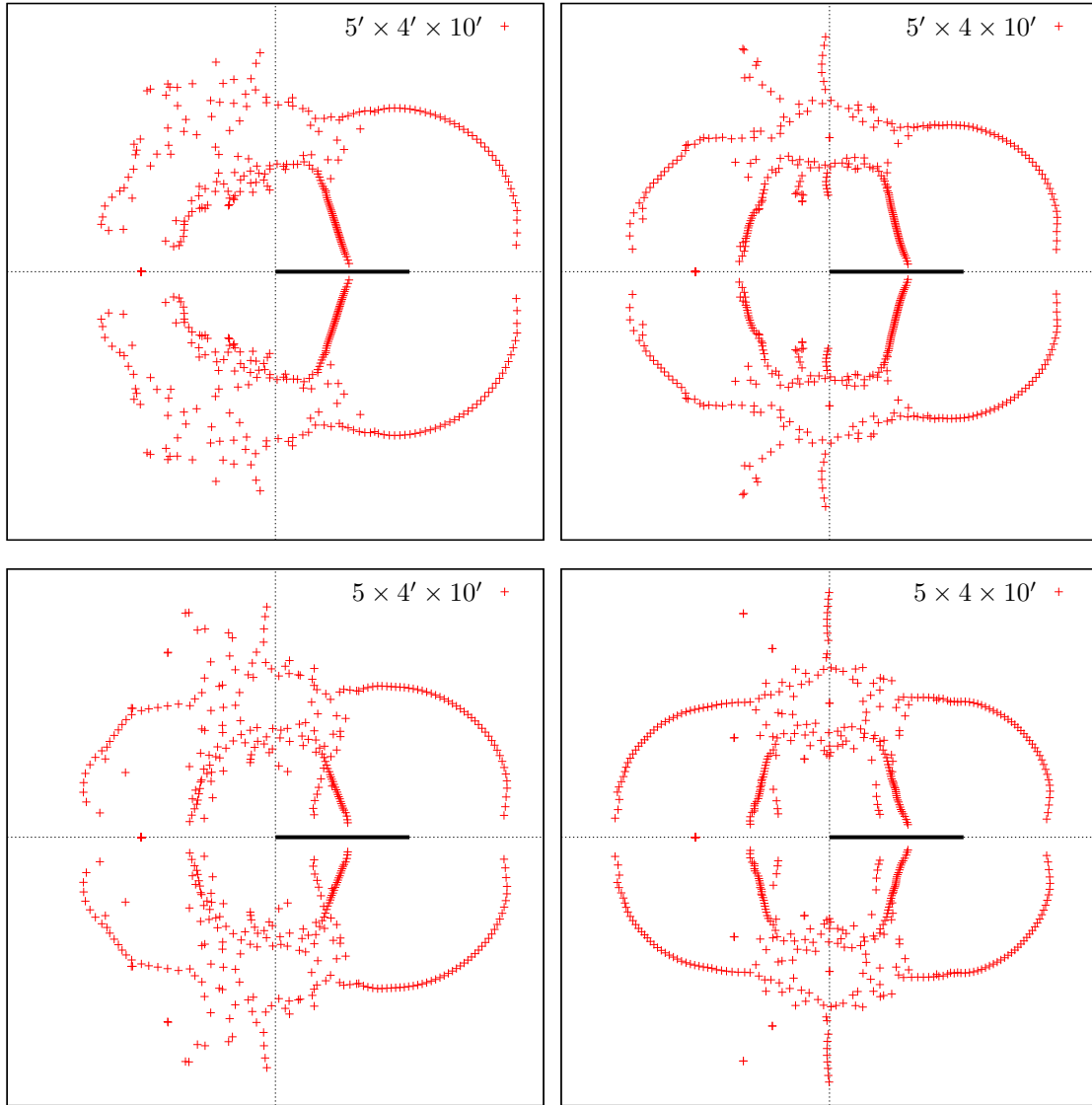


Figure 3.12: Control boundary conditions I. $N_x = \{5, 5'\}, N_y = \{4, 4'\}, N_z = 10'$. The degree of Z in sub-figure: (a) is 490; (b) is 530; (c) is 540 (d) is 580.

Figure 3.12, highlights the effect that boundary conditions have on our zero distribution. The arm of zeros approaching \mathfrak{F} for this lattice size do not seem to be considerably affected by changes in boundary conditions.

Notice the zeros approaching anti-ferromagnetic of $5 \times 4' \times 10'$. Here we can see the zeros approaching the region at two different points. Compare this to $5' \times 4' \times 10'$. and $5' \times 4 \times 10'$. We see that it is only a boundary effect.

Computationally, the lattice sizes represented here provide an excellent check when testing code for improvements on speed or memory usage. We are able to profile the programs full run-time for

this size. See Appendix C for further details.

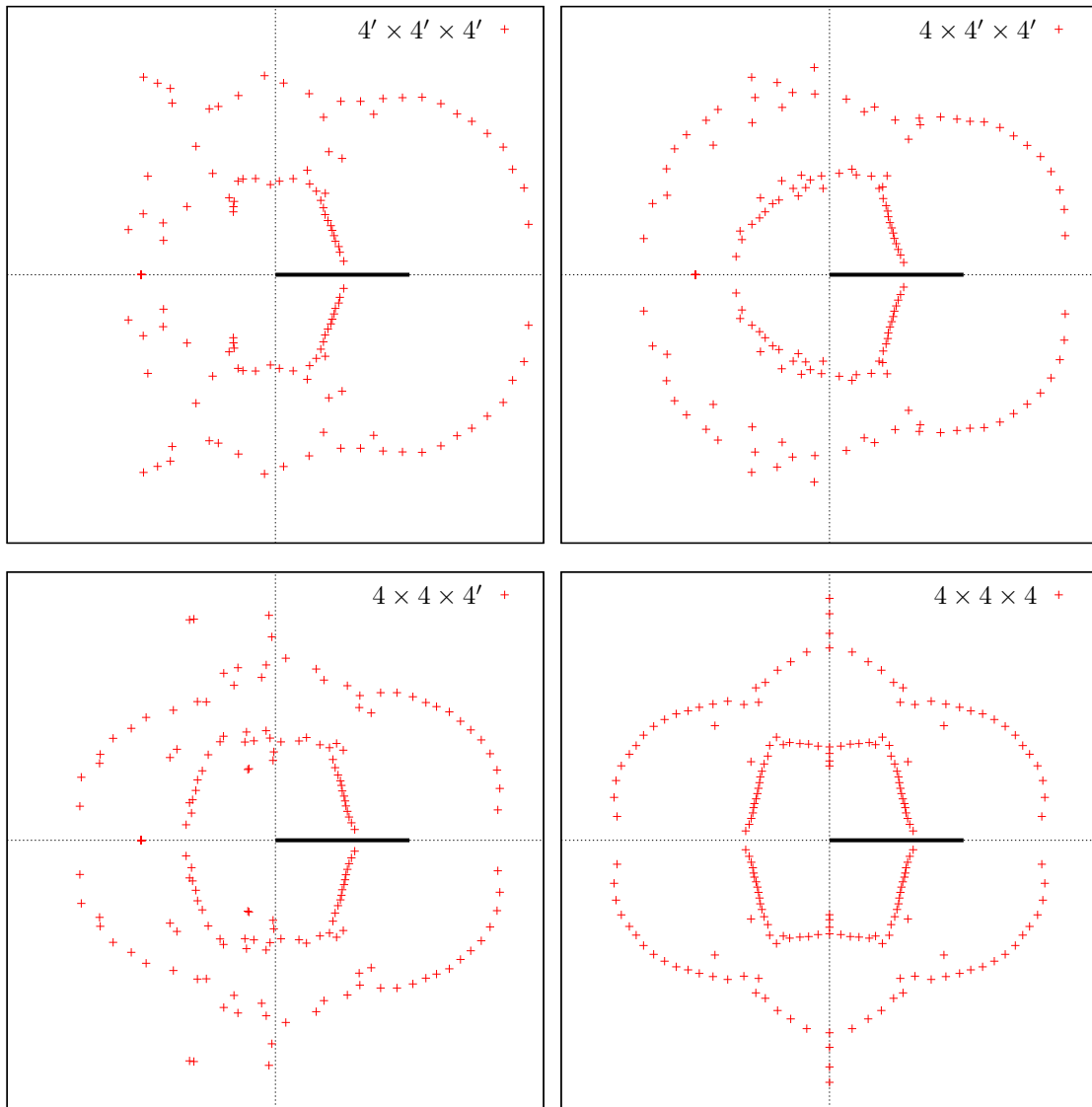


Figure 3.13: Control boundary conditions II. $N_x = N_y = N_z = \{4, 4'\}$. The degree of Z in sub-figure: (a) is 144; (b) is 160; (c) is 176 (d) is 192.

In Figure 3.13, we fix the lattice size to be the same in all directions, and vary between open and periodic boundary conditions. Note the $4 \times 4 \times 4$ (Figure 3.13(d)), was first calculated by Pearson [81] in 1982. Notice the perfect 8 fold symmetry present in this model.

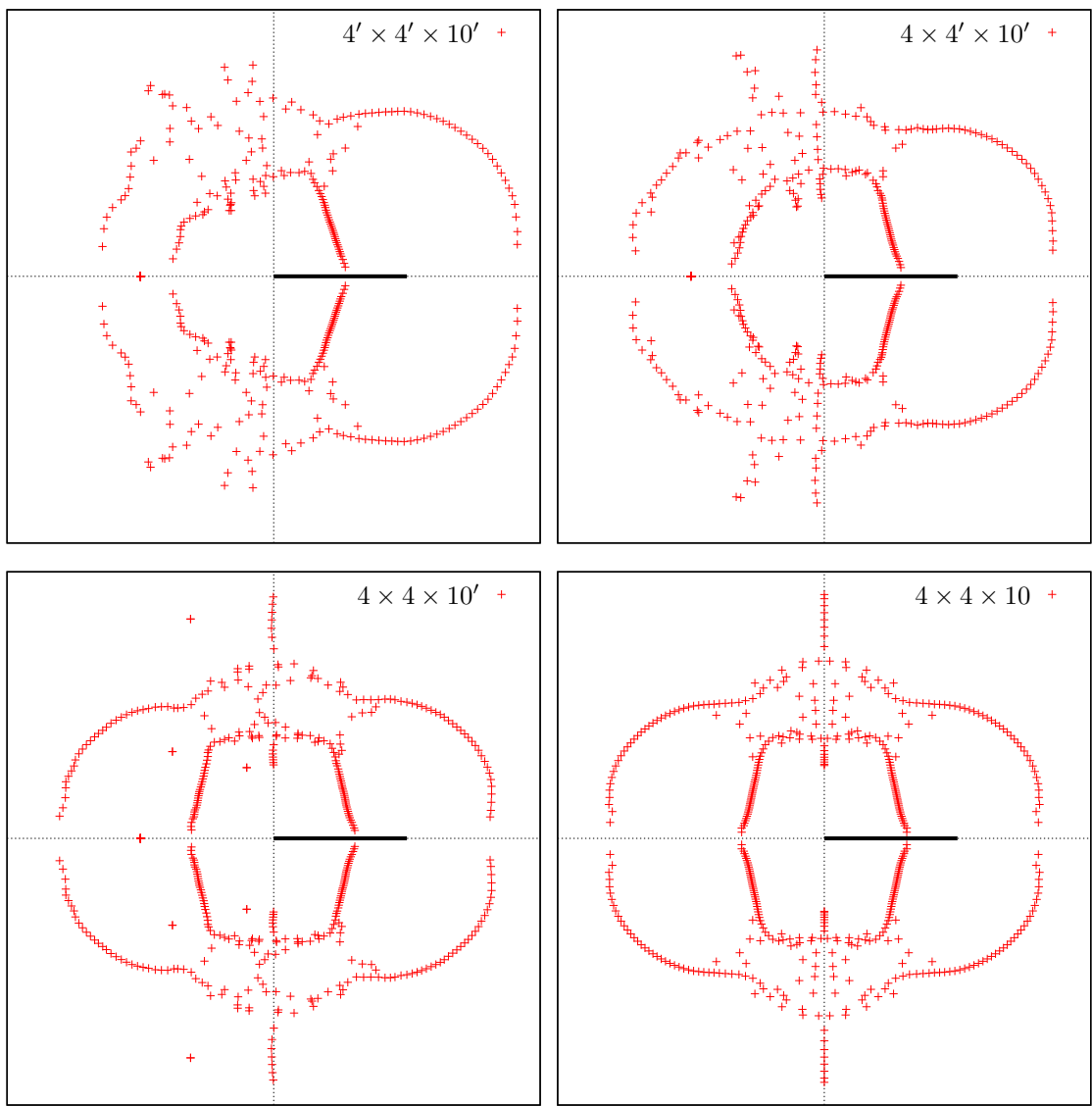


Figure 3.14: Control boundary conditions III. $N_x = N_y = \{4, 4'\}$, $N_z = \{10, 10'\}$. The degree of Z in sub-figure: (a) is 384; (b) is 424; (c) is 464 (d) is 480.

Due to computational restrictions, for large lattices we can only compute the long direction with open boundary conditions. For comparison, we test the $4 \times 4 \times 10$ lattice, to see what the effect may be. Here we see there is not much difference between the $4 \times 4 \times 10'$ and the $4 \times 4 \times 10$.

3.2.2 Checking dependence on size

Recall our simple model described in Section 3.2, $Z = x^{2M} + 1$, where $x = \exp(\beta)$. Denote the j th zero of the partition function as $z_j = r \exp(i\theta_j)$. Note, the argument θ_j of z_j is known as the *phase*.

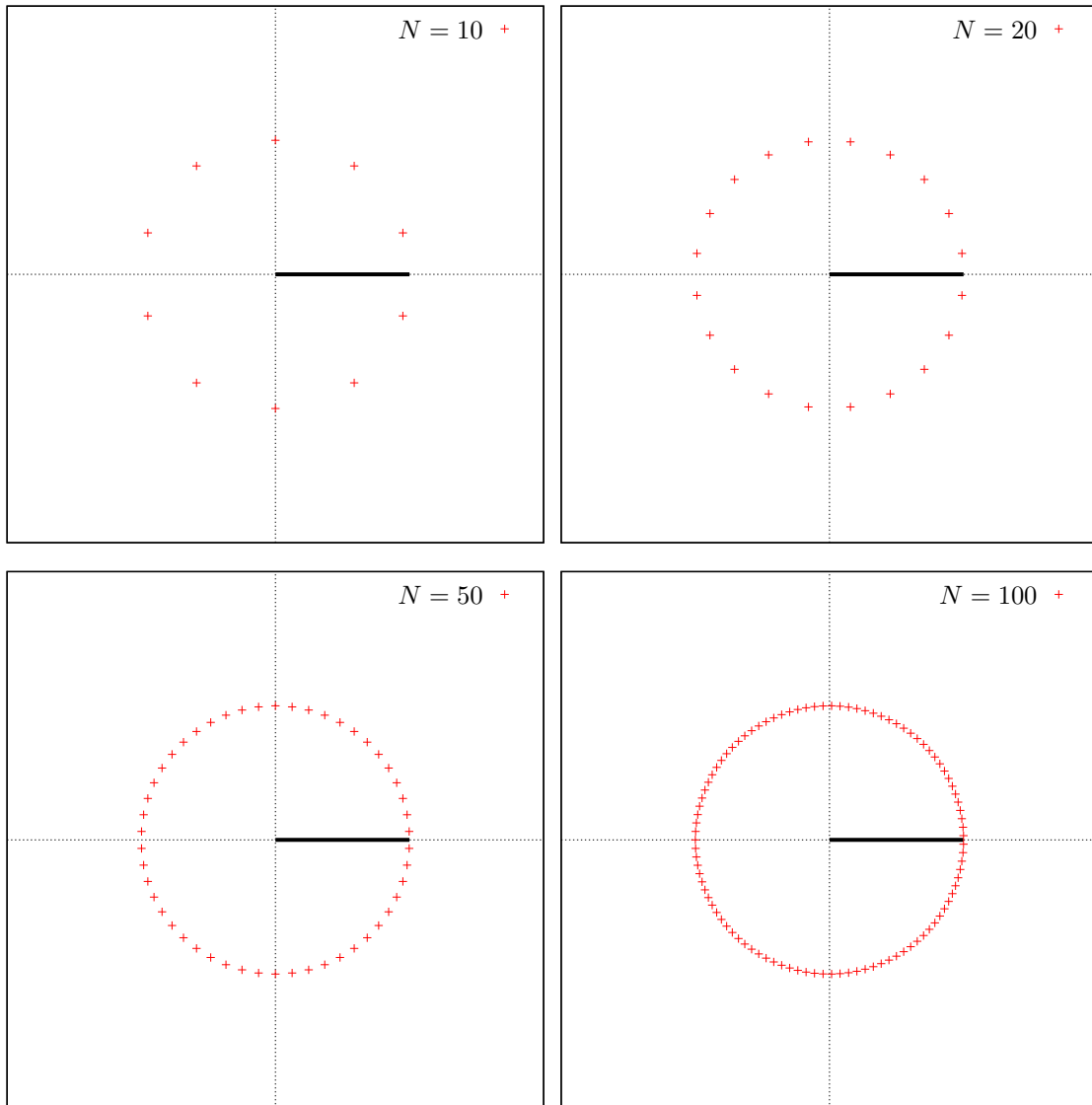


Figure 3.15: Showing the zeros of $Z = x^N + 1$, for various N

Notice as $N = 2M$ increase, the zero get closer to the real axis (ie. θ_j becomes smaller), see Figure 3.15. This simple model, shows that the zeros cut the real axis at $e^\beta = 1$. That is, only at zero temperature, does this model show a phase transition.

We now show the results for a series of controlled experiments, on various lattice sizes.

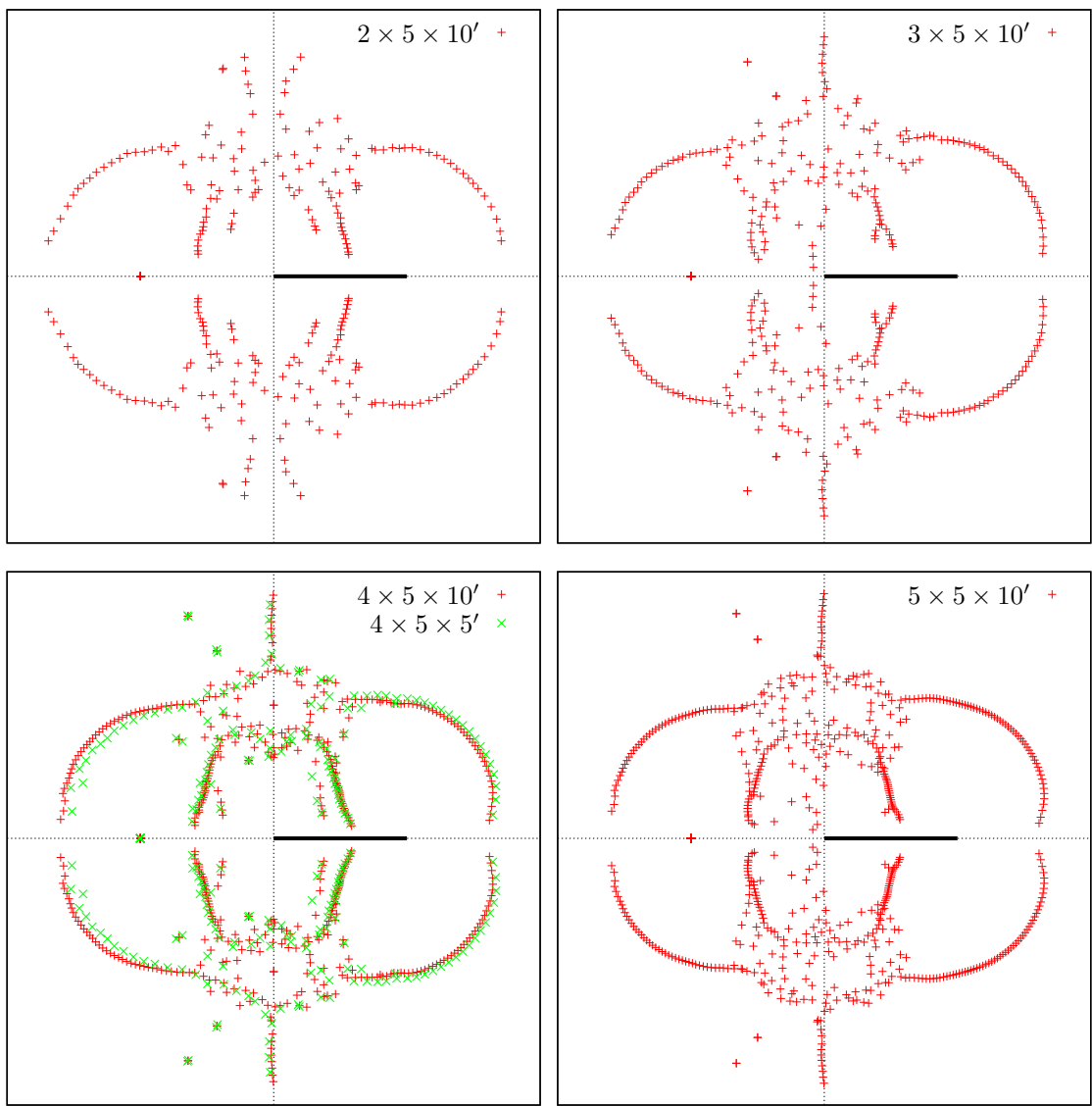


Figure 3.16: Control lattice size I. $N_x \times 5 \times 10'$: (a) $N_x = 2$; (b) $N_x = 3$; (c) $N_x = 4$; (d) $N_x = 5$. In sub-figure (c) we overlay a result from [10].

In 1990, Bhanot et al. [10] computed the $5 \times 4 \times 5'$. We overlay this result with the $5 \times 4 \times 10'$ in Figure 3.16(c), as check to show that our computation is correct.

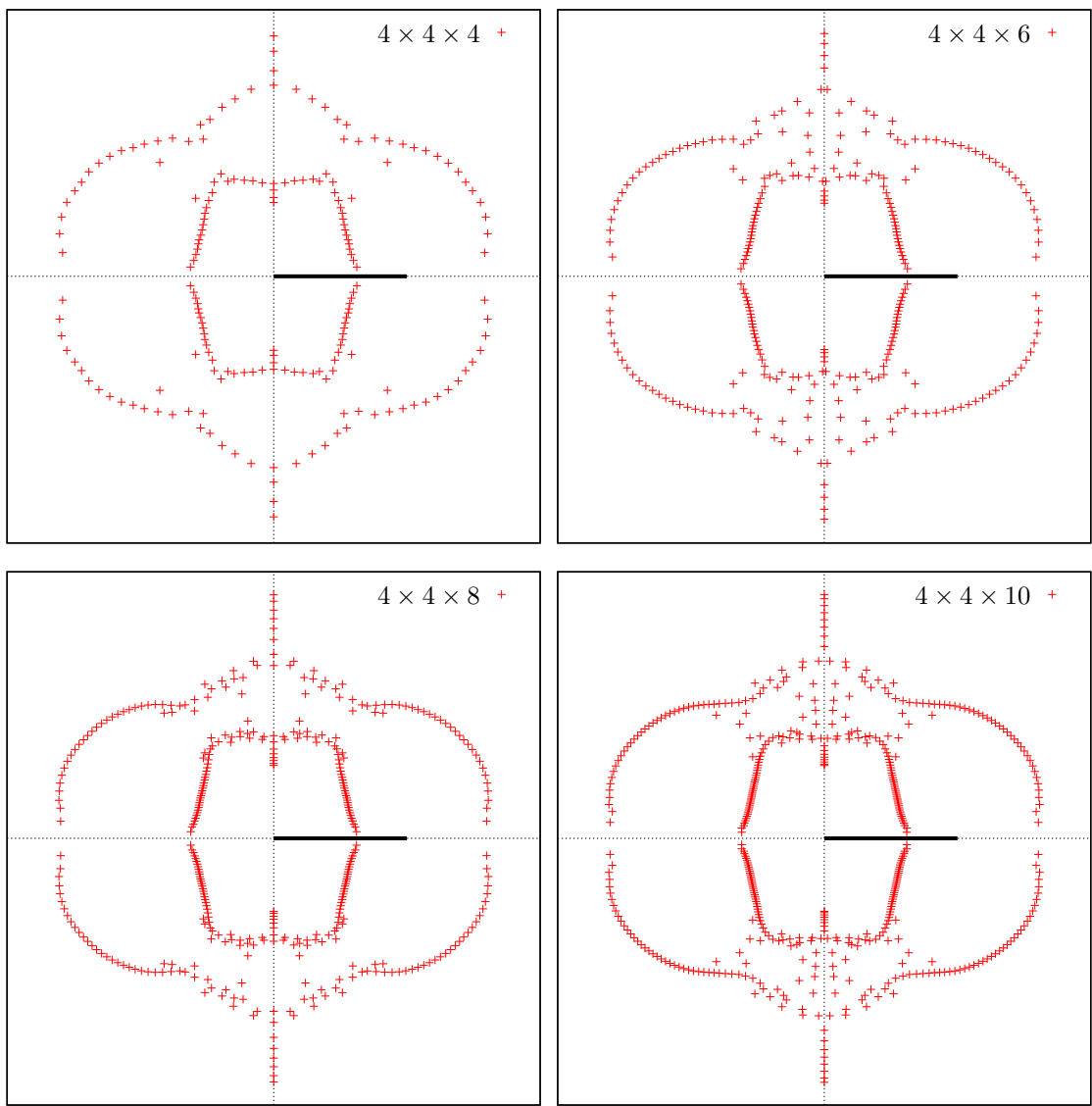


Figure 3.17: Control lattice size II. $4 \times 4 \times N_z$: (a) $N_z = 4$; (b) $N_z = 6$; (c) $N_z = 8$; (d) $N_z = 10$.

In Figure 3.17(d), notice the zeros on the large arm all seem to lie on some curve, except the zero closest to \mathfrak{F} . We investigate this further in the next section.

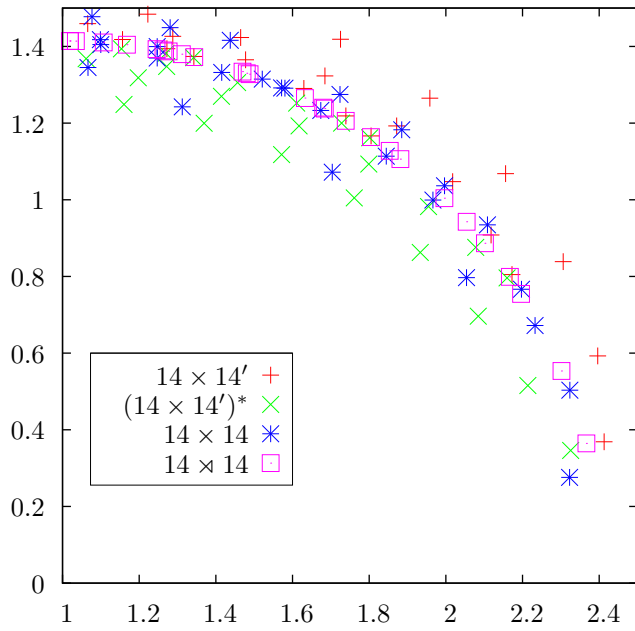
3.3 Further analysis: Specific heat

Recall Section 1.1.3, the specific heat C_V can be calculated from the partition function

$$C_V/k_B\beta^2 = -\frac{\partial^2 \ln(Z)}{\partial \beta^2}.$$

Also recall Section 2.3.1. We relate the zeros of the partition function to the specific heat. In the following figures we show a blow up of the zeros in the 1st quadrant near \mathfrak{F} , along with their corresponding specific heat curves.

Figure 3.18(a), we overlay the zero distributions of the 2d Ising model from Figure 3.8. We have focused on the zeros close to \mathfrak{F} , and plotted the corresponding specific heat curves.

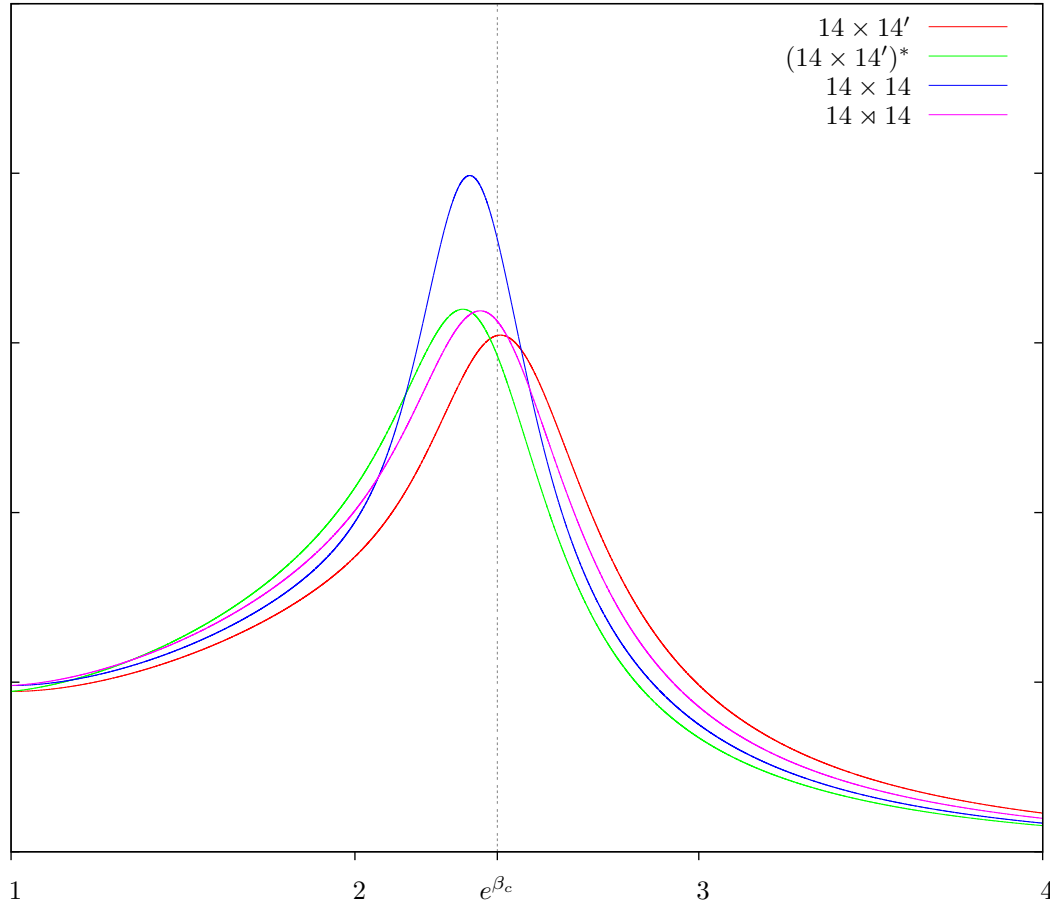


(a) An overlay of the zeros distributions, for the 14×14 lattice, under various boundary conditions.

Notice the position of the peak along the real axis is the position of the zero closest to \mathfrak{F} . Also the height of the peak corresponds to the distance between the zero closest to \mathfrak{F} and \mathfrak{F} .

Care has to be taken, as we see the peak of the $14 \times 14'$ is closer to e^{β_c} than the 14×14 model. The close up (Figure 3.18(a)), shows the position of the peak is dominated by the position of the zero closest to \mathfrak{F} .

Next we look at the 3d Ising models.



(b) A plot of the specific heat for the 2d Ising model on a 14×14 lattice

Figure 3.18: With reference to Figure 3.8: (a) overlays the zeros distributions close to \mathfrak{F} in the first quadrant; (b) overlays the corresponding specific heat curves.

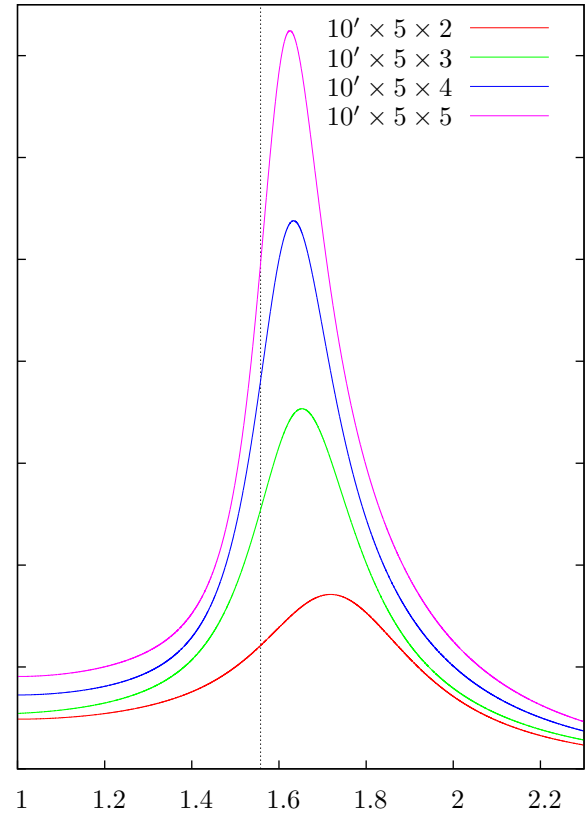
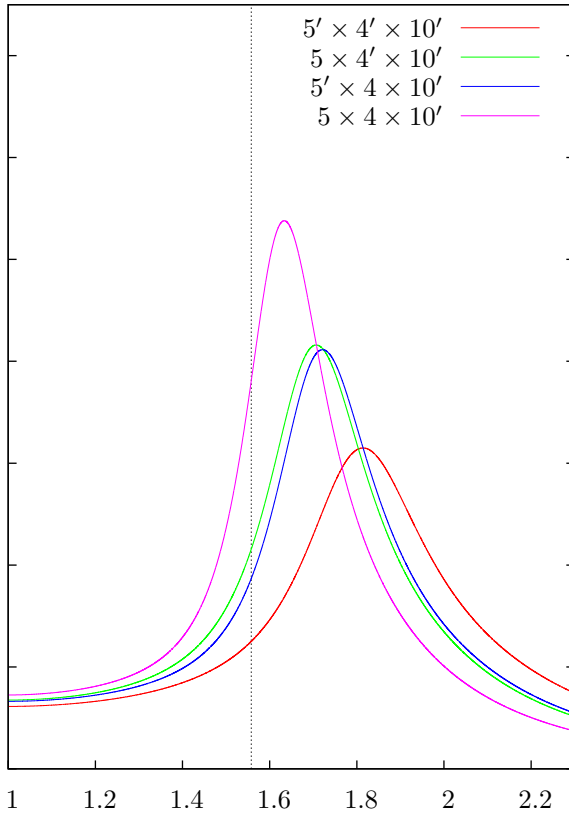
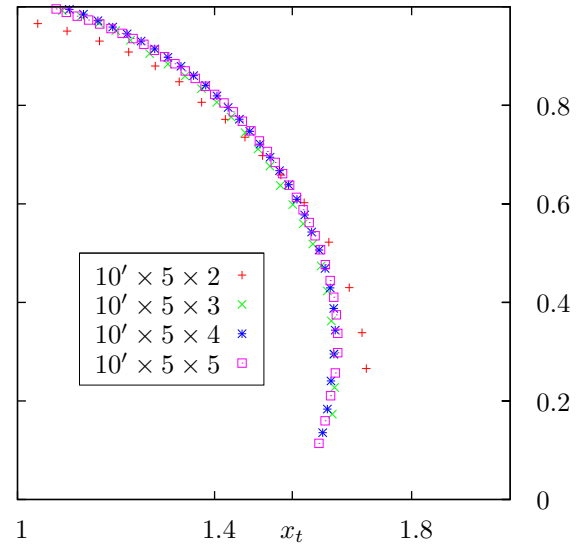
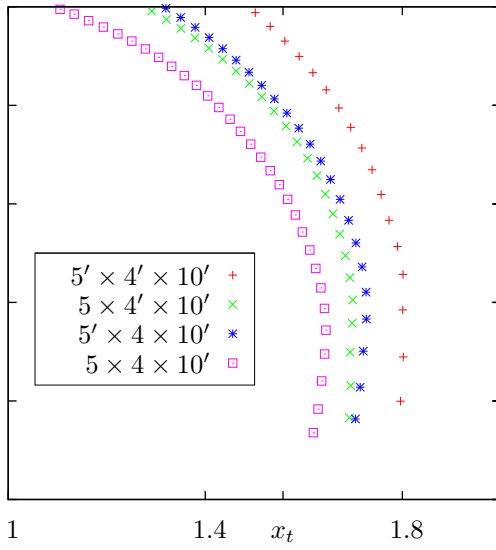


Figure 3.19: $N_x \times N_y \times 10'$:
 $N_x = \{5, 5'\}; N_y = \{4, 4'\}$

Figure 3.20: $10' \times 5 \times N_z$ for $N_z = \{2, 3, 4, 5\}$

Here we see that $5 \times 4' \times 10'$ and $5' \times 4 \times 10'$ zero distributions slightly vary, thus indicating a small dependence on boundary conditions at this lattice size. However there is still quite a significant difference in the $5' \times 4' \times 10'$ and $5 \times 4 \times 10'$ distributions.

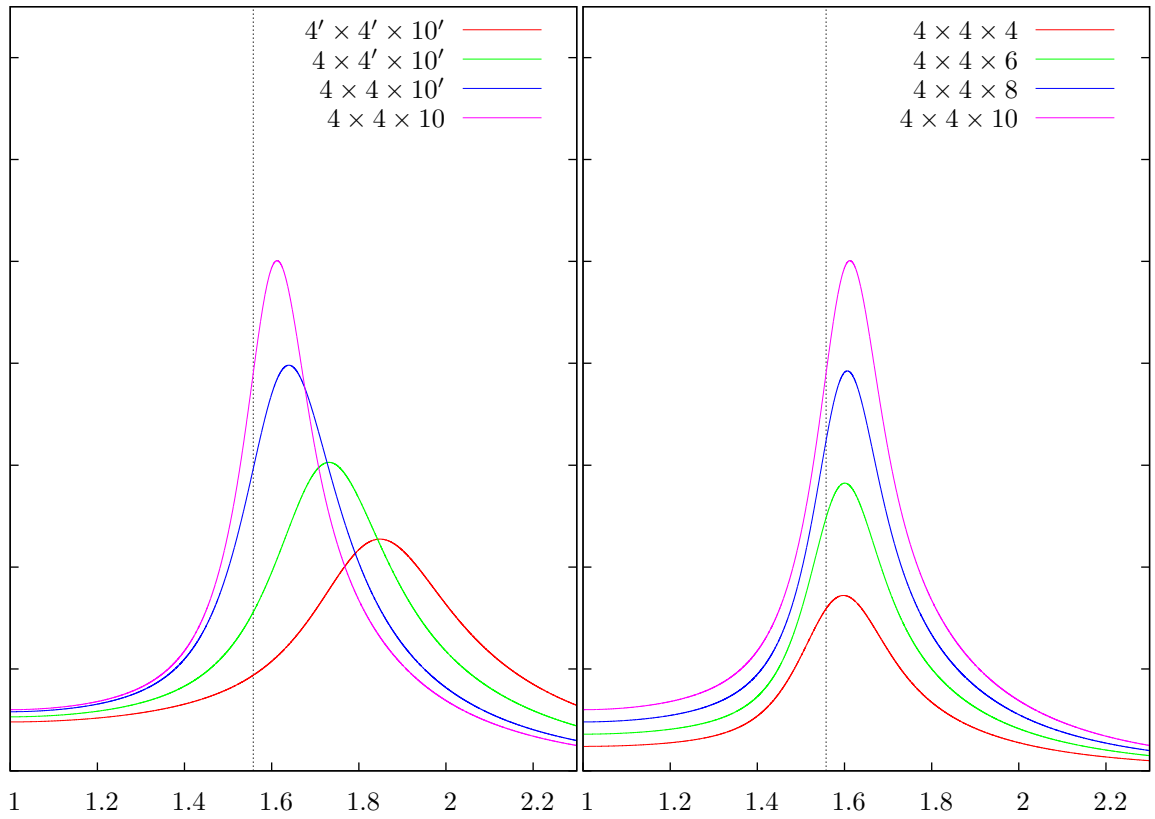
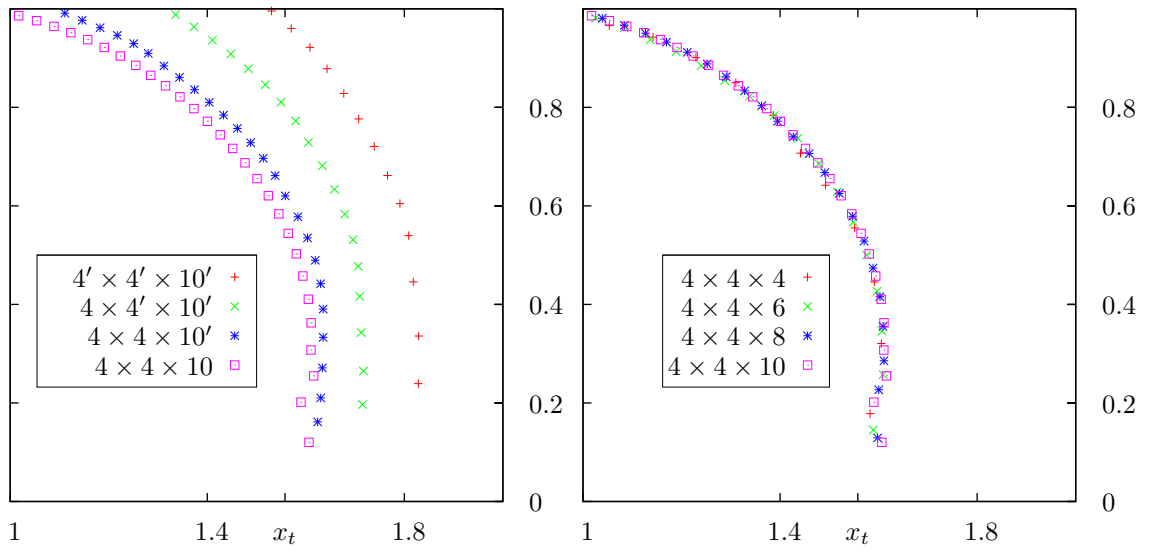


Figure 3.21: $N_x = N_y = \{4', 4\}$, $N_z = \{10', 10\}$

Figure 3.22: $4 \times 4 \times N_z$ for $N_z = \{4, 6, 8, 10\}$

The close up in Figure 3.21(a) shows that there is not much dependence on boundary conditions in the curve's position between $4 \times 4 \times 10'$ and $4 \times 4 \times 10$. However notice the unusual behaviour of the zeros in Figure 3.22.

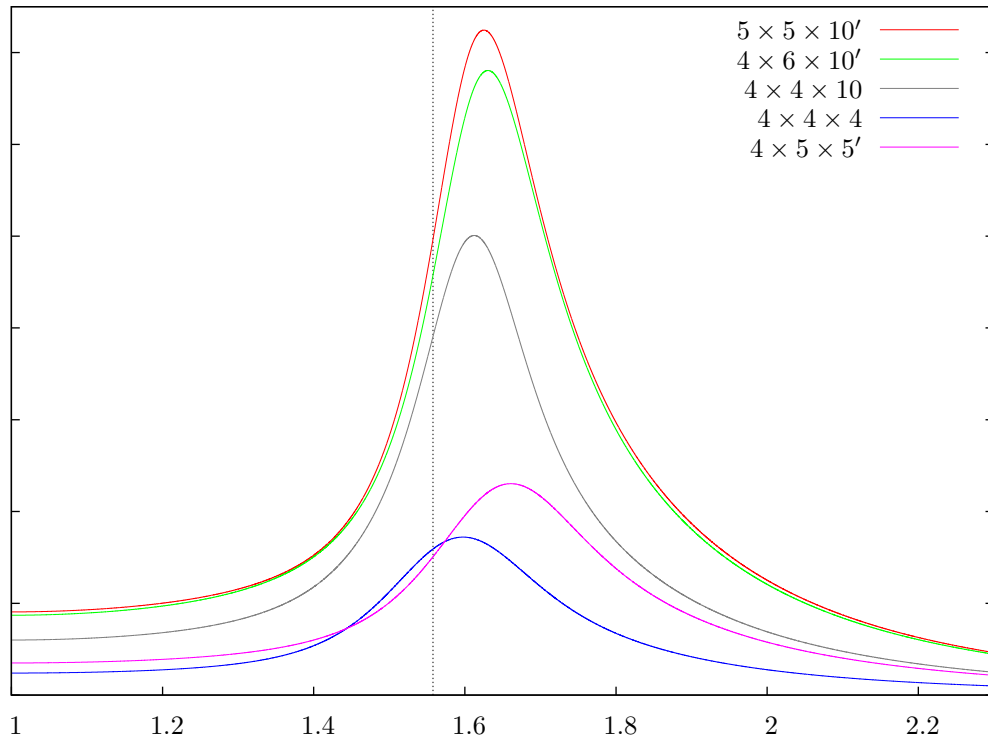
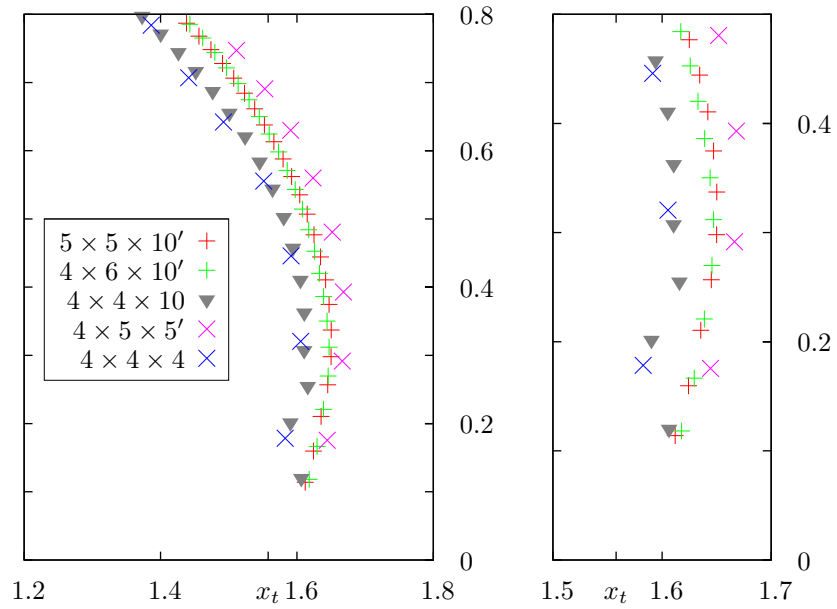


Figure 3.23: An overlay of zero distributions of large lattices close to \mathfrak{F} , along with their corresponding specific heat curves.

If we compare the $5 \times 5 \times 10'$, $6 \times 4 \times 10'$ and $4 \times 4 \times 10$, we notice the endpoints all lie very close to each other. But the specific heat curves show a far bigger difference in the height of each peak. Notice the density of zeros close to the real line. We see this also contributes to the height of the peak.

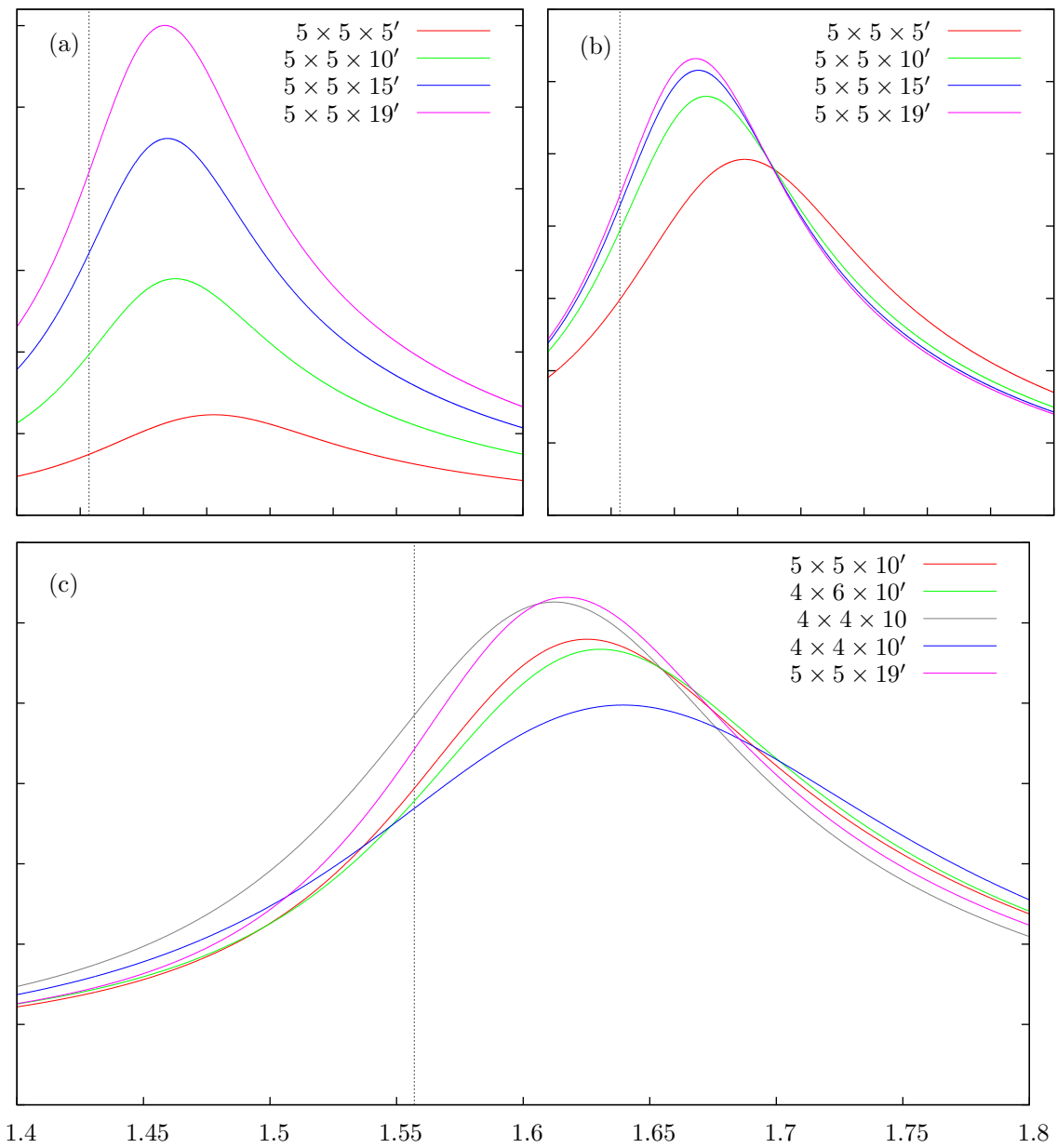


Figure 3.24: A look at the $5 \times 5 \times N_z$ on various axis.

Recall [2.3]. Here we compare c_V and C_V . Figure 3.24(a) is our usual plot of $C_V/k_B \beta^2$ vs. e^β . Figures 3.24(b) and 3.24(c), we plot $c_V := C_V/N$ vs e^β , where N is the number of spins on the lattice. Notice in Figure 3.24(c) the height of the peak for the $4 \times 4 \times 10$ is same as the $5 \times 5 \times 19'$, and higher than the $5 \times 5 \times 10'$, and $6 \times 4 \times 10'$ peaks.

3.4 Eigenvalue analysis

Here we look at the analytic structure of the transfer matrices in a 2d and 3d Ising model. Figure 3.25 shows the zero distribution for the 2d Ising model on a $10 \times N'_y$ lattice, where $N_y = \{10, 20, 50, 99\}$.

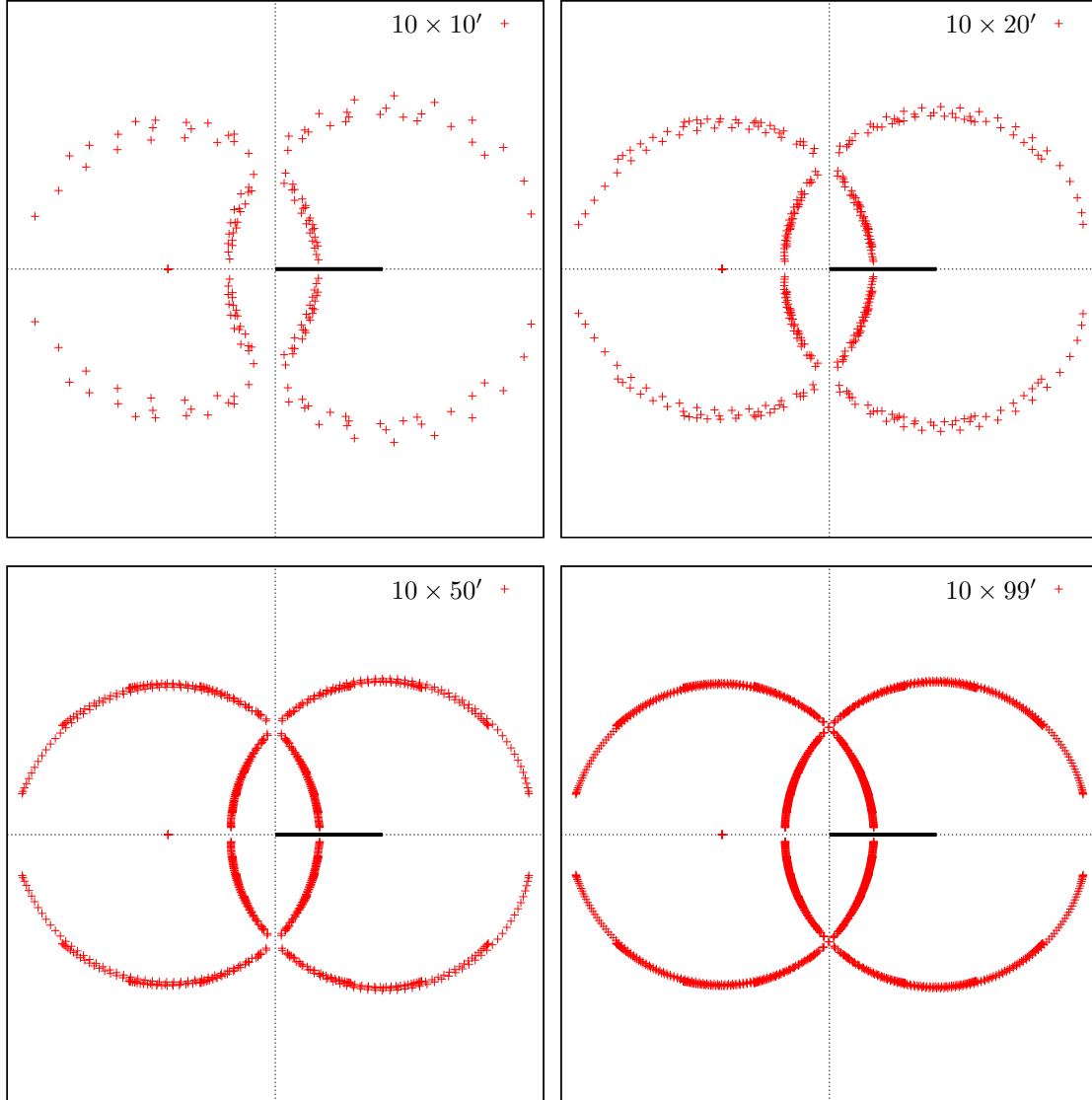


Figure 3.25: Zeros of the partition function Z for the $10 \times N_y$ Ising model, $N_y = \{10', 20', 50', 99'\}$. The degree of Z in sub-figure: (a) is 190; (b) is 390; (c) is 990; (d) is 1970;

As discussed in Section 2.3 we can see from the sequence of figures, that the zeros lie on curves whose shape and endpoints are determined by \mathcal{T} and not by the number of layers l . That is, the zeros get denser on these curves, but do not get closer to the real axis, as l increases.

Nevertheless we can still consider a $N \times N \times (N + L)$ (where $l = N + L$), a 3d sequence.

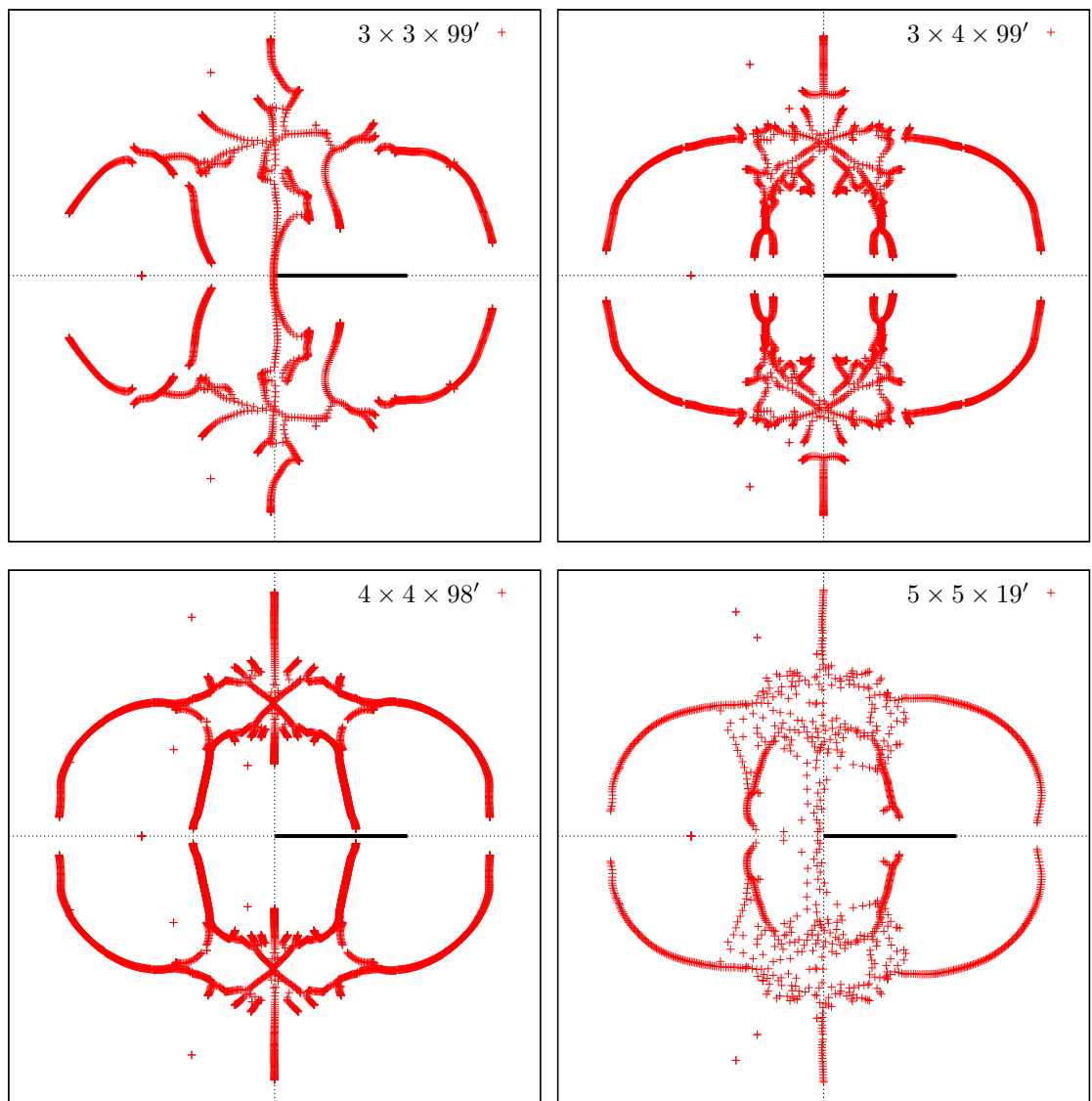


Figure 3.26: Zeros of the partition function Z in $x = e^\beta$. The degree of Z for sub-figure: (a) is 2664 (b) is 3552 (c) is 4688 (d) is 1400.

In Figure 3.26(c), we show the distribution of zeros for the Ising model on a $4 \times 4 \times 98'$ lattice. This is a partition function summed over more than 10^{472} configurations! Recall Section 2.3, this distribution allows us to probe the analytic structure of the largest magnitude eigenvalues for this $2^{16} \times 2^{16}$ transfer matrix. Comparing this to Pearson's results, this result gives a much clearer indication of where the eigenvalues of such a large matrix are degenerate.

3.5 Q -state: 2d Potts models ($Q > 2$)

Here we display our zeros distribution for $Q > 2$ -state Potts model on various 2d lattices (Figures 3.27 and 3.28) and 3d lattices (Figure 3.31).

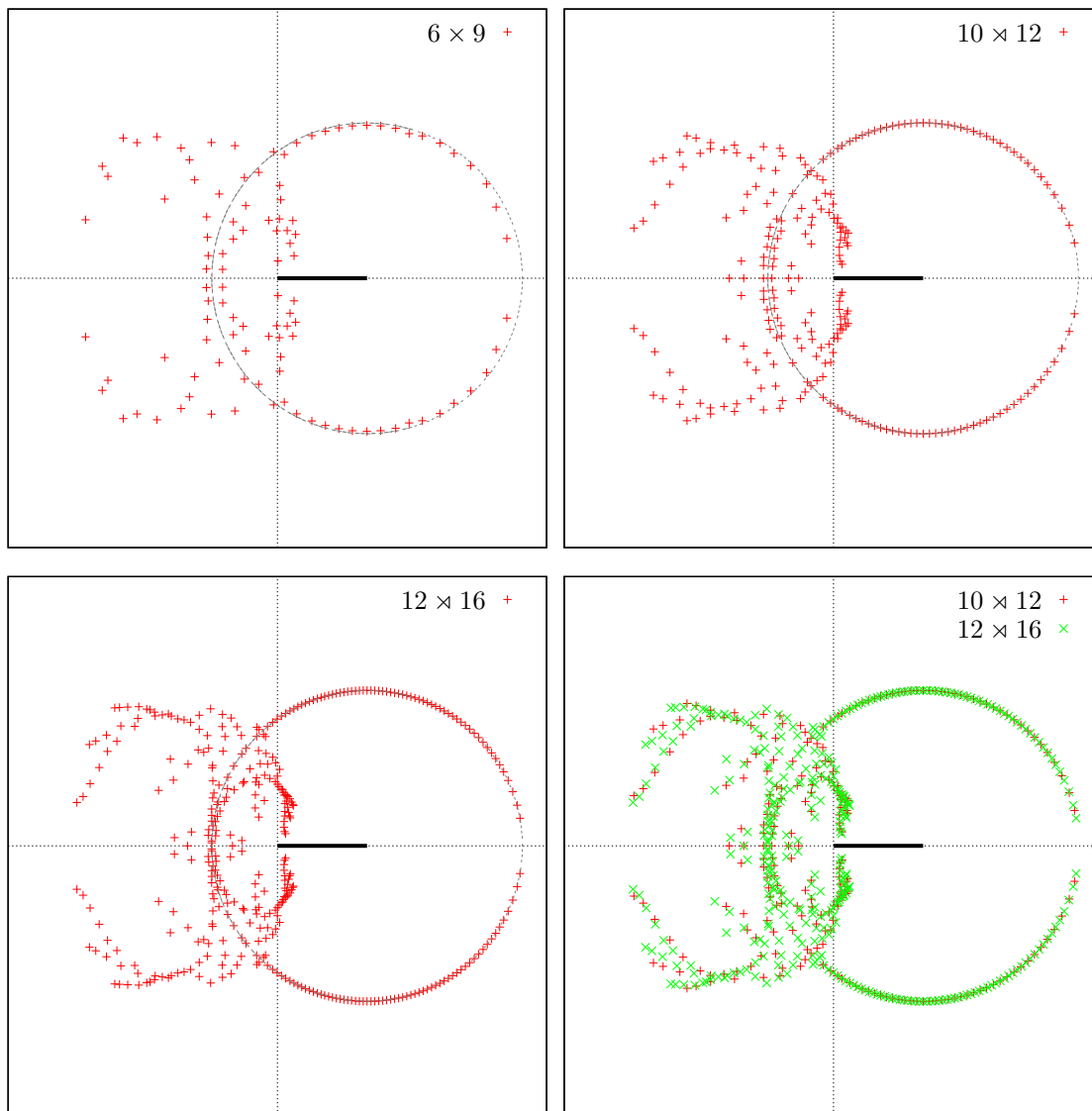


Figure 3.27: The zeros of the partition functions in Z in $x = e^\beta$ for various $Q = 3$ -state 2d Potts models

It has been shown that the distribution of zeros lie, in part, on an arc of known circle determined similarly to the locus computed in Section 1.2.3 (c.f. [38]), but not all zeros are confined to it.

This circle is the locus of points for which the duality transformation corresponds to complex conjugation:

$$e^\beta = \frac{1-Q}{1+\sqrt{Q}e^{i\theta}} \quad \text{for } 0 \leq \theta \leq 2\pi \quad (3.5.1)$$

Note, the $Q = 3$ -state 10×12 , and $Q = 5$ -state 7×9 (Figure 3.28) Potts models are computed by Martin [66].

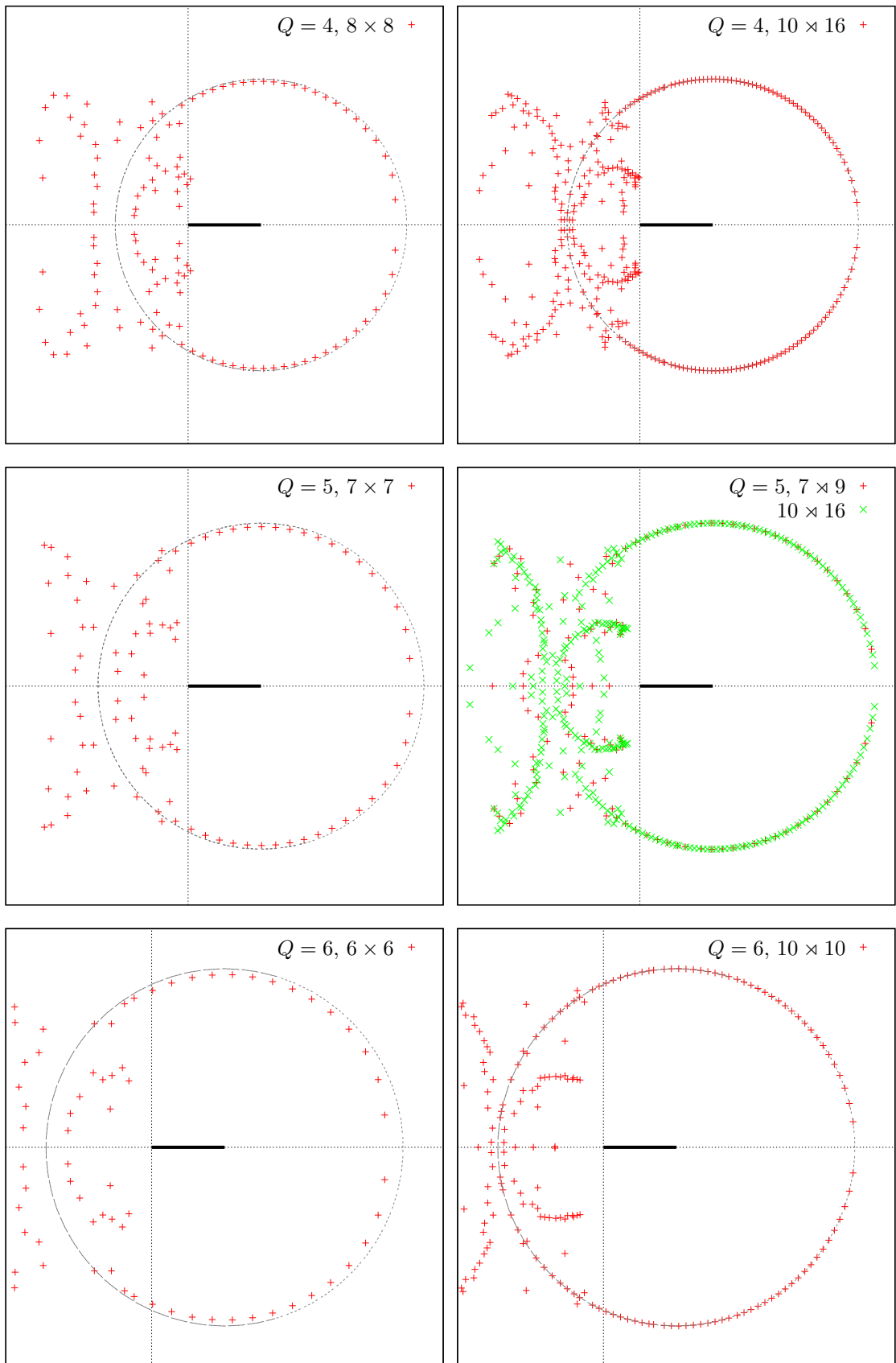


Figure 3.28: The zeros of the partition functions in Z in $x = e^\beta$ for various $(Q > 2)$ -state 2d Potts model

3.6 Q -state: 3d Potts models ($Q > 2$)

Figure 3.29, is a sequence of zeros distributions, $Q = 3$ -state 3d Potts model (the $3 \times 3 \times 9'$ result in Figure 3.29(b), was first computed by Martin [60]). Note, that in this sequence, the arm of zeros approaching \mathfrak{F} tend to be settled and well defined. However the zeros approaching the anti-ferromagnetic region have not stabilised. For example, notice the difference in the zeros in the anti-ferromagnetic region of Figures 3.29(b) and 3.29(f).

Consider the anti-ferromagnetic ground-state configurations in a 3d lattice. If we look at any line of adjacent spins through the lattice (which would be like a 1d sub-lattice), then this must also be a ground-state. With open boundary conditions there is no problem forming such lines, which are anti-ferromagnetic ground-states by a pattern (ie. in the line path through the 3d lattice) 12121212... from one edge to the other; or 123123123... or various others. But with a short periodic direction, some of these ground-state patterns are frustrated by the periodicity [24]. For example, if we have a configuration 12121, then 1 meets 1, and it is not an anti-ferromagnetic ground-state at all.

We check size and boundary dependence for a $Q = 3$ -state Potts model in Figures 3.29 and 3.30 respectively.

In Figure 3.31, we plot the distribution of zeros for some further Q -state Potts models.

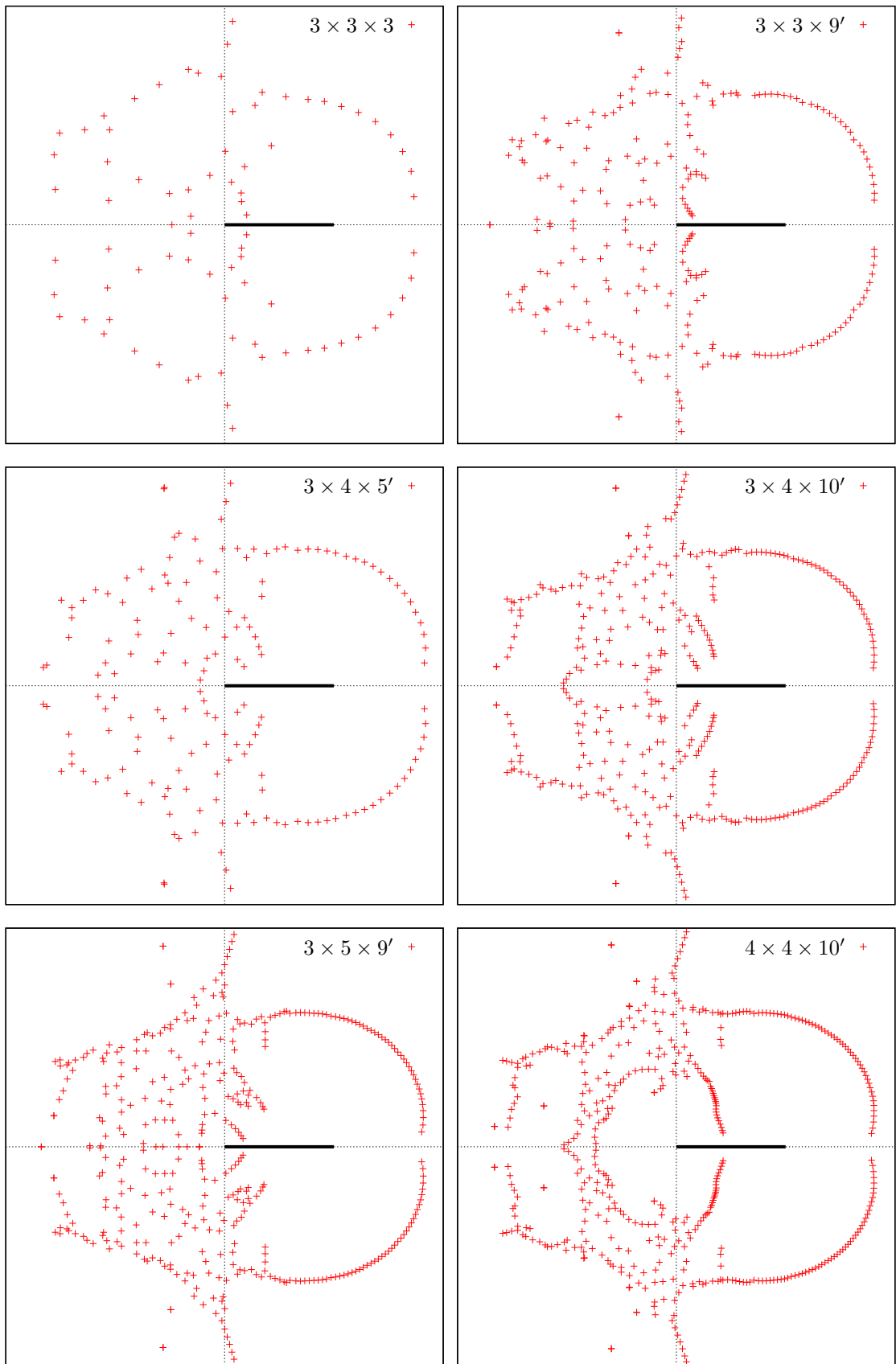


Figure 3.29: The zeros of the partition functions in Z in $x = e^\beta$ for $(Q = 3)$ -state models on various 3d lattices.

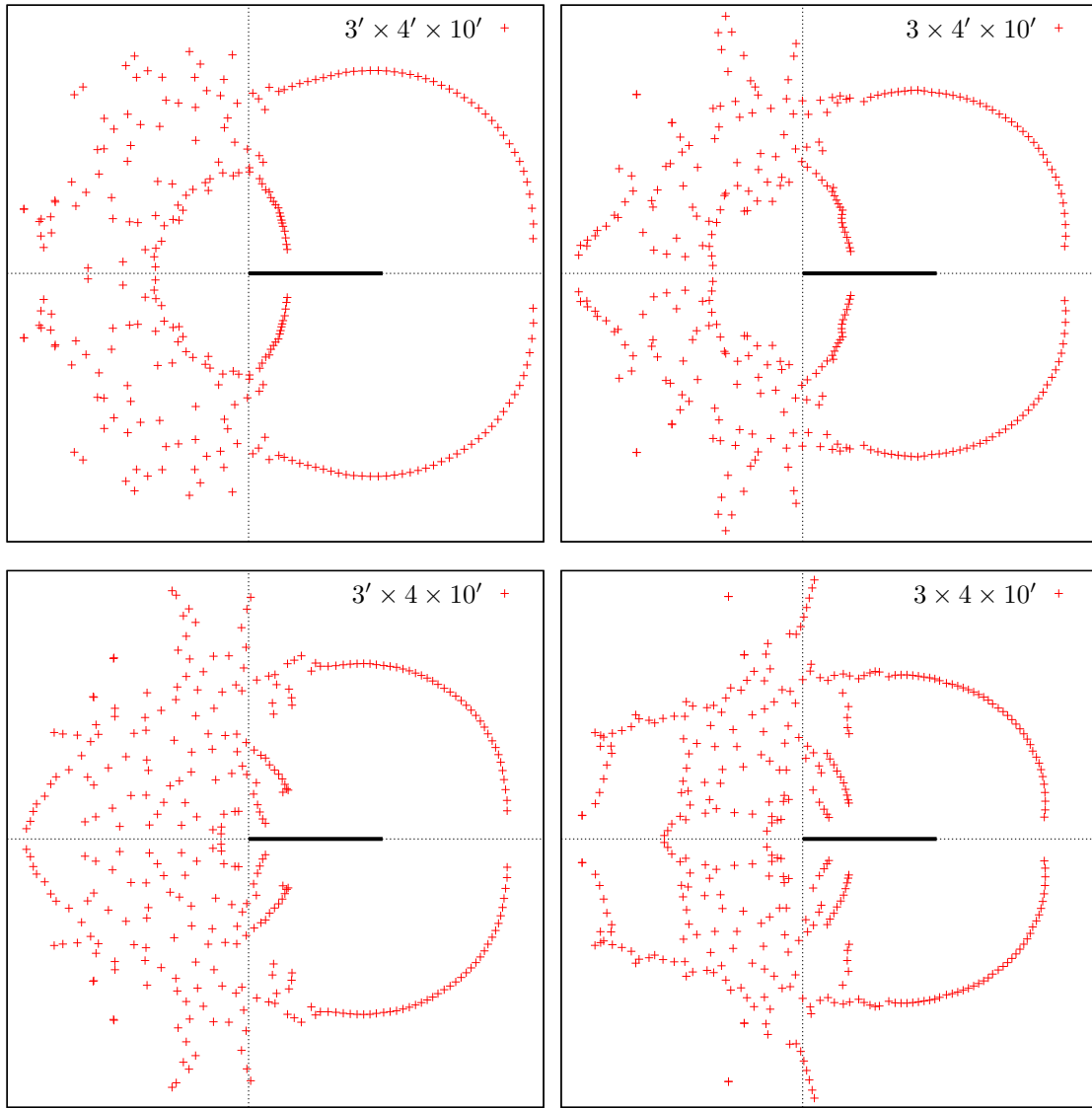


Figure 3.30: The zeros of the partition functions in Z in $x = e^\beta$ for $(Q = 3)$ -state models on a $3 \times 4 \times 10'$ lattice with various boundary conditions.

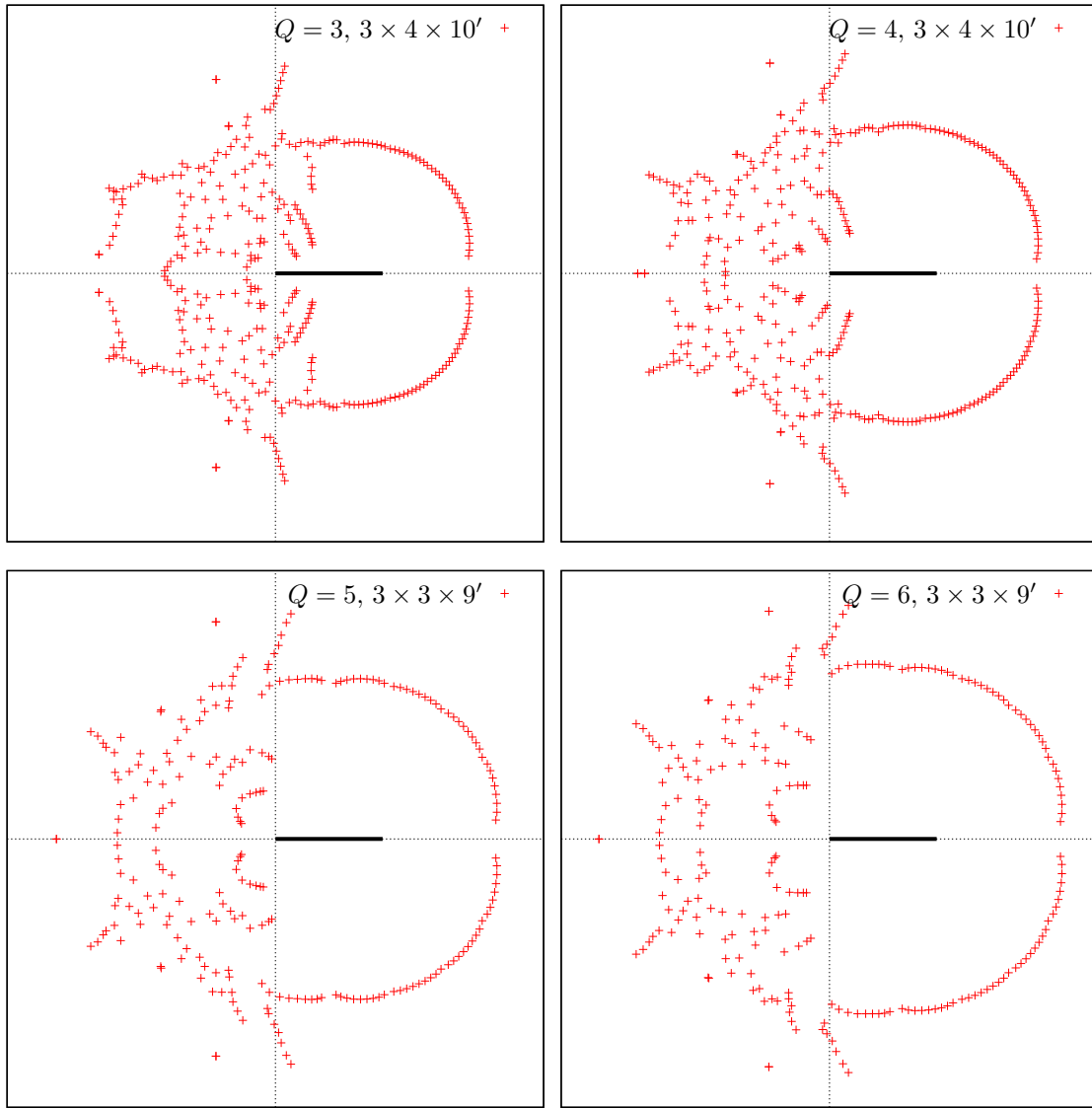


Figure 3.31: The zeros of the partition functions in Z in $x = e^\beta$ for various $(Q > 2)$ -state models on various 3d lattices.

Chapter 4

Discussion

We have studied the zeros of the Potts model partition function on finite 3d lattices $N_x \times N_y \times N_z$. Using a transfer matrix formalism, we compute the exact partition function in a polynomial expression, in the variable $x = e^\beta$. Our results show a diminishing dependence on lattice size and boundary conditions close to the ferromagnetic region. We also explain the difficulties that arise in the formalism close to the anti-ferromagnetic region.

Our aim is to locate the critical points of the 3d Ising model. In Table 4.1, we estimate the value for the critical point of the 3d Ising model using our largest results. We have numerically extrapolated the line of N zeros closest the ferromagnetic region, for the $5 \times 5 \times 10'$ and $6 \times 4 \times 10'$ Ising model results. The estimated points have been obtained using various in-built curve fitting functions of Maple [98]. (The process of estimating the critical points by extrapolating the zeros in the complex plane has been carried out by: Abe 1967 [1]; Katsura 1967 [47]; Ono et al 1967 [77]; Abe and Katsura 1970 [2]. Although the zeros are calculated for much smaller lattice sizes).

By studying a sequence of finite lattice results we infer that the 3d Ising model does exhibit co-operate phenomena (§1.1). Our results also seem to agree with an estimate of the critical temperature (§1.2.4) by Talapov (1996) [92]. However, an exception to this, is the zeros distributions

lattice size	N	Polynomial	Least square	Thiele	Cubic spline
$5 \times 5 \times 10'$	45	n/a	n/a	1.57456	1.58941
$5 \times 5 \times 10'$	4	1.56071	1.58656	1.59617	1.58860
$5 \times 5 \times 10'$	3	1.57201	1.58486	1.56560	1.58844
$5 \times 5 \times 10'$	2	1.58140	1.58140	1.58140	1.58140
$6 \times 4 \times 10'$	39	n/a	n/a	1.56893	1.59965
$6 \times 4 \times 10'$	4	1.56461	1.59772	1.98972	1.59874
$6 \times 4 \times 10'$	3	1.57594	1.59452	1.55325	1.59917
$6 \times 4 \times 10'$	2	1.58942	1.58942	1.58942	1.58942

Table 4.1: Extrapolating the critical point, using various curve fitting techniques.

in Figure 3.22(a). Our results also agree with previous work by Martin 1983 [61], Pearson 1982 [81], and Bhanot and Sastry 1990 [10]. For other Q -state models, such as the ones shown in Figures 3.27 and 3.28, our results agree with the findings of Hintermann (1978) [38].

Another interesting outcome of our results is that we are able to probe the analytic structure of the largest eigenvalues, for typically large matrices. However, we assume that the thermodynamic functions have the same functional features in the complex plane as they have in the real variable [90].

The specific heat observables of these partition functions results are also studied. We see the strong relation between the zero distribution close to the real ferromagnetic region and the position of the peak of the specific heat curve [43] (cf. §1.3). However, we find this is not true when we plot the specific heat per $N_x N_y N_z$ spins (such as in Figure 3.24(c)).

The computation of such large partition functions, requires a sophisticated level of programming. Computing results, such as the $5 \times 5 \times 19'$, requires solving many *time and space complexity* problems (cf [84]). That is, we are restricted computational limits, such as CPU processing time and memory usage required. However, we resist the temptation to present the vast amount of C++ programming code used. Instead, in Appendix B, we use the mathematical tools and notation introduced in Section 2.2 to describe our code. The code and all our exact partition function results are available to download at www.priyena.com [93].

We have considered the zeros of the partition function in the $x = e^\beta$ -plane. There are other variables that we could present our results in. For example, the high temperature expansion (§1.2.2) variable $\tanh \beta$ (cf. Pearson [81]). Or we could follow Martin [60], who plots the zeros of the 3-state Potts model in $x = \exp(-\frac{3}{2}\beta)$. That is, to consider the model as an Ising model with spin variables that take values from $\sqrt[3]{\pm 1}$.

Another interesting variation to the Potts model, is to consider anisotropic interactions. This is known as the clock model. See Martin [63, 64] for zero distributions of clock models.

So how may we compute partition function on *even* larger lattices? The tools we have describe, leave open a wide range of ways to grow the lattice, such that a computation maybe manageable in terms of time and memory. One possible method could be to consider some sort of hybrid version of the parallel computing method used by Bhanot and Sastry, and our method described in Appendix B.

Appendix A

Onsager's Exact Solution proof

In 1944, Lars Onsager solved the 2d Ising model in a zero field [78]. Onsager's solution is too complex to interpret for the context of this thesis. Instead, we use a simplification of his result, as derived by Martin [61, §2].

Recall Section 2.2.1, the partition function Z is expressed by transfer matrix \mathcal{T} with suitable boundary conditions. That is, for spins on a $N \times M$ lattice, $Z = \text{Tr}(\mathcal{T}^M)$, where \mathcal{T} is a 2^N square matrix. Further if $\{\lambda_i\}$ are the eigenvalues of \mathcal{T} , then

$$Z = \sum_i (\lambda_i^M). \quad (\text{A.0.1})$$

Unfortunately the eigenvalues of \mathcal{T} are not known and cannot be easily found.

A.1 Notations and background maths

A.1.1 Matrix algebra

Although matrices A and B may not commute (ie. $AB \neq BA$), we find that the trace of their product does ie. $\text{Tr}(AB) = \text{Tr}(BA)$. Further if a matrix S is used to diagonalise matrix A , ie. SAS^{-1} , then

$$\text{Tr}(SAS^{-1}) = \text{Tr}(S^{-1}SA) = \text{Tr}(A) \quad (\text{A.1.1})$$

For two arbitrary matrices A and B , we have the direct product (Kronecker product) defined as

$$A \otimes B = \begin{bmatrix} a_{11}B & a_{12}B & \cdots & a_{1n}B \\ \vdots & \vdots & \ddots & \vdots \\ a_{m1}B & a_{m2}B & \cdots & a_{mn}B \end{bmatrix}. \quad (\text{A.1.2})$$

If A is an $m \times n$ matrix and B is a $p \times q$ matrix, then their Kronecker product $A \otimes B$ is an $mp \times nq$ matrix.

Let $\mathbb{1}_i$ ($i \in \mathbb{N}$), denote an $i \times i$ identity matrix. Further, let $\mathbb{1}_i^{\otimes k}$ be the result of applying

$$\mathbb{1}_i^{\otimes k} = \underbrace{\mathbb{1}_i \otimes \mathbb{1}_i \otimes \cdots \otimes \mathbb{1}_i}_k \quad (\text{A.1.3})$$

k times.

The Kronecker product is not commutative. If A and B are both $k \times k$ matrices, then for fixed $N \in \mathbb{N}$ denote

$$A_i = (\mathbb{1}_k^{\otimes i-1} \otimes A \otimes \mathbb{1}_k^{\otimes N-i}), \quad \text{and} \quad B_j = (\mathbb{1}_k^{\otimes j-1} \otimes B \otimes \mathbb{1}_k^{\otimes N-j}).$$

Every A_i and B_j will commute for every $\{i, j \in \mathbb{N} | i \neq j\}$. Note for matrices A and B , if A and B are the same dimension and AB exists then

$$\mathbb{1}_a^{\otimes i} \otimes AB \otimes \mathbb{1}_b^{\otimes j} \equiv (\mathbb{1}_a^{\otimes i} \otimes A \otimes \mathbb{1}_b^{\otimes j}) \times (\mathbb{1}_a^{\otimes i} \otimes B \otimes \mathbb{1}_b^{\otimes j}) \quad (\text{A.1.4})$$

$$\mathbb{1}_a^{\otimes i} \otimes (A + B) \otimes \mathbb{1}_b^{\otimes j} \equiv (\mathbb{1}_a^{\otimes i} \otimes A \otimes \mathbb{1}_b^{\otimes j}) + (\mathbb{1}_a^{\otimes i} \otimes B \otimes \mathbb{1}_b^{\otimes j}) \quad (\text{A.1.5})$$

There are three Pauli matrices, denoted σ^x , σ^y , σ^z where

$$\sigma^x = \begin{pmatrix} 0 & 1 \\ 1 & 0 \end{pmatrix}, \quad \sigma^y = \begin{pmatrix} 0 & -i \\ i & 0 \end{pmatrix}, \quad \sigma^z = \begin{pmatrix} 1 & 0 \\ 0 & -1 \end{pmatrix}. \quad (\text{A.1.6})$$

The following properties are easily verified

$$(\sigma^x)^2 = (\sigma^y)^2 = (\sigma^z)^2 = \mathbb{1}_2 \quad (\text{A.1.7})$$

$$\sigma^x \sigma^y = -\sigma^y \sigma^x, \quad \forall x, y \in \{x, y, z\} \quad (\text{A.1.8})$$

$$\sigma^x \sigma^y = i\sigma^z, \quad \sigma^y \sigma^z = i\sigma^x, \quad \sigma^z \sigma^x = i\sigma^y \quad (\text{A.1.9})$$

Notation: For $x \in \{x, y, z\}$ and $i, n \in \mathbb{N}$ where $i \leq n$, denote

$$\sigma_i^x = \mathbb{1}_2^{\otimes i-1} \otimes \sigma^x \otimes \mathbb{1}_2^{\otimes n-i}. \quad (\text{A.1.10})$$

By using Equation (A.1.4) the following can also be verified:

$$(\sigma_i^x)^2 = \mathbb{1}_{2^n} \quad \forall x \in \{x, y, z\} \quad (\text{A.1.11})$$

$$\sigma_i^x \sigma_i^y = -\sigma_i^y \sigma_i^x, \quad \forall x, y \in \{x, y, z\} \quad (\text{A.1.12})$$

$$\sigma_i^x \sigma_i^y = \sigma_i^z \sqrt{-1}, \quad \sigma_i^y \sigma_i^z = \sigma_i^x \sqrt{-1}, \quad \sigma_i^z \sigma_i^x = \sigma_i^y \sqrt{-1} \quad (\text{A.1.13})$$

See the proofs of propositions A.3.4 and A.3.5 for an example of how to verify A.1.12 and A.1.13 respectively. Also note as $(\sigma_i^x)^2 = \mathbb{1}_{2^n}$ then $e^{\theta i \sigma_i^x} = \cosh(\theta) \mathbb{1}_{2^n} + \sinh(\theta) \sigma_i^x$.

A.1.2 Clifford algebra

Here we introduce the algebra that is used to link rotation matrices to transfer matrices. We give a formal definition of the algebra, and prove its existence by example.

Proposition A.1.1 (Clifford Relations [14]). *For each n there exists matrices $\Gamma_1, \Gamma_2, \dots, \Gamma_{2n}$ of size $2^n \times 2^n$, obeying*

$$\Gamma_i^2 = \mathbb{1}_{2^n} \quad (\text{A.1.14})$$

$$\Gamma_i \Gamma_j = -\Gamma_j \Gamma_i, \quad i \neq j \quad (\text{A.1.15})$$

Such a set is called a set of gamma-matrices (Γ -matrices).

Example A.1. We prove Proposition A.1.1 by existence. Suppose Γ_i is a set of Γ -matrices, and suppose S is an invertible matrix of size $2^n \times 2^n$, then

Proposition A.1.2. $\{S\Gamma^i S^{-1}\}_i$ is a set of Γ -matrices.

Proof. For every i , $S\Gamma^i S^{-1}$ is a $2^n \times 2^n$ matrix, such that

$$\begin{aligned}
(S\Gamma^i S^{-1})^2 &= (S\Gamma^i S^{-1})(S\Gamma^i S^{-1}) \\
&= S\Gamma^i (S^{-1}S)\Gamma^i S^{-1} \\
&= S\Gamma^i \Gamma^i S^{-1} \\
&= S\mathbb{1}_{2^n} S^{-1} \\
&= \mathbb{1}_{2^n}
\end{aligned} \tag{A.1.16}$$

and

$$\begin{aligned}
(S\Gamma^i S^{-1})(S\Gamma^j S^{-1}) &= S\Gamma^i (S^{-1}S)\Gamma^j S^{-1} \\
&= S(-\Gamma^j \Gamma^i) S^{-1} \\
&= -(S\Gamma^j S^{-1})(S\Gamma^i S^{-1})
\end{aligned} \tag{A.1.17}$$

□

In order to link transfer matrices to rotational matrices, we can express Pauli matrices (Equation (A.1.6)) as Γ -matrices (Proposition A.1.1).

Example A.2. For $n = 1$, then Γ_1, Γ_2 are 2×2 matrices. Suppose $\Gamma_1 = \sigma^x$ and $\Gamma_2 = \sigma^z$.

Then

$$(\Gamma_1)^2 = \begin{pmatrix} 0 & 1 \\ 1 & 0 \end{pmatrix} \begin{pmatrix} 0 & 1 \\ 1 & 0 \end{pmatrix} = \begin{pmatrix} 1 & 0 \\ 0 & 1 \end{pmatrix} = \mathbb{1}_2 \tag{A.1.18}$$

$$(\Gamma_2)^2 = \begin{pmatrix} 1 & 0 \\ 0 & -1 \end{pmatrix} \begin{pmatrix} 1 & 0 \\ 0 & -1 \end{pmatrix} = \begin{pmatrix} 1 & 0 \\ 0 & 1 \end{pmatrix} = \mathbb{1}_2 \tag{A.1.19}$$

$$\Gamma_1 \Gamma_2 = \sigma^x \sigma^z = \begin{pmatrix} 0 & 1 \\ 1 & 0 \end{pmatrix} \begin{pmatrix} 1 & 0 \\ 0 & -1 \end{pmatrix} = \begin{pmatrix} 0 & -1 \\ 1 & 0 \end{pmatrix} \tag{A.1.20}$$

$$\Gamma_2 \Gamma_1 = \sigma^z \sigma^x = \begin{pmatrix} 1 & 0 \\ 0 & -1 \end{pmatrix} \begin{pmatrix} 0 & 1 \\ 1 & 0 \end{pmatrix} = -\begin{pmatrix} 0 & -1 \\ 1 & 0 \end{pmatrix} \tag{A.1.21}$$

therefore

$$\Gamma_2 \Gamma_1 = -\Gamma_1 \Gamma_2 \tag{A.1.22}$$

A.2 Rotational matrices

A.2.1 Rotations in $2n$ -dimensions

Every rotation in $2n$ -dimensions can be defined by a $2n$ -square matrix. For example, the matrix for the rotation by θ in the 1-2 plane is

$$\begin{pmatrix} \cos(\theta) & \sin(\theta) & 0 & 0 & \dots & 0 \\ -\sin(\theta) & \cos(\theta) & 0 & 0 & \dots & 0 \\ 0 & 0 & 1 & 0 & \dots & 0 \\ 0 & 0 & 0 & 1 & \dots & 0 \\ \vdots & \vdots & \vdots & \vdots & \ddots & \vdots \\ 0 & 0 & 0 & 0 & \dots & 1 \end{pmatrix} \begin{pmatrix} x \\ y \\ z \\ t \\ \vdots \\ a \end{pmatrix} = \begin{pmatrix} x \cos(\theta) + y \sin(\theta) \\ -x \sin(\theta) + y \cos(\theta) \\ z \\ t \\ \vdots \\ a \end{pmatrix} = \begin{pmatrix} x' \\ y' \\ z \\ t \\ \vdots \\ a \end{pmatrix} \quad (\text{A.2.1})$$

Let

$$M(\theta) = \begin{pmatrix} \cos(\theta) & \sin(\theta) \\ -\sin(\theta) & \cos(\theta) \end{pmatrix}. \quad (\text{A.2.2})$$

The following properties of M are easily verified $M(\theta + \theta') = M(\theta)M(\theta') = M(\theta')M(\theta)$ and $M(2\pi) = M(0) = \mathbb{1}_2$. Also $\det(M) = 1$, so the complex eigenvalues are $\exp(\pm i\theta)$.

Notation: Let W be the group of rotational matrices. Let $W_{ab}(\theta)$ denote the matrix representing rotation by θ in the ab plane. Then for any i , we have

$$W_{i \ i+1}(\theta) = \mathbb{1}_{i-1} \oplus M(\theta) \oplus \mathbb{1}_{(2n-i-1)} \quad (\text{A.2.3})$$

where the spectrum of $W_{i \ i+1}$ is $\{e^{\pm i\theta}, 1\}$. For example, the eigenvalues of say $W_{12}(\theta)$ are

$$\begin{pmatrix} \cos \theta & \sin \theta & & & & \\ -\sin \theta & \cos \theta & & & & \\ & & 1 & & & \\ & & & 1 & & \\ & & & & \ddots & \\ & & & & & 1 \end{pmatrix} \rightsquigarrow \begin{pmatrix} e^{i\theta} & & & & & \\ & e^{-i\theta} & & & & \\ & & 1 & & & \\ & & & 1 & & \\ & & & & \ddots & \\ & & & & & 1 \end{pmatrix} \quad (\text{A.2.4})$$

For any rotation group element of W , the spectrum is of the form $\text{diag}(e^{i\theta}, e^{-i\theta}, e^{i\theta'}, e^{-i\theta'}, \dots)$.

A.2.2 Rotational matrices and Clifford algebra

We now show how rotational matrices $W_{ab}(\theta)$ (§A.2.1) can be expressed in terms of Γ -matrices (§A.1.2).

Fact A.2.1. *Given a set of $2^n \times 2^n$ Γ -matrices $\{\Gamma_i\}_i$, then $\{\Gamma'_i\}_i$, the set of $2^n \times 2^n$ matrices given by*

$$\Gamma'_i = \cos(\theta)\Gamma_i + \sin(\theta)\Gamma_{i+1} \quad (\text{A.2.5})$$

$$\Gamma'_{i+1} = -\sin(\theta)\Gamma_i + \cos(\theta)\Gamma_{i+1} \quad (\text{A.2.6})$$

$$\Gamma'_j = \Gamma_j, \quad \forall j \neq i, i+1, \quad (\text{A.2.7})$$

is a set of Γ -matrices, ie. $\{\Gamma'_i\}_i$ obey (A.1.14) and (A.1.15).

Proof. Firstly we show for all i Equation (A.1.14) holds true.

$$\begin{aligned}
(\Gamma'_i)^2 &= (\cos(\theta)\Gamma_i + \sin(\theta)\Gamma_{i+1})^2 \\
&= \cos^2(\theta)\Gamma_i^2 + \sin^2(\theta)\Gamma_{i+1}^2 + \cos(\theta)\sin(\theta)\Gamma_i\Gamma_{i+1} + \cos(\theta)\sin(\theta)\Gamma_{i+1}\Gamma_i \\
&= \cos^2(\theta)\mathbb{1}_{2^n} + \sin^2(\theta)\mathbb{1}_{2^n} + \cos(\theta)\sin(\theta)\Gamma_i\Gamma_{i+1} + \cos(\theta)\sin(\theta)(-\Gamma_i\Gamma_{i+1}) \\
&= \mathbb{1}_{2^n}.
\end{aligned} \tag{A.2.8}$$

Similarly

$$\begin{aligned}
(\Gamma'_{i+1})^2 &= (-\sin(\theta)\Gamma_i + \cos(\theta)\Gamma_{i+1})^2 \\
&= \cos^2(\theta)\Gamma_{i+1}^2 + \sin^2(\theta)\Gamma_i^2 - \cos(\theta)\sin(\theta)\Gamma_i\Gamma_{i+1} - \cos(\theta)\sin(\theta)\Gamma_{i+1}\Gamma_i \\
&= \mathbb{1}_{2^n}.
\end{aligned} \tag{A.2.9}$$

Next we show that Equation (A.1.15) holds true for all i .

$$\begin{aligned}
\Gamma'_i\Gamma'_{i+1} &= (\cos(\theta)\Gamma_i + \sin(\theta)\Gamma_{i+1})(-\sin(\theta)\Gamma_i + \cos(\theta)\Gamma_{i+1}) \\
&= -\cos(\theta)\sin(\theta)\Gamma_i^2 + \cos^2(\theta)\Gamma_i\Gamma_{i+1} - \sin^2(\theta)\Gamma_{i+1}\Gamma_i + \sin(\theta)\cos(\theta)\Gamma_{i+1}^2 \\
&= -\cos(\theta)\sin(\theta)\Gamma_i^2 + \cos^2(\theta)(-\Gamma_{i+1}\Gamma_i) - \sin^2(\theta)(-\Gamma_i\Gamma_{i+1}) + \sin(\theta)\cos(\theta)\Gamma_{i+1}^2 \\
&= (-\sin(\theta)\Gamma_i + \cos(\theta)\Gamma_{i+1})(-\cos(\theta)\Gamma_i - \sin(\theta)\Gamma_{i+1}) \\
&= -(-\sin(\theta)\Gamma_i + \cos(\theta)\Gamma_{i+1})(\cos(\theta)\Gamma_i + \sin(\theta)\Gamma_{i+1}) \\
&= -\Gamma'_{i+1}\Gamma'_i
\end{aligned} \tag{A.2.10}$$

For all $i, j (j \neq i, i+1)$

$$\begin{aligned}
\Gamma'_i\Gamma'_j &= (\cos(\theta)\Gamma_i + \sin(\theta)\Gamma_{i+1})\Gamma_j \\
&= \cos(\theta)\Gamma_i\Gamma_j + \sin(\theta)\Gamma_{i+1}\Gamma_j \\
&= \cos(\theta)(-\Gamma_j\Gamma_i) + \sin(\theta)(-\Gamma_j\Gamma_{i+1}) \\
&= -\Gamma_j(\cos(\theta)\Gamma_i + \sin(\theta)\Gamma_{i+1}) \\
&= -\Gamma'_j\Gamma'_i
\end{aligned} \tag{A.2.11}$$

□

We now show how rotational matrices are linked Γ -matrices. Take the $W_{12}(\theta)$ matrix as an example, but it is trivial to extend the concept to any W_{ab} matrix.

$$\begin{pmatrix} \cos(\theta) & \sin(\theta) & 0 & 0 & \dots & 0 \\ -\sin(\theta) & \cos(\theta) & 0 & 0 & \dots & 0 \\ 0 & 0 & 1 & 0 & \dots & 0 \\ 0 & 0 & 0 & 1 & \dots & 0 \\ \vdots & \vdots & \vdots & \vdots & \ddots & \vdots \\ 0 & 0 & 0 & 0 & \dots & 1 \end{pmatrix} \begin{pmatrix} \Gamma_1 \\ \Gamma_2 \\ \Gamma_3 \\ \Gamma_4 \\ \vdots \\ \Gamma_{2n} \end{pmatrix} = \begin{pmatrix} \Gamma_1 \cos(\theta) + \Gamma_2 \sin(\theta) \\ -\Gamma_1 \sin(\theta) + \Gamma_2 \cos(\theta) \\ \Gamma_3 \\ \Gamma_4 \\ \vdots \\ \Gamma_{2n} \end{pmatrix} = \begin{pmatrix} \Gamma'_1 \\ \Gamma'_2 \\ \Gamma'_3 \\ \Gamma'_4 \\ \vdots \\ \Gamma'_{2n} \end{pmatrix}$$

A.2.3 Product of rotational matrices

Let W_1 and W_2 be rotational matrices given by

$$W_1 = \prod_{i=1}^n W_{2i \ 2i-1}(2i\theta), \quad (\text{A.2.12})$$

and

$$W_2 = \prod_{i=1}^n W_{2i+1 \ 2i}(2i\beta). \quad (\text{A.2.13})$$

Example A.3. For $n = 2$, let $c = \cos(2i\theta)$, $s = \sin(2i\theta)$, $c' = \cos(2i\beta)$, and $s' = \sin(2i\beta)$. Then

$$\begin{aligned} W_1 &= W_{21}(2i\theta)W_{43}(2i\theta) \\ &= \begin{pmatrix} c & s & & \\ -s & c & & \\ & & 1 & \\ & & & 1 \end{pmatrix} \begin{pmatrix} 1 & & & \\ & 1 & & \\ & & c & s \\ & & -s & c \end{pmatrix} \\ &= \begin{pmatrix} c & s & & \\ -s & c & & \\ & & c & s \\ & & -s & c \end{pmatrix} \end{aligned}$$

and

$$\begin{aligned} W_2 &= W_{32}(2i\beta)W_{04}(2i\beta) \\ &= \begin{pmatrix} 1 & & & \\ & c' & s' & \\ & -s' & c' & \\ & & & 1 \end{pmatrix} \begin{pmatrix} c' & & & -s' \\ & 1 & & \\ & & 1 & \\ s' & & & c' \end{pmatrix} \\ &= \begin{pmatrix} c' & & & -s' \\ & c' & s' & \\ & -s' & c' & \\ s' & & & c' \end{pmatrix} \end{aligned}$$

Example A.4. For $n = 4$

$$W_1 = \begin{pmatrix} c & s & & & & \\ -s & c & & & & \\ & & c & s & & \\ & & -s & c & & \\ & & & & c & s \\ & & & & -s & c \\ & & & & & & c & s \\ & & & & & & -s & c \end{pmatrix} \quad W_2 = \begin{pmatrix} c' & & & & & & & -s' \\ & c' & s' & & & & & \\ & -s' & c' & & & & & \\ & & & c' & s' & & & \\ & & & -s' & c' & & & \\ & & & & & c' & s' & \\ & & & & & -s' & c' & \\ s' & & & & & & & c' \end{pmatrix}$$

Then let matrix $W = W_1W_2$. Expanding out the products

$$\begin{aligned} W &= W_1W_2 \\ &= \prod_{i=1}^n W_{2i \ 2i-1}(2i\theta) \prod_{i=1}^n W_{2i+1 \ 2i}(2i\beta) \\ &= W_{21}(2i\theta)W_{43}(2i\theta)W_{56}(2i\theta) \dots W_{32}(2i\beta)W_{54}(2i\beta)W_{76}(2i\beta) \dots \\ &= \prod_i^{2n} W_{a_i b_i}(\theta_i) \end{aligned} \quad (\text{A.2.14})$$

where all $\{a_i, b_i\}$ are distinct.

Define \mathfrak{T} as a $2n \times 2n$ shift operator matrix, ie. (when $n = 3$)

$$\mathfrak{T} = \begin{pmatrix} 0 & 1 & & & & \\ & 0 & 1 & & & \\ & & 0 & 1 & & \\ & & & 0 & 1 & \\ & & & & 0 & 1 \\ 1 & & & & & 0 \end{pmatrix} \quad (\text{A.2.15})$$

Then $\mathfrak{T}^{2n} = \mathbb{1}$ and for any i ,

$$\mathfrak{T}^i W_1 \mathfrak{T}^{-i} = W_1 \quad (\text{A.2.16})$$

$$\mathfrak{T}^i W_1 = W_1 \mathfrak{T}^i \quad (\text{A.2.17})$$

Define variable $z = e^{i\pi k/n}$, such that $z^{2n} = 1$.

Proposition A.2.2. z is an eigenvalue of \mathfrak{T} .

Proof.

$$\mathfrak{T} \begin{pmatrix} 1 \\ z \\ z^2 \\ z^3 \\ \vdots \\ z^{2n-1} \end{pmatrix} = \begin{pmatrix} z \\ z^2 \\ z^3 \\ \vdots \\ z^{2n-1} \\ 1 = z^{2n} \end{pmatrix} = z \begin{pmatrix} 1 \\ z \\ z^2 \\ z^3 \\ \vdots \\ z^{2n-1} \end{pmatrix}, \quad (\text{A.2.18})$$

hence z is an eigenvalue of \mathfrak{T} . □

Using Fourier transforms we define vector f_z , as

$$f_z = \begin{pmatrix} 1 \\ z^2 \\ z^4 \\ z^6 \\ \vdots \\ z^{2n-2} \end{pmatrix}, \quad (\text{A.2.19})$$

and also vectors v_1 and v_2 as

$$v_1^z = f_z \otimes \begin{pmatrix} 1 \\ 0 \end{pmatrix}, \quad \text{and} \quad v_2^z = f_z \otimes \begin{pmatrix} 0 \\ 1 \end{pmatrix} \quad (\text{A.2.20})$$

Then

$$W_1 v_1^z = \begin{pmatrix} c \\ -s \\ cz^2 \\ -sz^2 \\ \vdots \end{pmatrix} = c \begin{pmatrix} 1 \\ 0 \\ z^2 \\ 0 \\ \vdots \end{pmatrix} - s \begin{pmatrix} 0 \\ 1 \\ 0 \\ z^2 \\ \vdots \end{pmatrix} \quad (\text{A.2.21})$$

$$= c v_1^z - s v_2^z \quad (\text{A.2.22})$$

Also

$$W_2 v_1^z = \begin{pmatrix} c' \\ s'z^2 \\ c'z^2 \\ s'z^4 \\ \vdots \end{pmatrix} = c' \begin{pmatrix} 1 \\ 0 \\ z^2 \\ 0 \\ \vdots \end{pmatrix} + s'z^2 \begin{pmatrix} 0 \\ 1 \\ 0 \\ z^2 \\ \vdots \end{pmatrix} \quad (\text{A.2.23})$$

$$= c' v_1^z + s'z^2 v_2^z \quad (\text{A.2.24})$$

Similarly

$$W_1 v_2^z = s v_1^z + c v_2^z \quad (\text{A.2.25})$$

$$W_2 v_2^z = -s'z^{-2} v_1^z + c' v_2^z \quad (\text{A.2.26})$$

Leading to

$$W_1(W_2 v_1^z) = (c'c + s'sz^2)v_1^z + (s'cz^2 - c's)v_2^z \quad (\text{A.2.27})$$

$$W_1(W_2 v_2^z) = (-s'cz^{-2} + c's)v_1^z + (s'sz^{-2} + c'c)v_2^z \quad (\text{A.2.28})$$

and finally

$$W_1 W_2 \begin{pmatrix} v_1^z \\ v_2^z \end{pmatrix} = W \begin{pmatrix} v_1^z \\ v_2^z \end{pmatrix} = \begin{pmatrix} c'c + s'sz^2 & s'cz^2 - c's \\ -s'cz^{-2} + c's & s'sz^{-2} + c'c \end{pmatrix} \begin{pmatrix} v_1^z \\ v_2^z \end{pmatrix} \quad (\text{A.2.29})$$

Proposition A.2.3. *The determinant of the image matrix $W^{(z)}$ is 1.*

Proof.

$$\begin{aligned} \det(W^{(z)}) &= (c'c + s'sz^2)(s'sz^{-2} + c'c) - (-s'cz^{-2} + c's)(s'cz^2 - c's) \\ &= (c'c + s'sz^2)(s'sz^{-2} + c'c) + (s'cz^{-2} - c's)(s'cz^2 - c's) \\ &= c'cs'sz^{-2} + (c'c)^2 + (s's)^2 + c'cs'sz^2 + (s'c)^2 - c'ss'cz^{-2} - c'ss'cz^2 + (c's)^2 \\ &= (c'c)^2 + (s's)^2 + c's'cs(z^2 + z^{-2}) + (s'c)^2 + (c's)^2 - c'ss'c(z^2 + z^{-2}) \\ &= (c'c)^2 + (s's)^2 + (s'c)^2 + (c's)^2 \\ &= (c')^2(c^2 + s^2) + (s')^2(c^2 + s^2) \\ &= (c')^2 + (s')^2 \\ &= 1 \end{aligned} \quad (\text{A.2.30})$$

□

Then as the determinant of a matrix is equal to the product of its eigenvalues. Proposition A.2.3 implies that the eigenvalues of W must be reciprocal ie. $\lambda_1 = \lambda_2^{-1}$.

A.2.4 Eigenvalues of W

As W is rotational matrix, we note that the eigenvalues will be of the form $e^{\pm l_z}$. Then as the sum of the eigenvalues is equal to the trace of the $W^{(z)}$ [87, Pg. 249]

$$e^{l_z} + e^{-l_z} = 2 \left(cc' + \frac{z^2 + z^{-2}}{2} ss' \right) \quad (\text{A.2.31})$$

Then using the identities $\cosh(x) \equiv \frac{e^x + e^{-x}}{2}$, $\cosh(x) \equiv \cos(ix)$ and $\sinh(x) \equiv i \sin(ix)$, gives

$$\cosh(l_z) = \left(\cosh(2\theta) \cosh(2\beta) - \frac{z^2 + z^{-2}}{2} \sinh(2\theta) \sinh(2\beta) \right) \quad (\text{A.2.32})$$

Since z is any solution to $z^{2n} = 1$, the complete set of l_z is obtained from $z = e^{\pi ik/n}$ with $k = 1, \dots, n$. By the Perron-Frobenius theorem each l_z is positive for physical parameters.

The eigenvalues of z can be written more precisely as

$$\lambda = \exp \left(\frac{1}{2} \sum_{k=1}^n \pm l_{e^{i\pi k/n}} \right). \quad (\text{A.2.33})$$

A.3 Formulation

A.3.1 Local transfer matrices

In this section we provide a link between $2N \times 2N$ rotational matrices and the exponentially larger $2^N \times 2^N$ transfer matrix \mathcal{T} . To begin with we introduce *local horizontal* and *vertical bond* transfer matrices. We then express \mathcal{T} as a product of these matrices. These local transfer matrices are then expressed as Γ -matrices, thus allowing a connection to rotational matrices to be made.

Notation: Let \mathcal{T}_i denote the local horizontal bond transfer matrix that adds a horizontal bond in the i th row; $\mathcal{T}_{i(i+1)}$ be the local vertical transfer matrix for the vertical bond between the spins in i -th and $(i+1)$ -th row; Let $\mathbb{1}_2$ denote a 2×2 identity matrix, such that for $k \in \mathbb{N}$

$$\mathbb{1}_2^{\otimes k} := \underbrace{\mathbb{1}_2 \otimes \mathbb{1}_2 \otimes \dots \otimes \mathbb{1}_2}_k, \quad (\text{A.3.1})$$

that is a $2k \times 2k$ identity matrix.

For spins on a $N \times M$ lattice, we have

$$\mathcal{T}_i = \mathbb{1}_2^{\otimes i-1} \otimes \begin{pmatrix} x & 1 \\ 1 & x \end{pmatrix} \otimes \mathbb{1}_2^{\otimes N-i}, \quad (\text{A.3.2})$$

and

$$\mathcal{T}_{i(i+1)} = \mathbb{1}_2^{\otimes i-1} \otimes \begin{pmatrix} x & 0 & 0 & 0 \\ 0 & 1 & 0 & 0 \\ 0 & 0 & 1 & 0 \\ 0 & 0 & 0 & x \end{pmatrix} \otimes \mathbb{1}_2^{\otimes N-(i+1)}. \quad (\text{A.3.3})$$

In terms of local transfer matrices, \mathcal{T} is

$$\mathcal{T} = \left(\prod_i^N \mathcal{T}_i \right) \left(\prod_i^N \mathcal{T}_{i(i+1)} \right). \quad (\text{A.3.4})$$

where $N+1 = 1$.

Example A.5. In Figure A.1, we show how an extra column of spins can be added to a 3×2 model.

To write \mathcal{T}_i and $\mathcal{T}_{i(i+1)}$ in terms of Γ -matrices, we first need to express them as Pauli matrices (Equation (A.1.6)). To do this we redefine our Hamiltonian such that

$$H = \sum_{ij} \delta_{\sigma_i \sigma_j} = \sum_{ij} (2\delta_{\sigma_i \sigma_j} - 1). \quad (\text{A.3.5})$$

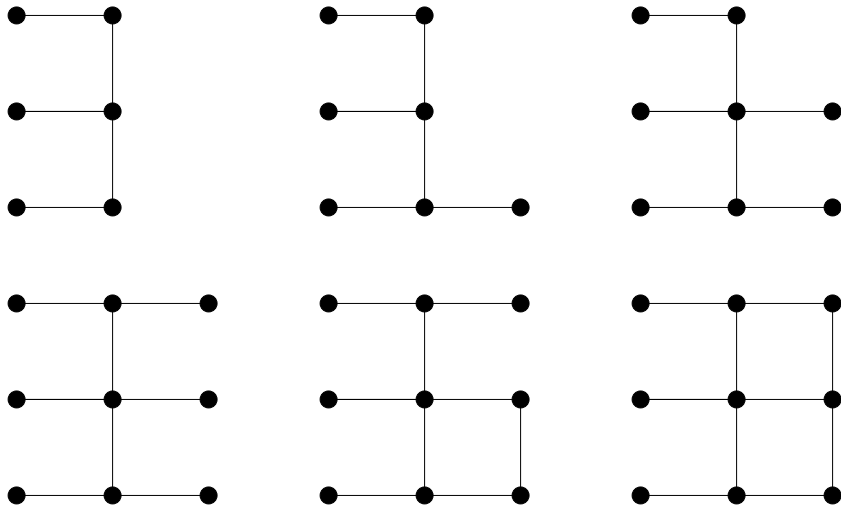


Figure A.1: Adding a sequence of horizontal and vertical bonds to a lattice

Then \mathcal{T}_i and $\mathcal{T}_{i(i+1)}$ can be written as

$$\mathcal{T}_i = \mathbb{1}_2^{\otimes i-1} \otimes \begin{pmatrix} x & x^{-1} \\ x^{-1} & x \end{pmatrix} \otimes \mathbb{1}_2^{\otimes N-i}, \quad (\text{A.3.6})$$

and

$$\mathcal{T}_{i(i+1)} = \mathbb{1}_2^{\otimes i-1} \otimes \begin{pmatrix} x & 0 & 0 & 0 \\ 0 & x^{-1} & 0 & 0 \\ 0 & 0 & x^{-1} & 0 \\ 0 & 0 & 0 & x \end{pmatrix} \otimes \mathbb{1}_2^{\otimes N-(i+1)} \quad (\text{A.3.7})$$

Proposition A.3.1. *Each local horizontal transfer matrix can be expressed in terms of Pauli matrices, as*

$$\mathcal{T}_i = \frac{x}{\cosh(\theta)} \exp(\theta \sigma_i^x) \quad (\text{A.3.8})$$

Proof. For all \mathcal{T}_i , the matrix in Equation (A.3.6), is written as

$$\begin{aligned} \begin{pmatrix} x & x^{-1} \\ x^{-1} & x \end{pmatrix} &= x \begin{pmatrix} 1 & 0 \\ 0 & 1 \end{pmatrix} + x^{-1} \begin{pmatrix} 0 & 1 \\ 1 & 0 \end{pmatrix} \\ &= x(\mathbb{1}_2) + x^{-1}\sigma^x \\ &= x(\mathbb{1}_2 + x^{-2}\sigma^x) \end{aligned} \quad (\text{A.3.9})$$

Therefore $\mathcal{T}_i = \mathbb{1}_2^{\otimes i-1} \otimes x(\mathbb{1}_2 + x^{-2}\sigma^x) \otimes \mathbb{1}_2^{\otimes N-i}$. Simplifying

$$\mathcal{T}_i = x(\mathbb{1}_2^{\otimes N} + x^{-2}\sigma_i^x) \quad (\text{A.3.10})$$

Using $(\sigma_i^x)^2 = \mathbb{1}_2^{\otimes N}$, and Taylor's series expansion,

$$\begin{aligned} e^{\theta \sigma_i^x} &= 1 + \theta \sigma_i^x + \frac{(\theta \sigma_i^x)^2}{2!} + \frac{(\theta \sigma_i^x)^3}{3!} + \frac{(\theta \sigma_i^x)^4}{4!} + \dots \\ &= \left(1 + \frac{\theta^2}{2!} + \frac{\theta^4}{4!} + \dots\right) \mathbb{1}_2^{\otimes N} + \left(\theta + \frac{\theta^3}{3!} + \dots\right) \sigma_i^x \\ &= \cosh(\theta) \mathbb{1}_2^{\otimes N} + \sinh(\theta) \sigma_i^x \end{aligned} \quad (\text{A.3.11})$$

Therefore

$$\frac{e^{\theta\sigma^x}}{\cosh(\theta)} = (\mathbb{1}_2 + x^{-2}\sigma^x) \quad (\text{A.3.12})$$

where

$$x^{-2} = \tanh(\theta). \quad (\text{A.3.13})$$

Thus by equations (A.3.12) and (A.3.10)

$$\mathcal{T}_i = \frac{xe^{\theta\sigma_i^x}}{\cosh(\theta)} \quad (\text{A.3.14})$$

□

Proposition A.3.2. *Local vertical transfer matrices $\mathcal{T}_{i(i+1)}$ can be expressed in terms of Pauli matrices, more precisely*

$$\mathcal{T}_{i(i+1)} = \exp(\beta\sigma_i^z\sigma_{i(i+1)}^z) \quad (\text{A.3.15})$$

Proof. Identities (A.1.4) and (A.1.5) are used in the following proof. Note:

$$\begin{aligned} \sigma_i^z\sigma_{i+1}^z &= (\mathbb{1}_2^{\otimes i-1} \otimes \sigma^z \otimes \mathbb{1}_2^{\otimes N-i}) (\mathbb{1}_2^{\otimes i} \otimes \sigma^z \otimes \mathbb{1}_2^{\otimes N-i-1}) \\ &= (\mathbb{1}_2^{\otimes i-1} \otimes (\sigma^z \otimes \mathbb{1}_2) \otimes \mathbb{1}_2^{\otimes N-i-1}) (\mathbb{1}_2^{\otimes i-1} \otimes (\mathbb{1}_2 \otimes \sigma^z) \otimes \mathbb{1}_2^{\otimes N-i-1}) \\ &= \mathbb{1}_2^{\otimes i-1} \otimes (\sigma^z \otimes \mathbb{1}_2) (\mathbb{1}_2 \otimes \sigma^z) \otimes \mathbb{1}_2^{\otimes N-i-1} \\ &= \mathbb{1}_2^{\otimes i-1} \otimes (\sigma^z \otimes \sigma^z) \otimes \mathbb{1}_2^{\otimes N-i-1} \end{aligned} \quad (\text{A.3.16})$$

and

$$\begin{aligned} (\sigma_i^z\sigma_{i+1}^z)^2 &= (\mathbb{1}_2^{\otimes i-1} \otimes (\sigma^z \otimes \sigma^z) \otimes \mathbb{1}_2^{\otimes N-i-1})^2 \\ &= \mathbb{1}_2^{\otimes i-1} \otimes (\sigma^z \otimes \sigma^z)^2 \otimes \mathbb{1}_2^{\otimes N-i-1} \\ &= \mathbb{1}_2^{\otimes i-1} \otimes (\mathbb{1}_2^{\otimes 2}) \otimes \mathbb{1}_2^{\otimes N-i-1} \\ &= \mathbb{1}_2^{\otimes N} \end{aligned} \quad (\text{A.3.17})$$

As $x = e^\beta$, $\mathcal{T}_{i(i+1)}$ can be written as

$$\mathcal{T}_{i(i+1)} = \mathbb{1}_2^{\otimes i-1} \otimes \begin{pmatrix} e^\beta & & & \\ & e^{-\beta} & & \\ & & e^{-\beta} & \\ & & & e^\beta \end{pmatrix} \otimes \mathbb{1}_2^{\otimes N-i-1} \quad (\text{A.3.18})$$

Using the identity $e^{\pm\beta} = \cosh(\beta) \pm \sinh(\beta)$, we have

$$\begin{pmatrix} e^\beta & & & \\ & e^{-\beta} & & \\ & & e^{-\beta} & \\ & & & e^\beta \end{pmatrix} = \cosh(\beta) \begin{pmatrix} 1 & & & \\ & 1 & & \\ & & 1 & \\ & & & 1 \end{pmatrix} + \sinh(\beta) \begin{pmatrix} 1 & & & \\ & -1 & & \\ & & -1 & \\ & & & 1 \end{pmatrix} \quad (\text{A.3.19})$$

$$= \cosh(\beta)\mathbb{1}_2^{\otimes 2} + \sinh(\beta)(\sigma^z \otimes \sigma^z) \quad (\text{A.3.20})$$

Therefore $\mathcal{T}_{i(i+1)}$ can be written as

$$\begin{aligned} \mathcal{T}_{i(i+1)} &= \mathbb{1}_2^{\otimes i-1} \otimes (\cosh(\beta)\mathbb{1}_2^{\otimes 2} + \sinh(\beta)(\sigma^z \otimes \sigma^z)) \otimes \mathbb{1}_2^{\otimes N-i-1} \\ &= \cosh(\beta) [\mathbb{1}_2^{\otimes i-1} \otimes \mathbb{1}_2^{\otimes 2} \otimes \mathbb{1}_2^{\otimes N-i-1}] + \sinh(\beta) [\mathbb{1}_2^{\otimes i-1} \otimes (\sigma^z \otimes \sigma^z) \otimes \mathbb{1}_2^{\otimes N-i-1}] \\ &= \cosh(\beta)\mathbb{1}_2^{\otimes N} + \sinh(\beta)\sigma_i^z\sigma_{i+1}^z \\ &= \exp(\beta\sigma_i^z\sigma_{i+1}^z) \end{aligned} \quad (\text{A.3.21})$$

A.3.2 Local transfer matrices and gamma matrices

Define a set of $2n$ matrices, $\gamma_1^\bullet, \gamma_2^\bullet, \dots, \gamma_{2n}^\bullet$, as follows: For all $1 \leq i \leq 2n$, define γ_i^\bullet by

$$\gamma_i^\bullet = \left(\prod_{j=1}^{k-1} \sigma_j^x \right) \sigma_k^z. \quad (\text{A.3.22})$$

if $i = 2k - 1$ is odd, else by

$$\gamma_i^\bullet = \left(\prod_{j=1}^{k-1} \sigma_j^x \right) \sigma_k^y \quad (\text{A.3.23})$$

if $i = 2k$ is even. Note: The set $\gamma_1^\bullet, \gamma_2^\bullet, \dots, \gamma_{2n}^\bullet$ is **not** a set of Γ -matrices as

$$\gamma_2^\bullet \gamma_4^\bullet \neq -\gamma_4^\bullet \gamma_2^\bullet \quad (\text{A.3.24})$$

Proposition A.3.3. *The set of $2n$ matrices, $\gamma_1^\bullet, \gamma_2^\bullet, \dots, \gamma_{2n}^\bullet$, forms a set of quasi Γ -matrices obeying*

$$(\gamma_i^\bullet)^2 = \mathbb{1}_2^{\otimes n} \quad (\text{A.3.25})$$

$$\gamma_i^\bullet \gamma_{i+1}^\bullet = -\gamma_{i+1}^\bullet \gamma_i^\bullet \quad (\text{A.3.26})$$

Proof. For all i ,

$$\begin{aligned} (\gamma_{2i}^\bullet)^2 &= (\sigma_1^x \dots \sigma_{i-1}^x) (\sigma_i^y) (\sigma_1^x \dots \sigma_{i-1}^x) (\sigma_i^y) \\ &= (\sigma_1^x \sigma_1^x) \dots (\sigma_{i-1}^x \sigma_{i-1}^x) (\sigma_i^y \sigma_i^y) \\ &= \mathbb{1}_2^{\otimes n} \end{aligned} \quad (\text{A.3.27})$$

$$\begin{aligned} (\gamma_{2i-1}^\bullet)^2 &= (\sigma_1^x \dots \sigma_{i-1}^x) (\sigma_i^z) (\sigma_1^x \dots \sigma_{i-1}^x) (\sigma_i^z) \\ &= (\sigma_1^x \sigma_1^x) \dots (\sigma_{i-1}^x \sigma_{i-1}^x) (\sigma_i^z \sigma_i^z) \\ &= \mathbb{1}_2^{\otimes n} \end{aligned} \quad (\text{A.3.28})$$

Also

$$\begin{aligned} \gamma_{2i}^\bullet \gamma_{2i-1}^\bullet &= (\sigma_1^x \dots \sigma_{i-1}^x \sigma_i^y) (\sigma_1^x \dots \sigma_{i-1}^x \sigma_i^z) \\ &= (\sigma_1^x \sigma_1^x) \dots (\sigma_{i-1}^x \sigma_{i-1}^x) (\sigma_i^y \sigma_i^z) \\ &= \sigma_i^y \sigma_i^z, \end{aligned} \quad (\text{A.3.29})$$

and therefore

$$\begin{aligned} \gamma_{2i-1}^\bullet \gamma_{2i}^\bullet &= (\sigma_1^x \dots \sigma_{i-1}^x \sigma_i^z) (\sigma_1^x \dots \sigma_{i-1}^x \sigma_i^y) \\ &= (\sigma_1^x \sigma_1^x) \dots (\sigma_{i-1}^x \sigma_{i-1}^x) (\sigma_i^z \sigma_i^y) \\ &= \sigma_i^z \sigma_i^y \\ &= -\sigma_i^y \sigma_i^z \quad (\text{by A.1.12}) \\ &= -\gamma_{2i}^\bullet \gamma_{2i-1}^\bullet \end{aligned} \quad (\text{A.3.30})$$

Proposition A.3.4. For all $1 \leq i \leq 2n$,

$$\gamma_{2i+1}^\bullet \gamma_{2i}^\bullet = \sigma_i^z \sigma_{i+1}^z \sqrt{-1} \quad (\text{A.3.31})$$

Proof.

$$\begin{aligned} \gamma_{2i+1}^\bullet \gamma_{2i}^\bullet &= (\sigma_1^x \cdots \sigma_i^x \sigma_{i+1}^z) (\sigma_1^x \cdots \sigma_{i-1}^x \sigma_i^y) \\ &= (\sigma_1^x \sigma_1^x) \cdots (\sigma_{i-1}^x \sigma_{i-1}^x) (\sigma_i^x \sigma_{i+1}^z \sigma_i^y) \\ &= \sigma_i^x \sigma_i^y \sigma_{i+1}^z \\ &= (\mathbb{1}_2^{\otimes i-1} \otimes \sigma^x \sigma^y \otimes \mathbb{1}_2^{\otimes n-i}) \sigma_{i+1}^z \\ &= (\mathbb{1}_2^{\otimes i-1} \otimes \sqrt{-1} \begin{pmatrix} 1 & 0 \\ 0 & 1 \end{pmatrix} \otimes \mathbb{1}_2^{\otimes n-i}) \sigma_{i+1}^z \\ &= \sigma_i^z \sigma_{i+1}^z \sqrt{-1} \end{aligned}$$

□

Proposition A.3.5. For all $1 \leq i \leq 2n$,

$$\gamma_{2i}^\bullet \gamma_{2i-1}^\bullet = \sigma_i^x \sqrt{-1} \quad (\text{A.3.32})$$

Proof.

$$\begin{aligned} \gamma_{2i}^\bullet \gamma_{2i-1}^\bullet &= (\sigma_1^x \cdots \sigma_{i-1}^x \sigma_i^y) (\sigma_1^x \cdots \sigma_{i-1}^x \sigma_i^z) \\ &= \sigma_i^y \sigma_i^z \\ &= \sigma_i^x \sqrt{-1} \end{aligned}$$

□

By Propositions A.3.4 and A.3.5, \mathcal{T}_i and $\mathcal{T}_{i(i+1)}$ (equations A.3.8 and A.3.15 respectively) are expressed as

$$\mathcal{T}_i = k e^{-i\theta \gamma_{2i}^\bullet \gamma_{2i-1}^\bullet} \quad (\text{A.3.33})$$

where $k = x / \cosh(\theta)$, and

$$\mathcal{T}_{i(i+1)} = e^{-i\phi \gamma_{2i+1}^\bullet \gamma_{2i}^\bullet} \quad (\text{A.3.34})$$

A.3.3 Rotational and transfer matrices

For any given set of Γ -matrices define function

$$S : \{W_{ab}(\theta) | a \neq b \in 1, 2, \dots, 2n; \theta \text{ angle}\} \rightarrow M_{2^n}(\mathbb{C}) \quad (\text{A.3.35})$$

where

$$S(W_{ab}(\theta)) = \cos(\theta/2) - \sin(\theta/2) \Gamma_a \Gamma_b. \quad (\text{A.3.36})$$

Proposition A.3.6. The function $S(W_{ab}(\theta))$ is also expressed in the form

$$S(W_{ab}(\theta)) = \exp\left(-\frac{1}{2}\theta \Gamma_a \Gamma_b\right). \quad (\text{A.3.37})$$

Proof. Using $(\Gamma_a \Gamma_b)^2 = \Gamma_a \Gamma_b \Gamma_a \Gamma_b = -\Gamma_a \Gamma_a \Gamma_b \Gamma_b = -\mathbb{1}_2$, it follows that

$$\begin{aligned}
S(W_{ab}(\theta)) &= \exp\left(-\frac{1}{2}\theta \Gamma_a \Gamma_b\right) \\
&= 1 + \left(-\frac{1}{2}\theta \Gamma_a \Gamma_b\right) + \frac{\left(-\frac{1}{2}\theta \Gamma_a \Gamma_b\right)^2}{2!} + \frac{\left(-\frac{1}{2}\theta \Gamma_a \Gamma_b\right)^3}{3!} + \dots \\
&= \left(1 - \frac{\left(-\frac{1}{2}\theta\right)^2}{2!} + \dots\right) + \left(\left(-\frac{1}{2}\theta\right) + \frac{\left(-\frac{1}{2}\theta\right)^3}{3!} + \dots\right) \Gamma_a \Gamma_b \\
&= \cos(\theta/2) - \sin(\theta/2) \Gamma_a \Gamma_b
\end{aligned}$$

□

Proposition A.3.7. *For a fixed width N , the transfer matrix \mathcal{T} is*

$$\mathcal{T} = k^N \prod_{j=1}^N S(W_{2j \ 2j-1}(2i\theta)) S(W_{2j+1 \ 2j}(2i\phi)). \quad (\text{A.3.38})$$

where θ and ϕ distinguish between horizontal and vertical bonds respectively.

Proof. Using equations (A.3.33) and (A.3.34), we have

$$\mathcal{T}_j = k \exp(-i\theta \gamma_{2j}^\bullet \gamma_{2j-1}^\bullet) \quad (\text{A.3.33})$$

$$= k S(W_{2j \ 2j-1}(2i\theta)). \quad (\text{A.3.39})$$

and

$$\mathcal{T}_{j(j+1)} = e^{-i\phi \gamma_{2j+1}^\bullet \gamma_{2j}^\bullet} \quad (\text{A.3.34})$$

$$= S(W_{2j+1 \ 2j}(2i\phi)) \quad (\text{A.3.40})$$

Recall Equation (A.3.4).

$$\mathcal{T} = k^N \left(\prod_{j=1}^N S(W_{2j \ 2j-1}(2i\theta)) \right) \left(\prod_{j=1}^N S(W_{2j+1 \ 2j}(2i\phi)) \right) \quad (\text{A.3.41})$$

Note, we use periodic boundary conditions. That is, let $N+1=0$ such that $S(W_{2j+1 \ 2j}(2i\phi)) = S(W_{1 \ 2N}(2i\phi))$. Also note that we could add a horizontal bond then a vertical bond, then horizontal etc. In that case Equation (A.3.41) simplifies to

$$\mathcal{T} = k^N \left(\prod_i^N S(W_{2i \ 2i-1}(2i\theta)) S(W_{2i+1 \ 2i}(2i\phi)) \right). \quad (\text{A.3.42})$$

□

For convenience let

$$S(W_{a_j b_j}(2i\theta_j)) = S(W_{2j \ 2j-1}(2i\theta)) S(W_{2j+1 \ 2j}(2i\phi)) \quad (\text{A.3.43})$$

where θ_j distinguishes between horizontal and vertical bonds. Equation (A.3.38) is now written as

$$\mathcal{T} = k^N \prod_j^{2N} S(W_{a_j b_j}(2i\theta_j)). \quad (\text{A.3.44})$$

The transfer matrix as a realisation of a rotation

Proposition A.3.8. For any product of $S(W_{ab})$, by conjugating we find the relationship

$$\prod_j S(W_{a_j b_j}(\theta_j)) \rightsquigarrow S\left(\prod_j W_{a_j b_j}(\theta_j)\right) \quad (\text{A.3.45})$$

Proof. Let $W = W_{ab}(\theta)$, and $W' = W_{a'b'}(\theta')$. Then for

$$S(W)\Gamma_x S^{-1}(W) = \cos(\theta)\Gamma_a + \sin(\theta)\Gamma_b = R_{ab}(\theta)(\Gamma_x) \quad (\text{A.3.46})$$

we have

$$S(W')(S(W)\Gamma_x S^{-1}(W))S^{-1}(W') = S(W')R_{ab}(\theta)(\Gamma_x)S^{-1}(W') \quad (\text{A.3.47})$$

$$= R_{a'b'}(\theta)\left(R_{ab}(\theta)(\Gamma_x)\right) \quad (\text{A.3.48})$$

and

$$S(W')(S(W)\Gamma_x S^{-1}(W))S^{-1}(W') = (S(W')S(W))\Gamma_x(S^{-1}(W)S^{-1}(W')) \quad (\text{A.3.49})$$

$$= S(W'W)\Gamma_x S^{-1}(W'W). \quad (\text{A.3.50})$$

□

So

$$\mathcal{T} = k^N \prod_{ab} S(W_{ab}(\theta_{ab})) \rightsquigarrow S\left(\prod_{ab} W_{ab}(\theta_{ab})\right) \quad (\text{A.3.51})$$

Claim: \mathcal{T} is a “realisation” of a rotation, given that

$$S(W_{ab}(\theta))\Gamma_a S^{-1}(W_{ab}(\theta)) = \cos \theta \Gamma_a + \sin \theta \Gamma_b \quad (\text{A.3.52})$$

and

$$S(W_{ab}(\theta))\Gamma_b S^{-1}(W_{ab}(\theta)) = \cos \theta \Gamma_b - \sin \theta \Gamma_a \quad (\text{A.3.53})$$

Proposition A.3.9.

$$S(W_{ab}(\theta))\Gamma_a S^{-1}(W_{ab}(\theta)) = \cos \theta \Gamma_a + \sin \theta \Gamma_b \quad (\text{A.3.54})$$

Proof. As $S(W_{ab}(\theta)) = e^{-\frac{1}{2}\theta\Gamma_a\Gamma_b}$, and $S^{-1}(W_{ab}(\theta)) = e^{\frac{1}{2}\theta\Gamma_a\Gamma_b}$

$$\begin{aligned} S(W_{ab}(\theta))\Gamma_a S^{-1}(W_{ab}(\theta)) &= \left(\cos \frac{\theta}{2} - \sin \frac{\theta}{2}\Gamma_a\Gamma_b\right)\Gamma_a\left(\cos \frac{\theta}{2} + \sin \frac{\theta}{2}\Gamma_a\Gamma_b\right) \\ &= \left(\cos \frac{\theta}{2}\Gamma_a + \sin \frac{\theta}{2}\Gamma_b\right)\left(\cos \frac{\theta}{2} + \sin \frac{\theta}{2}\Gamma_a\Gamma_b\right) \\ &= \left(\cos^2 \frac{\theta}{2} - \sin^2 \frac{\theta}{2}\right)\Gamma_a + \left(2\cos \frac{\theta}{2}\sin \frac{\theta}{2}\right)\Gamma_b \\ &= \cos(\theta)\Gamma_a + \sin(\theta)\Gamma_b \\ &= \Gamma'_a \end{aligned} \quad (\text{A.3.55})$$

□

Proposition A.3.10.

$$S(W_{ab}(\theta)) \Gamma_b S^{-1}(W_{ab}(\theta)) = \cos \theta \Gamma_b - \sin \theta \Gamma_a \quad (\text{A.3.56})$$

Proof.

$$\begin{aligned} S(W_{ab}(\theta)) \Gamma_b S^{-1}(W_{ab}(\theta)) &= \left(\cos \frac{\theta}{2} - \sin \frac{\theta}{2} \Gamma_a \Gamma_b \right) \Gamma_b \left(\cos \frac{\theta}{2} + \sin \frac{\theta}{2} \Gamma_a \Gamma_b \right) \\ &= \left(\cos \frac{\theta}{2} \Gamma_b - \sin \frac{\theta}{2} \Gamma_a \right) \left(\cos \frac{\theta}{2} + \sin \frac{\theta}{2} \Gamma_a \Gamma_b \right) \\ &= \left(\cos^2 \frac{\theta}{2} - \sin^2 \frac{\theta}{2} \right) \Gamma_b - \left(2 \cos \frac{\theta}{2} \sin \frac{\theta}{2} \right) \Gamma_a \\ &= \cos(\theta) \Gamma_b - \sin(\theta) \Gamma_a \\ &= \Gamma'_b \end{aligned} \quad (\text{A.3.57})$$

□

A.3.4 Eigenvalues of $S(W)$

Our next task is to connect eigenvalues of proper rotations W to the eigenvalues of $S(W)$. Note the eigenvalues of the rotational matrix are explained in Section A.2.1.

Proposition A.3.11. *The spectrum of $S(W_{ab}(\theta))$ is $e^{\frac{\pm i\theta}{2}}$, of which there are 2^{n-1} copies.*

Proof. Let $\Gamma = \gamma^\bullet$, then

$$\begin{aligned} S(W_{ab}(\theta)) &= \exp\left(-\frac{1}{2}\theta \Gamma_a \Gamma_b\right) \\ &= \exp\left(-\frac{1}{2}\theta \sigma_a^z \sigma_a^y\right) \quad (\text{by A.3.29}) \\ &= \exp\left(\frac{i}{2}\theta \sigma_a^x\right) \quad (\text{by A.1.13}) \\ &= \mathbb{1}_2^{\otimes a-1} \otimes \exp\left(\frac{i}{2}\theta \sigma^x\right) \otimes \mathbb{1}_2^{\otimes N-a} \end{aligned} \quad (\text{A.3.58})$$

and this holds true for all a, b , where $\Gamma_a \Gamma_b = \sigma_a^z \sigma_a^y$. The spectrum of Equation (A.3.58) is the same the spectrum of $\mathbb{1}_2^{\otimes a-1} \otimes \exp\left(\frac{i}{2}\theta \mathbb{1}_2\right) \otimes \mathbb{1}_2^{\otimes N-a}$. ie. $e^{i\frac{\theta}{2}}$ and $e^{-i\frac{\theta}{2}}$ □

A.3.5 The indeterminate solution

The largest eigenvalue for \mathcal{T} , is

$$\lambda_0 = \exp\left(\frac{1}{2} \sum_{k=1}^n +l_{e^{i\pi k/n}}\right) \quad (\text{A.3.59})$$

If the lattice is M sites long and with a fixed width N , then

$$Z = \text{Tr}(\mathcal{T}^M) \quad (\text{A.3.60})$$

$$= \sum \lambda^M \quad (\text{A.3.61})$$

$$= \lambda_0^m \left(1 + \sum_{i \neq 0} \left(\frac{\lambda_i}{\lambda_0} \right)^M \right) \quad (\text{A.3.62})$$

Then for large M

$$Z \sim \lambda_0^M \quad (\text{A.3.63})$$

The free energy density $f = \frac{-k_B T}{NM} \ln Z$, can then be approximated as

$$f \sim \frac{-k_B T}{N} \ln \lambda_0. \quad (\text{A.3.64})$$

Equation A.3.64 becomes an equality in the large M limit.

Using

$$\sinh(2\beta) = \sinh(2\theta)^{-1} \quad \text{and} \quad \coth(2\beta) = \cosh(2\theta), \quad (\text{A.3.65})$$

in isotropic case $\beta = \theta$ Equation (A.2.32) is then

$$\cosh(l_z) = \coth(2\beta) \cosh(2\beta) - \frac{z^2 + z^{-2}}{2}. \quad (\text{A.3.66})$$

To find l_z we need to find

$$l_z = \cosh^{-1} \left(\coth(2\beta) \cosh(2\beta) - \frac{z^2 + z^{-2}}{2} \right). \quad (\text{A.3.67})$$

Using standard trigonometric identities

$\cosh^{-1} x = \ln(x + \sqrt{x^2 - 1}) = \ln(x) + \ln(1 + \sqrt{1 - x^{-2}})$ and

$\pi \ln(1 + \sqrt{1 - t^2}) = \int_0^\pi \ln(1 + t \cos w) .dw$, leads to

$$\cosh^{-1} x = \ln(x) + \frac{1}{\pi} \int_0^\pi \ln(1 + x \cos y) .dy \quad (\text{A.3.68})$$

$$= \frac{1}{\pi} \int_0^\pi dy \ln(2x - 2 \cos(y)). \quad (\text{A.3.69})$$

So

$$l_z = \frac{1}{\pi} \int_0^\pi dy \ln(2(\coth(2\beta) \cosh(2\beta) - \frac{z^2 + z^{-2}}{2}) - 2 \cos(y)) \quad (\text{A.3.70})$$

Substitute l_z into Equation (A.3.59), then

$$\ln \lambda_0 = \frac{1}{2} \sum_{k=1}^n \frac{1}{\pi} \int_0^\pi dy \ln(2 \coth(2\beta) \cosh(2\beta) - 2 \cos(2\pi k/n) - 2 \cos(y)) \quad (\text{A.3.71})$$

From this point, we have a choice of proceeding in two directions. Either we take the large N limit, (which converts the sum to a integral) or we discretise the integral to a sum over M terms using:

$$\int_0^\pi f(y) dy \sim \frac{\pi}{M} \sum_{r=1}^M f(\pi r/M) \quad (\text{A.3.72})$$

A.3.6 Thermodynamic limit solution

We choose to discretise the integral, for which we get

$$\ln \lambda_0 = \frac{1}{2} \sum_{k=1}^N \frac{1}{M} \sum_{r=1}^M \ln(2 \coth(2\beta) \cosh(2\beta) - 2 \cos(2\pi k/N) - 2 \cos(\pi r/M)) \quad (\text{A.3.73})$$

$$Z_{MN} = \prod_{r=1}^M \prod_{s=1}^N \left\{ 1 - \frac{1}{2} K \left(\cos \frac{2\pi r}{M} + \cos \frac{2\pi s}{N} \right) \right\}, \quad (\text{A.3.74})$$

where

$$K = \frac{\exp(-2\beta) \{1 - \exp(-4\beta)\}}{\{1 + \exp(-4\beta)\}^2} \quad (\text{A.3.75})$$

In Section 1.2.1, we continue with further analysis of this solution.

Appendix B

Code

In this section, the code that computes the exact partition functions of Chapter 3 is explained. We begin this section with a discussion on the problems associated to such computations.

Consider the $5 \times 5 \times 10'$ Ising model result given in Figure 3.10(b) (Page 47), for example. (The exact partition function for this result is presented in Appendix E). Computing the partition function Z_G on this lattice by enumerating over all 2^{250} states would take at least 10^{62} years! Thus, it is not yet possible to compute Z_G in a reasonable time frame using say, a brute-force enumeration program. On the other hand, suppose we use the transfer matrix method described in Section 2.2.1. The size of the transfer matrix is $2^{25} \times 2^{25}$, where each element is a large polynomial. This requires using much more memory than is currently available.

So we introduce some transfer matrix organisation, that makes the computation possible. Note, we shall use the notation from Section 2.1 to explain our method.

B.1 Hamiltonian symmetries

Recall Section 2.2.2, we use the layer transfer matrix to add an extra layer of spins to a lattice. For example in Figure B.1 step **1**, we have the $4 \times 4 \times L$ lattice. Then by layer transfer matrix computation we have the $4 \times 4 \times (L+1)$ lattice, ie **1** \rightarrow **2**. The white spins in the figure are external outgoing spins, and the black ones are internal.

Consider the computation

$$D^T \mathcal{T}^{L+1} = (D^T \mathcal{T}^L) \mathcal{T}, \quad (\text{B.1.1})$$

where D is a column vector such that $D^T \mathcal{T}^L$ is then just the partition vector indexed by the external spins of \mathcal{T}^L . That is $Z_G^\xi = D^T \mathcal{T}^L$.

We compute the symmetries of $\Omega_\mathcal{E}$ that are equivalent by translations and spin symmetries of the Hamiltonian. We denote the set of representatives of each equivalence class $[\Omega_\mathcal{E}]$.

It is only necessary to store the $(Z_G^\xi)_i$ for representatives of each equivalence class, since $(Z_G^\xi)_i = (Z_G^\xi)_j$ if i, j are in the same equivalence class. Let $[Z_G^\xi]$ be the partition vector indexed by $[\Omega_\mathcal{E}]$

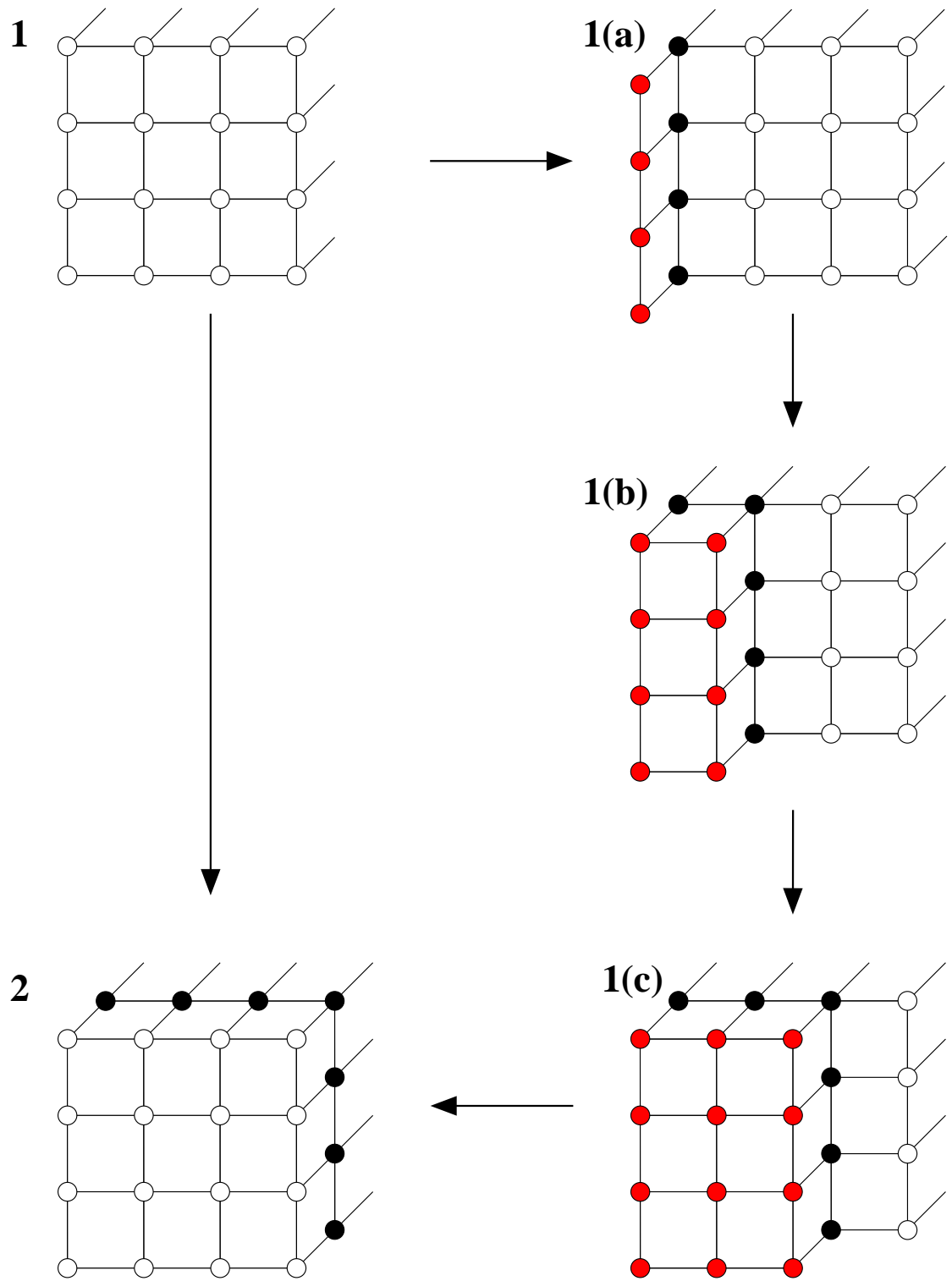


Figure B.1: Showing two possible routes that an extra layer is added to the $4 \times 4 \times L$ lattice (1). The resultant is a $4 \times 4 \times (L + 1)$ lattice (2).

(the set of configuration representatives). Then for each $[i] \in [\Omega_{\mathcal{E}}]$ we have

$$(D^T \mathcal{T}^{L+1})_{[i]} = \sum_{j \in \Omega_V} (Z_G^{\mathcal{E}})_j \mathcal{T}_{[i],j}. \quad (\text{B.1.2})$$

Back to our $5 \times 5 \times 10'$ example. For this, we find $|\Omega_{\mathcal{E}}| = 86056$. The required number of vector multiplications is reduced, but still not enough to compute Z_G in a reasonable time frame.

B.2 Transfer matrix symmetries

We now describe an alternate method to add an extra layer of spins. This method is graphically outlined in Figure B.1. We add the extra layer by following steps $\mathbf{1} \rightarrow \mathbf{1(a)} \rightarrow \mathbf{1(b)} \rightarrow \mathbf{1(c)} \rightarrow \mathbf{2}$.

For a lattice with N_z layers of $N_x \times N_y$ spins per layer. We divide each layer into a subset column spins. That is $V = V_1 \cup V_2 \cup \dots \cup V_{N_y}$. For example in Figure B.2 we have divided a layer of the $4 \times 4 \times L$ lattice into 4 columns of spins V_1, V_2, V_3, V_4 .

The partition vector is written in the form

$$Z_G^V := Z_G^{V_1, V_2, \dots, V_{N_y}}$$

We denote the added layer of spins as $V' = V'_1 \cup \dots \cup V'_{N_y}$. For the intermediate steps such as $\mathbf{1} \rightarrow \mathbf{1(a)}$ we have

$$Z_G^{V_2, \dots, V_{N_y}, V'_1} = Z_G^{V_1, V_2, \dots, V_{N_y}} \mathcal{T}'.$$

and for $\mathbf{1(a)} \rightarrow \mathbf{1(b)}$

$$Z_G^{V'_3, \dots, V_{N_y}, V'_1, V'_2} = Z_G^{V_2, \dots, V_{N_y}, V'_1} \mathcal{T}''.$$

Here \mathcal{T}' is a transfer matrix where the only interactions are between spins in V_1 and V'_1 , and the internal interaction in V' , see Figure B.3 for example. The solid lines represent interactions that are added, while the dashed lines are to show spacial awareness. \mathcal{T}'' is the same as \mathcal{T}' , but also includes the interaction between V'_1 and V'' . By the same method the rest of the layer can be built.

The dimension of \mathcal{T}' and \mathcal{T}'' is $Q^{N_x N_y} \times Q^{N_x N_y}$ and $Q^{N_x N_y} \times Q^{N_x(N_y-1)}$ respectively. In general, suppose we label $\mathcal{T}', \mathcal{T}'' \dots$ as $\mathcal{T}^1, \mathcal{T}^2, \dots, \mathcal{T}^{N_y}$, then each \mathcal{T}^i is a $Q^{N_x N_y} \times Q^{N_x(N_y-i)}$ matrix. Further if we only consider only the equivalence classes, ie. $[\Omega_{V'_1, \dots, V'_i}]$ then the required number of dot product computations is reduced even further.

To highlight this reduction we use the ‘‘big Oh’’ notation (see [84]). Let N be the number of terms in a dot product. Let $O(N)$ be the total number of polynomial product computations required to add a layer to the lattice.

So for example, for each layer in the $5 \times 5 \times 10$ computation, $O(N) = 86056 \cdot 2^{25} \approx 2.89 \times 10^{12}$. By our method

$$O(N) = 4 \cdot 2^{25} + 37 \cdot 2^{20} + 570 \cdot 2^{15} + 9511 \cdot 2^{10} + 86056 \cdot 2^5 \approx 2.04 \times 10^8.$$

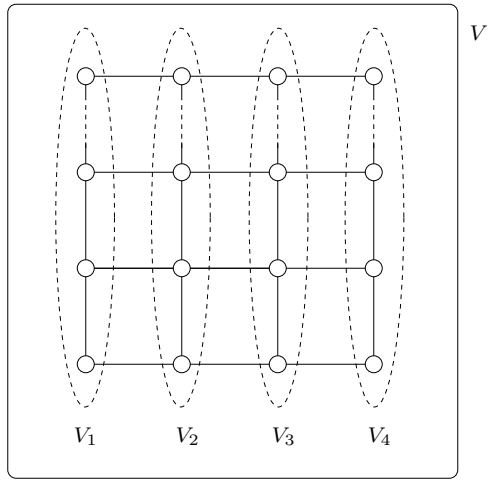


Figure B.2: The spins on a layer of $4 \times 4 \times L$ lattice are organised into columns and the sets labelled V_1, \dots, V_4

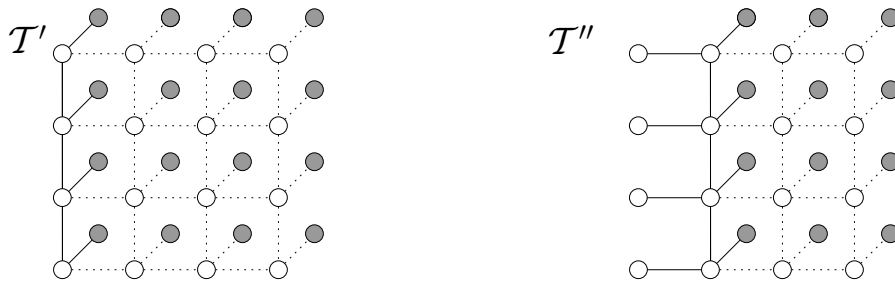


Figure B.3: Examples of local transfer matrices

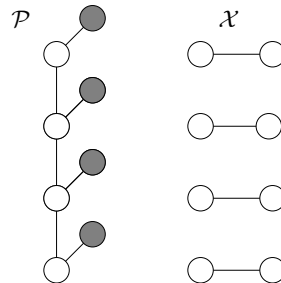


Figure B.4: A transfer matrix used in the code

Computationally, we do not even need create \mathcal{T}^i 's of this size. We replace each \mathcal{T}^i with $\mathcal{T}_{\mathcal{P}}$ and $\mathcal{T}_{\mathcal{X}}$, where \mathcal{P} is a “comb” graph and \mathcal{X} a parallel line graph (see Figure B.4) for example.

The following code extract shows how we use $\mathcal{T}_{\mathcal{P}}$.

```

1 int h = 0;
2 for (int i = 0; i < ZNEW.size(); i++){
3     int k = 0;
4     for (int j = 0; j < ZG.size(); j++){
5         ZNEW[i] = ZNEW[i] + ZG[j]*TP[h][k];
6         k++;
7         if(k == QCOL)
8             k=0;
9     }
10    h++;
11    if(h == QCOL)
12        h=0;
13 }

```

In this code segment ZNEW denotes $Z_{\mathcal{G}}^{V_1, V_2, V_3, V_4}$; ZG denotes $Z_{\mathcal{G}}^{V_2, V_3, V_4, V'_1}$; TP denotes $\mathcal{T}_{\mathcal{P}}$; QCOL = Q^{Nx} (the number of spin configurations per column).

The $5 \times 5 \times 19'$ in Figure 3.10(c) (Page 47, is found by computing the dot product on the $5 \times 5 \times 10'$ partition vector with itself. In general, we have

$$Z_{\mathcal{G}} = \sum_{\sigma \in [\Omega_V]} \left(m_{\sigma}([Z_{\mathcal{G}}^V]_i \cdot ([Z_{\mathcal{G}}^V]_i / x^{H(\sigma)})) \right), \quad (\text{B.2.1})$$

where m_{σ} is the multiplicity of each equivalence class, and the common edges $x^{H(\sigma)}$ between the two is factored out.

B.2.1 Spin configurations

In Section 2.1, we define the totally ordered set. In this section, we give an example of how the set of spin configurations can be mapped to a totally ordered set.

Let Ω_V be a set of spin configurations of Σ_V indexed by totally ordered set V . Note for fixed Q , $|\Omega_V| = Q^{|V|}$.

$$T : \Omega \rightarrow \{1 \dots Q^{|\Sigma|}\} \quad (\text{B.2.2})$$

$$T(\sigma) = 1 + \sum_{i=1}^{|\Omega|} Q^{i-1}(\sigma_i - 1), \quad (\text{B.2.3})$$

where $\sigma \in \Omega$, and $\sigma_i \in \{1, \dots, Q\}$ is the value of the i -th spin.

B.3 Large numbers, memory

The GNU general multiple precision (GMP) library is used for handling the large coefficients involved in our calculations.

We use the gnu C++ code profiling tool *gprof*, to analyse our code at run-time. By profiling the code, we identify where the majority of CPU speed and memory is used.

Our programs are computed on the AMD Opteron processor 6134, which has 2300Mhz CPU speed and 64GB ram available. The 2-state $5 \times 5 \times 10$ takes 121 hours to complete and requires 19GB of memory. The 2-state $4 \times 6 \times 10$ takes 28 hours to run and requires 10GB of memory.

Appendix C

Checking results

Here we describe the methods used to check our results. We use: series expansion; checking all possible configuration are accounted for; the structure of the code and the use of recursive functions; checks against published results;

[81, 10] and an alternate code is also used from comparison [59].

The partition function Z can be written in polynomial form

$$Z = a_N x^N + a_{N-1} x^{N-1} + \dots + a_1 x^1 + a_0 x^0 \quad (\text{C.0.1})$$

where $x = \exp(\beta)$.

We first check that all spin configurations are accounted for in the partition function. That is, if

$$\sum_i^N a_i = Q^{N_x N_y N_z}.$$

Recall Section 1.2.2, certain terms of this polynomial can be found using a *series expansion* method [50, 99].

Series expansion involves permuting the suitable spin states from a known “ground-state” configuration. A *ground-state* configuration is where the Hamiltonian and the number of equivalent configurations is easily obtained. For example, configuration with all spins aligned in the same direction (Figure C.1(a)). If we allow Q states, then the number of equivalent configurations is also Q .

Another ground-state would be one where its spin is pointing in a different direction to its nearest neighbour (see Figure C.1(b) for example). However this ground-state is harder to calculate the larger Q is.

The next largest (smallest) term is given by changing a spin’s configuration so that the change in energy is a minimum (maximum) (Figures C.1(c) and C.1(d)). By symmetry, we can find the number of equivalent configurations.

We continue to change spin configurations until the number of symmetric states is too large to calculate.

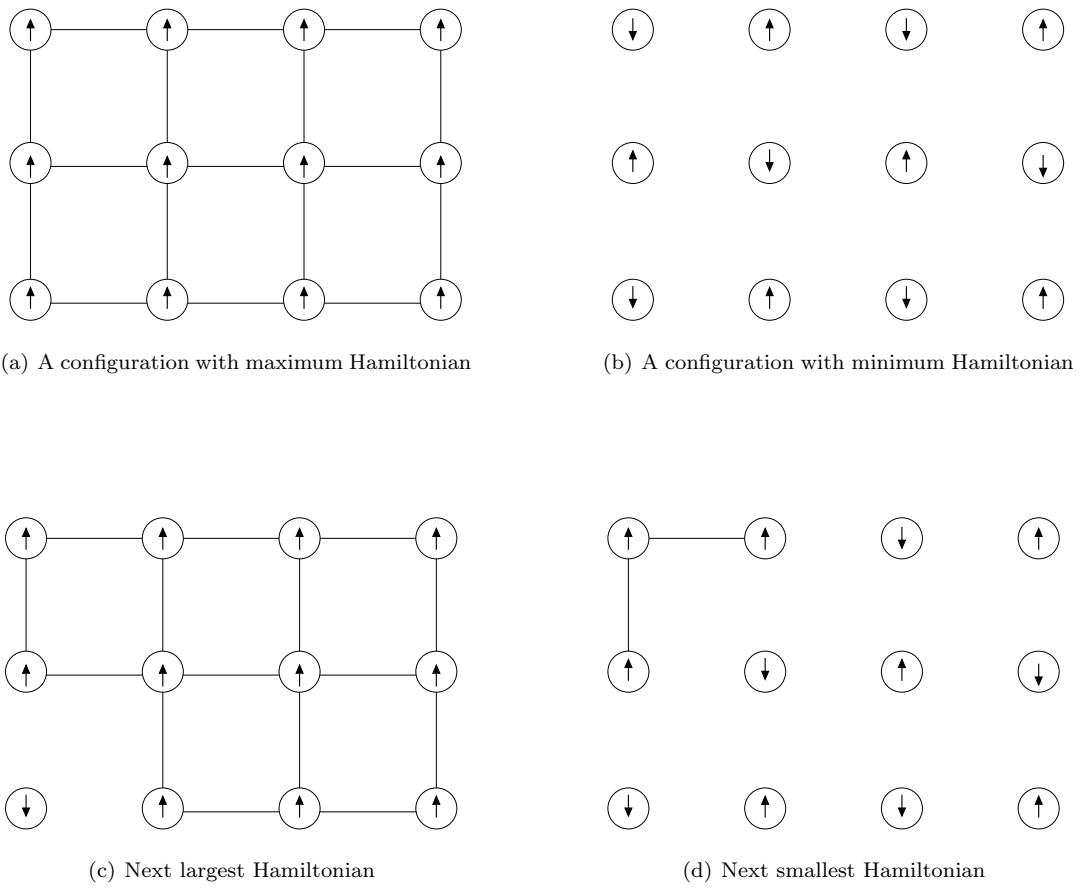


Figure C.1: 3×4 lattice, showing various states of the system

For a lattice spin system with N spins say Σ_S , we check the sum of the coefficients of Z is $|\Omega_S| = Q^N$

Using recursive functions and changing a minimal number of variables, Partition functions for over 2000 finite sized systems are found. Code variables are N_x, N_y, N_z, Q -states and boundary conditions. The probability of that there is an error in the code is significantly reduced, because the same code is used to produce known and unknown results with a minimal change in code.

Recall from Section 2.2.1. We fix the code so that the partition function Z is found using

$$Z = \text{Tr}(\mathcal{T}^{N_z}) \tag{C.0.2}$$

where N_z is the number of layers of the system. The size of \mathcal{T} depends on the size and dimension of the system, but is independent of the boundary conditions. In our code, \mathcal{T} is fixed to be a $Q^{N_x N_y}$ square matrix. If we require a 2d system then we set either $N_x = 1$ or $N_y = 1$. Similarly for a 1d system set $N_x = N_y = 1$.

Consider a $N_x \times N_y \times N_z$ and $N_y \times N_x \times N_z$ lattice. They both have the same partition function, but by using comb and parallel line graphs, their computation is different. That is, the elements of the local transfer matrices are different, as are the number of local transfer matrices. Similarly alternating boundary conditions, between open and periodic involves a changes in the elements of the transfer matrix. Thus another check is made by comparing suitable partition functions. A

shell script is used to compare all possible equivalent partition functions.

The 1d models are checked exactly using the indeterminate solution.

Previously published exact partition function results, by Pearson, Bhanot and Sastry and Martin (see §1.2.5 for details and references), are reproduced by our program.

A series of other programs have been created to calculate partition functions using different calculation techniques. Each has their limitations on size and/or time. The results produced are used to compare the results of the final program. In this section we describe a few of the programs made, and discuss their limitations.

The first program is known as a brute force program. This program permutes through all possible configurations. It calculates the Hamiltonian at each configuration, and simply adds the term to the polynomial. Although very little memory is required, we find that the program takes a too long for systems with more than 2^{50} possible configurations.

Our next program is known as a brute force transfer matrix program. The program computes matrix multiplication. This time the program is limited by the available memory of the computer. The size of the transfer matrices is a real restriction for computing larger systems, however more results are produced compared to the brute force program.

Next is a program that uses local transfer matrices. This produces significantly more results than the above two programs, but again memory is a restriction. The next program is an adaption of the previous one. Symmetry is used to identify alike elements in local transfer matrices. These elements are stored in a separate array, and the transfer matrix elements are changed to pointers. Thus reducing the memory required. A program to optimise polynomial arithmetic is then used. All these programs build up to the final program, producing larger lattices at each stage.

We also use P Martin's code [59], which calculates the partition function in a completely different manner. This is also used as a check.

Appendix D

Finding Zeros

The algorithm used to find all the roots of the partition function Z_G , is a combination of the Newton-Raphson method (NR), and polynomial division [59]. All roots are found to a minimum precision of $\epsilon = 1^{-300}$, and L is the number of initial NR iterations.

The NR algorithm is as follows:

$$x_{i+1} = x_i - \frac{f(x_i)}{f'(x_i)} \quad (\text{D.0.1})$$

for $0 < i < L$. For our program setting $L = 1000$ is usually sufficient. We iterate the above L times then check if $|x_L - x_{L-1}| < \epsilon$. If so, then accept x_L as a root. If not, then repeat the iteration for another L steps.

Let $z_1 = x_L$. By polynomial division, z_1 is factored out. That is $Z_G(x) = f_1(x)(x - z_1)$. Due to rounding errors, we find there will be a small remainder r_1 . The program checks $r_1 \leq \epsilon$. If $r_1 > \epsilon$, then we increase the precision of the program, by increasing L . Also if z_1 is a root then its complex conjugate is also a root. The iteration (D.0.1), is then repeated for $f_1(x)$, until we have Z_G expressed in terms of its roots, ie. $Z_G = (x - z_1)(x - z_2) \dots$

We reduce the impact of rounding errors as follows. The NR-algorithm finds real roots regardless of whether the initial guess is a real or complex number. However, if we find all real roots using a real initial guess, then the overall rounding error is significantly reduced.

Appendix E

Example of exact partition function

In this section we present an exact partition function for a $Q = 2$ -state 3d Potts model on a $5 \times 5 \times 10$ lattice.

Table E.1: Exact partition function for Ising model on a $5 \times 5 \times 10'$ lattice

H	Coefficient
100	2470
101	126000
102	3420000
103	63402800
104	893302500
105	10124284660
106	95912238200
107	780433955600
108	5570733156400
109	35479328490800
110	204501309891040
111	1079794524724300
112	5277959343607550
113	24100804163263000
114	103629681995796400
115	422489171516103360
116	1642905877211242200
117	6124964268162207100
118	21988829780205073400
119	76304616605068076500
120	256779654670214312390
121	840323833469132657900
122	2680769289845021320000
123	8354312965570402030500
124	25479785463590478364850
125	76174773659118734381430
126	223547654859325112237700
127	644784708562149149507100
128	1829896157867023042397950
129	5114870385823477500437200
130	14093659796007152886502240
131	38312416809680985837267000
132	102823839944517884609254900
133	272627097608189787830324700
134	714532134692591615887413400
135	1852191807372667449214697980
136	4750895331050662107087312350
137	12063862523707334023980364850
138	30338844078695591581591262800
139	75592665296033483243346194300
140	186673176405986726698065060540
141	457033636121630574736906310100
142	1109712784183195455191382629400
143	2672958491026065451111362170700
144	6388630411951050543068095900000
145	15155296595701216867714338496650
146	35691319349172115803784141101000
147	83463458850345531204815355834600
148	193844821891579153459592792004750

Continued on next page

H	Coefficient
149	447218029809502026252853960479350
150	1025109180018535958328075561147600
151	2334966815425374025329298960613400
152	5285926025146401057221940759934800
153	11894809793422055778090963746796750
154	26610485523806643214439406113123700
155	59192488671133000418872924960580380
156	130934944602800148390805830334358550
157	288053803877275434225791007140951200
158	630335956641161848053189022865633700
159	1372144732615084966925968305386801500
160	2971692434556287521979770251012495960
161	6403663769447206507020080510690553950
162	13731455836963702893262338464351969300
163	29302784365556864792467190277870719300
164	62236412390006464725741752355454303050
165	131571267475113485308388351664119864700
166	276881779660512277602587459223647450700
167	580068159859719458817771360047550762500
168	1209896343394298612240745363962545849650
169	2512659581274543540056836490346821021300
170	5195964077318022154685130504933271708460
171	10699786364904953415408162272807343024100
172	21942642921652070406570084449160190035600
173	4481619300392632347245111802339977466650
174	91167389766899757998747510493904417627500
175	184725987293551197348604593904198413037360
176	372842030618206459713330591462926320432200
177	749641691715508055433147303784246974949400
178	1501541618460237210381003451261937626766500
179	2996386070704033919337583556309152628280400
180	5957391381779377020957062065364396685244010
181	11801384076349726860236753884316535438825150
182	23294209675211207812707806763410554407452900
183	45816333942273498665251141260458888402806100
184	89798369711394805199106131592348373120454300
185	175392145444667118669726034875503227969769980
186	341399280884269618845743084404194561390375700
187	662281233227169820422371600907809896960373800
188	1280459137282460603846844887905038189045553100
189	2467447478943062013715726305790788082138097050
190	4739188532447051780386468541523078081252491260
191	9072946860763132772850935996947460923572528300
192	17313903591434838656116165077965866078861997250
193	32934973108194176569522920581853085710687885050
194	62452278847803469934827642098178609642892879500
195	118053924894702789403708896669233611189513252840
196	222467096734643102498341711156010378972081383050
197	417941957923384559296330556136531166339402672400
198	782784415636979012125960374760218719703320605100
199	1461689556881422302354175165349940769868850157800
200	2721229976741408321086258191904967341454135922220
201	5051058868248697504181105614430399716835637181700
202	9347947291554178745915042866561950307647021352000
203	17249475598361571581588298340268661849440579396800
204	31737312923913323907186631074112627511905114211400
205	58224726389684597146163937183354927875086021102850
206	106511345484713415700281999060342918537052197374400
207	194286716379084851506533216309508442168391587156000
208	353391850445114408960479780259978273824706957717300
209	640978043404337119284353310236860128434100269222200
210	1159336892783227387080705313595355902298621470153820
211	2091040215959763234719546115152544203856882510794800
212	3761034852975242268341436501388711195270261468758150
213	6746061062034166502407712510211948097276594874343500
214	12066921573553228439497015168499423008159470525261900
215	21525392774143301474884412830212535681235633970340760
216	38292947904408447461290216345673863462516816077809650
217	67936642592187532319178975075845318226950117719102750
218	120201824904824551016031932105063729497006969519705200
219	212101422312876848819289868011265306115034009156941500
220	373254609090668020241717581537741916940036233964106160
221	655087182043534127920640994585580762559282659720061150
222	1146643204353854439468108631776662664087522971711194800
223	2001683651325507185166309791265284693204085924142623300
224	3485000940822936731728814318700822660258691909982433000
225	6051356863003913163660166334978244889664183700716324340
226	10479651625538384495545865876055209995002714934855169000
227	18100337259404011530516895062822814554594774045409597400
228	31179810734530503578316971663480406400591580417231412350
229	53568345732500887613256598866450204283890856891936878800
230	91789211015487712598627256401234349127396767686754643600
231	156864291623759108740822709586249146589760435463168204200
232	267365729203056221638647322847249670067945162939494753650
233	454502668234611761341171905282975463411245434755672780200
234	770576525684052681125470935030484627409852887397243982600
235	1302995948288648565711415679982364307082485054838124849020
236	2197441632416466782779996390774000216061416358056070385400
237	3696046195094743366846709090567451386081743600378987813250
238	6200142703694546157727540508760670440060563447235007555300

Continued on next page

H	Coefficient
239	10373097328337847375022034952326682743262953796369200443100
240	17308348833135112394153733971439366359124492027678939467060
241	28803211819295612124515745616913573843257096716069901357050
242	47803719376916049005172170160397636929703931649181084096500
243	79125246160724891817239979393299371456751532309727823004200
244	130616464853658265170765222125095348657029218633581378359100
245	215033842756760048367094941372120705286747326055687833190620
246	353051486133324235209549234189813699131283366426203549422200
247	578079581682156353735321701174746806456489965947432667666200
248	943955056340376850875126343090567077375277803604906391299100
249	1537179450253762225822812137038271256519260470497506194770500
250	249633331998564813734886456874100299762459545308138644062520
251	4042781154332250085383321177654339087525455119847759169222500
252	65290827127851000936716094074647344564214880844102320775066050
253	10515083567705857074125353558001414283987217282758813746994850
254	16887134608025332600124374497532417361159993135703830629962900
255	27044294382926522417189530811534875534336980749592263652224440
256	43188218182616497697016735663786971161334963771390265519514300
257	68773015199193624743204920925132834293165947588316228669329450
258	109201073753279347521713488633811776713677125200889087488023300
259	172895801661560544202858688622325454280620546067765515143984200
260	272949954278455539911960711381033381794926190039755929373518000
261	429649884421672818807818930834626966296359137970045173350261300
262	674328065935723345437570268998172518544677944568945897892044700
263	1055222673942612329200240785023314726157875463812936752833244300
264	1646358943170219307425647199016419634401196836708778342707279450
265	2560963430634161110367456888657436460012666674452524947205160740
266	3971652838271488478687105163807202584827979394130672416635990600
267	6140709670073208748247273132744237351832328006940809413847966700
268	9465319415722841899794990421402917687157036202462812557110948800
269	14544914298239576036515374415572670946711329332781091115558987400
270	22281053248737975434204796320832644215740967289584072172190669860
271	34024998669909834184160720193718965737995652062673939092447404200
272	51794933651300967689760630964664796311288554720422141245093327700
273	78594443876178865527584188631271529483949037863783932378562258300
274	11887763906341901042287753383184103920312259855072151767623504300
275	179225726592751371644942905459232182077771933115470007744623738720
276	269327192112120168391457545391801126203963339319392992188508379400
277	403392009484207872775894743899286139001518385074274250277156847750
278	602183585772813976819507603519905499914855527822580083867569064100
279	895925947915278233955712993282814872832682554091477644268999403600
280	132844534614111054553263476913916945002008464472272415145596561430
281	19630447341684630251720601034552720366938625772511269415648714022400
282	2890799323673085893126072081463621465239921601203802776480095334100
283	4242218370054359715861894368665810185406482290119220519324904264200
284	6203564259220425018654506777309322899312847742067754935297106449100
285	903958275115254409163243410405738314059085837877367322626089109400
286	13125013443426323277636240022702182435361800512324740576751050199100
287	18988061972139592418328345071154663111576364845617065781987240120000
288	27370081112861169746713445476010302722975190331411378190769284278900
289	3930709582898718006895429240236027322896278982237947989520319958750
290	56240601639306938236988172536344348362714540622724822588053059285380
291	80167367764052837164027580086349247135145612130402050362050553608300
292	113840906504375402557899928404123165572243538142464678516174693236650
293	161040968324253765979677951361421851494822268535517591649220325290100
294	226932048427965097336474299652383675682830347172782843145269574500700
295	318537624534273829889743578060318584660856202551276036098259113749020
296	445363882084824099269886028028722707508649332257048974201911834332200
297	620215227152003169851022087568320079530702868465555911423617785021400
298	860254143990294687241592826336849173236878786765450658731949898365800
299	1188370114945859300946233131296478000015637813120948346750616297683100
300	1634936543558291644983535205078962297055480667753201541013182079999460
301	2240051006385738929458599823004383191941691717855939649881375079350700
302	3056372712557447907899280879199472736374407980836518735993953823649200
303	4152691646799120398063948826366041076059238661047213349279084028971000
304	5618386205085744591454796447882966245158031959540245612793880486913600
305	7568949658979303866599198036790531701628241397171109548535050171079190
306	10152789664316299117359513126211182900879626745216276522084681078774900
307	13559528059916035114734662649684083338493570865004810968818293485175800
308	18030048755895535465165200635842257421044795422742444690558034617494800
309	23868557482610341197877163031573352461806011502761756019343050717117400
310	31456925932572665552254041738420967648344122733567811657390919613070460
311	4127159121230804640001469488863635396716803813596846331774845012417800
312	53903265839864127810128799667832718703580010189912392771687647547131950
313	70079679627502818155009414182336176648595972672630562815949887371634300
314	90691518189850173934176023761648364125434075353198089643318702834885800
315	11682163887904844035270542567489321259429415333607187851089671666179200
316	149777529155954803452356764026025776876016211901965682105273834530299850
317	191126820723878795513855145888741629297111748812246185133925228939955250
318	242735482062391227780669986269926839707993897853929572231292330148292400
319	306808080627749255644059549380465710255320671277250162301841424178652100
320	385929234281624817665713382285765976756707219373601609789926745703127160
321	483105062460530745803713914813664027997565915191986171202655611515887300
322	601803107447200443774398235318099084776285110098567971082272540788251500
323	745988834901785367322193185292927921389381584606665905434230803743489200
324	920156454843758159622726910120395931092485630289947991155999766201183200
325	1129351448310453998266496422255763573176151689202670419253190369546986440
326	1379181864164591753264992959635867679019404249602189822737586048221757300
327	167581519225452921908301909244042386909999255944590059428283214432135400
328	202595745389387010089478624114796571210925230979262476934646935688821550

Continued on next page

H	Coefficient
329	2436811110989631971446831306852176481073980183936317922010170992298965700
330	2916008513970711957417202988904498021721551408648077045203162383043451440
331	3471517916912182767463102900177289530567355525793018274344290420281191200
332	4111519612390362946479011432691647745533787689716606941924999323178045450
333	4844250497755373707509059193698449298078560936563385532386405902698633000
334	5677816387445805655670125285780240101405626076647975289908149446078222300
335	6619972628242517451125392237058509686454533369476886098919613636203607220
336	7677875035767177229403211623082585797806409874553492999233860574870293000
337	88578048132550471453739064043473061374915301226142771644143412665189707550
338	10164872881284771167905750334119773401384350408517753590838159909979781300
339	11602710865036776031785917908415923278140797907439559417378381310938568900
340	13173157762445876704170525850016727191376517609205104420225547864038855800
341	14875952947562814107290724518707525935309683943866746733869829320815517650
342	16708447535158848038958057967437453538304206693805196841718304304533602600
343	18665347129317849424622845320989694647747214356297394903353069651432944300
344	20738499489726438498367481325571653730478085147016668357096128775991349600
345	2291674057713565384489909205065396721404771892149797673646555825573914120
346	2518581170833204261170354439503940984810503692455614932541590144288437600
347	27528359115090881606977302174681080432824074131104667685067933442105161700
348	299240250520350138727280802879114206680439235350055536126896678249473750
349	32349636768230448771098178744924723256110312724672103761246042393696456300
350	34779496224732728543579533722025155134858025412821197758980967720123577640
351	37185769527882711245907610882377364543445677482227567528183395996138469700
352	39538970819929698811077856251879977036281900802284584168495349967518204950
353	41808531022999926961392587788742500370186870464004948179766980187765977650
354	4396343759252493149027539099257872529892367913888201891647758918933162400
355	45972927536914756099077698440099504671161017652234628322394450150803190540
356	47807212633831623252217738976071960193599613822347129663984500829847232750
357	49438213234189495550324416729011478423798863470338637170335720233520649950
358	50840275474023854474373064870694846421275677586904594215639694757289832400
359	51990846245637296308047720747426782268323521681228928314812387377100414700
360	52871080988631266887300336551901893275591367694733497519901903100202244180
361	53466361258337376004840914957266811572708902354544803458916054808516842400
362	5376670205426173792027576091634514445178971610638854254380425244374234500
363	53767032917162101282895018544302968865253696636816644875022605389539506300
364	53467341641509406061803883836044976363144110416594820221488884249335861450
365	52872674860857418091719779098926425137192355273792265030524275809736983080
366	51992995471413941246029469449669574836880771279059387092802679743625525600
367	50842902569337465355019380473070596649757174443739905822761730500760991900
368	49441224995232954388273734096630932779489908779968924200740899937131526250
369	4781050442875577701414465833476132602497737790182834414966515770459527800
370	45976388016744297035800370794427841801183476375831857839053804735401756460
371	43966953559939258924028115300630266440323217376755914652213906477715946000
372	41811992197514517847311201434913569984559400883006355427191665318260321100
373	39542274254511119536734924568920342498609602438900999347333476083850639450
374	37188823463361268159638761327339913638986893007716307946323913120741553900
375	34782223211682111844428954615279346696723808331231100801011656249051569740
376	32351975937655595061019583221718393316735269547287007071453737156328630000
377	2992593347222047315857897486239946866734866148343779703685795862527495050
378	27529812228212566161443708965117418392618626076331043646701826714891651000
379	251868028930844925643385314139941841501665873063414825612391993998869757300
380	2291727992937895759102485527802530914352506997085834804692035679951588800
381	20738611949479171546989007237116540373216378557275288865909365752328578950
382	18665070107682037214797986926456809739376017731674438484194667482855888700
383	16707828208275777212846019356943087702422210203936894822737391144003438900
384	14875045386693721514746452263356300641472965440935475893535855317942348750
385	13172020060783882493849979994421820746029283991119781462015078304214365680
386	11601402404562444295853942363416087424266088579202587289250957880988201100
387	10163451858996615417329117407616240325733075209299050320152105080572896700
388	8856326117787093735451636924006061968172526346663734472173224136446376050
389	7676388535120467462402681475107603354356157628283271560215808372859315650
390	661852189931856850217099881334159362882773978150833290294999123555214580
391	5676437890183900872832572198745641859814457345108904134287162715972742800
392	4842973172440350351978686325516344230094582217595851646103315593059773650
393	4110364859148361835479151785765025259257048066384347698503764844545519150
394	3470499902110354639221386434885910748829394136152142785526977890531549200
395	2915134739300578581772202110096799438824966593399993196458738655681686320
396	2436083177175543705957953909474357801927100190676912129846615987985489500
397	2025371951656634418059930033562917531530599557268331925553080391129620400
398	1675364657591880466318367078160757894343523875688006318307662127994083000
399	1378855742280572484548410359964354850253117969899046522046186726604720500
400	1129137019696537808198127288482635058945390788388232413361371959239241500
401	920039687186358459101375405256025171913914069827240201794647587847563400
402	745955134860649282166845500319087528387353523964818719679181451169188600
403	601837956249584308226231151187572826621757190868084116920815229929612400
404	483194528176533149264931664639123853955477647266738210992482351411134350
405	386060361238701400458908377212595045426987933313633468819837851543361200
406	306969162494110759308501039371108493331256838839983542381996625165324800
407	242916229623575270200796125088902881741539398633791336096246504075829200
408	191318438350926133719109942705837036566869029997737691297889003829358450
409	149972715559212438896255706653002260119839992448972227616504356999936350
410	117014528157944243564935115705874321621403616174986019000808191699998960
411	90877576656688039290663930186410313715410535955509850553421072555614800
412	70255572641903270350795682190115516854930831987124747543539272216577550
413	54066707170144930983586937492864514684302625409622144890713801463659550
414	4142118544851301168875000280879373219859954745294769791549770566921600
415	31592012389486676246304011028800051198523593380479130513578350738397860
416	23989601990872947023241706420233027986286173472055424407980450884589150
417	18136347849816210891022320910314905226396200824686827794903002065014850
418	13652328401954336509184020820230633273128130966131244173582622368939700

Continued on next page

H	Coefficient
419	10233024138019025365423639030325698015880081989073176289219388299660400
420	7637690428534930259950470049028829665504144068474742513975766996330420
421	5676774174626231368915752907063671991468009790651732305670695660677950
422	4201881135689329778212720813142508050565800602510985452122889154481000
423	3097489764235545007590188194144871534152565082301940884924178380880400
424	2274163532837302197184405515031942094810747391036196830533675198511400
425	1663034438676538403416808526899766358965417105145011996389145088459760
426	1211353512483791142167809656914158626140048559115229490260568862788200
427	878928117254968322497809482037358987333663416060481136560760091852900
428	635289399977774768285189213796646616670006591333053318120897433309800
429	457455620710685719367457462364485787667501350405248778933639777407850
430	328177689456644795413949875092258031610008816343314690074912574522480
431	234571790399941711775531725439387134947509941952845449168437681424600
432	167060343872613514085499096643014801046153558606130040103887113182750
433	118556759619213183763056353700923012749391188088689179618401067343950
434	83841572635420169286288414629630700529066293048402020350379523930300
435	5908778553899962888355512866295414506026224677475656065993728181000
436	41501762146058703335210920068778113241594624595858704542648766066250
437	29053031920760956707597619644347264008715816701127391670867427730450
438	20272079761142353931244484956307447818386055811929622204051197251400
439	14099805533606498037803793759902245142243986906880132376087373935500
440	97760222031863612278978248392992742638694123580750002764222421435500
441	6757280491309534076616340201127147372420075230606501994222302631750
442	4656601596276525457949101863572632417033954852483688533774184203000
443	3199487472619908779359682872767469882348381579859632979571021693300
444	2191961476156213786946719685991415811412295195814148178637432301250
445	1497454714005125866779417666833600984447275316571451638607355870540
446	1020163936319960805009915754777582455846820518224366077273004615200
447	693120941128961554814949053359587355963560394724051555056490080500
448	469675828229577165730209311402608753810910752294040819505928947350
449	317442387959437581633524947188117346789272611944827056942108176200
450	214011211825133606184398898000274935858501901749462292774735994840
451	143926375955717928398058156393578324827803344253449168686662291000
452	96561455257220250190985825739462573201913771722399824236340886550
453	64632947557367444948013003481350947947891269689946400114050609200
454	43163627985050809502600027999593822766165312040741432984402780300
455	28762236023553282115377791799719665231431322409528623352374094200
456	19124706764863163176848069735151878483443690378543441634653847300
457	12689976839288257768792606008966886060563340664606492928357699650
458	8403244049477967219677066483508427069446119298982956170719682100
459	5553657748277405267922381708377513795386170671011058624164332600
460	3663386774192537168948156356247469125276402540682754197403516320
461	2412032249911649279140435085029167046768603863635940267269416050
462	1585275879583056230967830110362217050428526034883765788753064600
463	1040093226819378269602142169464958342229123926680346683546989400
464	681254113774080893614047517207861246583843231380324407201587800
465	445490773449889616067230687656882607026134862315172373872280940
466	290859795107670025226176645261370618084004560612566581093111700
467	189612162410692876038646933286066559173011613721621492585897800
468	123426299391838769989072875468525923560337169086502595007858950
469	80228581302475153170394188682161256949579076260559018174752450
470	52077558729267546653260378354461270145674566093952067891101260
471	33759170101656749134364030979732919269550518461297528307763200
472	21856036011830442442796984214136231367181124782435950273051450
473	14132131715687572616700034558184106815409399666638463788555150
474	9126789688812956793913007164107548919911173964164433662491400
475	5887341510677895434867742632363007924799667641440976326918340
476	3793387873792142189109516257503674622586024501295343772049100
477	2441503862736038357223264147562643123900923166724845664681350
478	1569727685452003599911861512691508650791742176713124493008400
479	1008188767763025606591968618139285024336716157631744789642300
480	646879266521337367573011439368575240058259043209499454839620
481	414649339104650333106853399528128558936645269170522235454000
482	265538170857719362138045310669743118273680849976419380935400
483	169891792747936446041343640672419322222569139343140594016400
484	108599517030265685852148478167859695586793760201934115381850
485	69359097812300780959496566087880349846633818415137825005580
486	44259696692223850747148253048073472500171666676564201630400
487	28219657456560131650883693039335079839859346447315306988000
488	17978011867152079708166955259663921012868007200107318148050
489	11444215081581197459087374854526586776739222059284141579000
490	7279341591192906542466482799033230549944981397605391346720
491	4626651437681723667535101611369794727869650212192877346100
492	2938437615458170185680682456421724121967945868844518174500
493	1864864071640062020121088994949147033363871469153240602450
494	1182672550339401885236885834644109654159907065005668166900
495	749503607334163118374198211580978548144400320569461885220
496	474656810227208867007051141322526225483395778665544825200
497	300391102131665746080790385043936412759876439471157223650
498	189976573172274071329900050141596440274332219787893481900
499	120066725823532559315017437272457230557448613038075461000
500	75833072159011277697048331778036073604566113793151216252
501	47864274768054379403159397113625013206053391286506754000
502	30191481177692314615920804567351608880871089910038313200
503	19031827871163630832032615191338495467683111681787786400
504	11989541262463491928332720142270570698294313751622033500
505	7548371543893727051884859084970795377151223869907489400
506	4749359943607441029206463250914292651478769326123595400
507	2986416179877020573089928791138289438973911092189754700
508	1876727269320163632049243111395992149745417370853013250

Continued on next page

H	Coefficient
509	1178662881310348340663079814973819342764574736389229950
510	739805474273539745604046603557402668140132454434514300
511	464073449975282567984622901401575945681720688198392000
512	290936889549688353657761022371803455868953122926276000
513	182286821422670984246646498420975491870893978369887250
514	114145181797015093840134282334773850127798613537757900
515	71434341544438576113391972748812065724409910851734160
516	44679147711461316637600381877708578630247335834127700
517	27928796246509993087369188799440943792864544950267200
518	17448178786446299560764326792571138483193368790552900
519	10894304136188875051840334957502664006733535829620300
520	6798314867613495701346038803323828638706302736769710
521	4239906163825310520568916926980663758805888903637800
522	2642805074532247705252467034968946183443071858943000
523	1646374350359484061061230956476116250775509731525900
524	1025055093053102730147667593894605352602307499022700
525	637854314546239840843092398025067499400748933094368
526	396690600379014686419602067688958128123623242730900
527	246569201760152508803716452134437430508673538876000
528	153173125884145490665568131641042463204609389128300
529	95100632514939175146144445211115529523893248107100
530	59012160499902153180649669954914631504413864804380
531	36597973461797334417222953529187076780695715926000
532	22684543735789303028450923121474950681151014354700
533	14052725433993975507851124827338469539841586748550
534	8700586536584375944943710393445362368068828176300
535	5383861195593081216860218448529325845413746549920
536	3329633029281942462951317021345198011814298958050
537	2058049708354888241012070809981287172749807779500
538	1271370252271019859430130439132136247190938316100
539	784954695469107000165820022910464776517291571000
540	484365394507175429966699295619750403336193320960
541	298715076338190117351783451489226191229594554500
542	184117975305084668746457986071193881427616859100
543	113420011439260578764608421596357338557891871400
544	6982919096236173475650149669032422241476346800
545	42967242350673825913802851899411743421199299970
546	26423501242893179169342968395627318094308905500
547	16240330429324025102612707456756474434516149500
548	9975854848243228276826345037790039433566076850
549	6124282769290890507152783045750547807229204400
550	3757588582635419391096889676908026465172540972
551	2304151744585981935178515014183186482540014700
552	1412081253496924049764212157468082987367401400
553	864876153020277188235722858020310509928680200
554	529410512812023134002158154567451638705498200
555	323872710087886446742933566583532601029754740
556	1980149377034296874371644455104329261856137100
557	120993488760600932508527717679111733868061000
558	73886484705549732566783765100036741264374000
559	45092624087120862977906962368058949694500200
560	27503114654387983080637687208937536909399100
561	16764575380875917665229433861211979112895850
562	10212586704388312208130284771077051296783900
563	6217414611448160787689116472351102967552200
564	3782795122298097034718974607672026603572100
565	2300080344175738876761954762881837745286100
566	1397649419533172120406976467262991280047900
567	848744088552919621129822233651720089098800
568	515081799820950711560588727669300091545150
569	312388293907825820001474032315388735510200
570	189334531282407044444322692633783122048200
571	114677865334689568046871575079655039535000
572	69413066425768496330176593539629943718550
573	41986812147253959080399558161049146745050
574	25379991950574580242888763463697935020200
575	15331166781770865219901187448721726388588
576	9254662884395119675506841299698663421100
577	5582722266241314143942235651324291671700
578	3365329374512340726798913389023200489500
579	2027233606834725398237013938323079956400
580	1220310415437203933116832365538989301620
581	734050477460906081648421399978204762400
582	441230665250093029687272629366768375900
583	265026157371581639234171453740739184200
584	159070439440302922226504221603369571950
585	95404202614601453956924505872876196040
586	57176349274944020690513352648927868200
587	34240210052142149555341048058237040000
588	20488971760863340902488022082289318250
589	12250917167238179282334524773130947500
590	7319362893624171276661676925216649740
591	4369543799085758770308576536792255300
592	2606437168744071876335541201772344200
593	1553494987606274278489182387566838550
594	925150746138266225352565488786400700
595	550503068671103330645199346576954340
596	327294200311903071596531925889535100
597	194426080475167354456771719821989550
598	115396561852384728015785181837775200

Continued on next page

H	Coefficient
599	68432410019307403338783350259243100
600	40545555204381046731350738654413252
601	24002042909418457951395143653868300
602	14195653457404317361170572440247900
603	8388397801363502090671037655499100
604	4952153042167812263992003817725550
605	2920912064824862844666090393418160
606	1721166385258626501087766942411000
607	1013280382856817227434680135713500
608	595942258183722150823477026597150
609	350166252063869947350120541466650
610	205541346960964208030339679378960
611	120534957643932833263183252061900
612	70610255959097289127846975373700
613	41324263670294290236702387335350
614	24158420998157315586360554399200
615	14109399762249343883673274917020
616	8231115294127388231232388734900
617	4797112284754064056622941210700
618	2792505126104941201198459448700
619	1623956259236266460547516392900
620	943254429301558532520031901850
621	547325151751758019801030730100
622	317187461363478926582975214600
623	183630747758591827008253523800
624	106171152403027540450539966100
625	61323193579140216967263632772
626	35371235131114374281399634500
627	20381289678152827770909339200
628	11727199887762108398616192500
629	6740838982703330423695345150
630	3868872950415594144294667060
631	2218279538629369975026396200
632	1269887907814166756375534050
633	726238691926574869074327150
634	414645712256087446640776200
635	236509480352165561391734280
636	134666410407314529831594650
637	76605399706491821858301300
638	43496110671331720857114800
639	24674068396090978554783000
640	13969539948900809541766520
641	7902147958143472690096500
642	4460521289001568141366500
643	2515854574506792664110100
644	1415761618865940888118550
645	796110098112800567110430
646	446608830289979755826900
647	250380849524845119659900
648	139991024705117335561400
649	78235418730452295338900
650	43594019669148411114848
651	24282569937621335723900
652	13486467155679455541450
653	7488195366237610313700
654	4142410789905605145400
655	2292062781467672003640
656	1263255299896042527300
657	696546420227846493350
658	382675228837926401000
659	210245661133910873400
660	114884213205807559760
661	62887040723294119150
662	34241658386899173300
663	18683028068624382600
664	10143579812914088950
665	5505134688850088080
666	2963434375313788100
667	1604542146818801300
668	862510064897144400
669	465797984160726950
670	249422941755644900
671	133172318644062200
672	70374908177438150
673	37800215439149200
674	20068363309906200
675	10725451951613092
676	5628809173927350
677	2931971129035650
678	1520412416550500
679	819134981009700
680	429210138822550
681	225761958083900
682	114247212825100
683	57453042751400
684	29685694023400
685	16392207489000
686	8360141145700
687	4245626650200
688	2009555521150

Continued on next page

H	Coefficient
689	978710551850
690	530978901840
691	304499669800
692	143789812200
693	68133738500
694	28904563900
695	14496144360
696	9032248700
697	5124764650
698	2024885700
699	869501100
700	313989378
701	199693950
702	147079300
703	71467600
704	20265700
705	8117750
706	2301300
707	2839200
708	2069900
709	697000
710	109240
711	51600
712	8900
713	39150
714	20500
715	3400
716	100
717	200
719	400
720	100
725	2

Bibliography

- [1] Ryuzo Abe. Logarithmic singularity of specific heat near the transition point in the ising model. *Progress of Theoretical Physics*, 37(6):1070–1079, 1967.
- [2] Yoshihiko Abe and Shigetoshi Katsura. Distribution of Zeros of the Partition Function in the Complex Temperature Plane. II. *Progress of Theoretical Physics*, 43(5):1402–1404, 1970.
- [3] Lars Ahlfors. *Complex Analysis*. McGraw-Hill, Inc., 3rd edition, 1979.
- [4] Philip W. Anderson. *Basic notions of condensed matter physics*. Westview Press, 1997.
- [5] Aruldas and Rajagopal. *Modern Physics*. PHI Learning Pvt. Ltd., 2004.
- [6] Michael Baake, Uwe Grimm, and Carmelo Pisani. Partition function zeros for aperiodic systems. *Journal of Statistical Physics*, 78:285–297, 1995. 10.1007/BF02183349.
- [7] Marc Baus and Carlos F. Tejero. *Equilibrium statistical physics: phases of matter and phase transitions*. Springer, 2008.
- [8] R J Baxter. Potts model at the critical temperature. *Journal of Physics C: Solid State Physics*, 6(23):L445, 1973.
- [9] R. J. Baxter. *Exactly Solved Models in Statistical Mechanics*. Academic Press, 1982.
- [10] Gyan Bhanot and Srikanth Sastry. Solving the ising model exactly on a 5x5x4 lattice using the connection machine. *Journal of Statistical Physics*, 60:333–346, 1990. 10.1007/BF01314924.
- [11] J.J. Binney, N.J. Dowrick, A.J. Fisher, and M.E.J. Newman. *The Theory of critical phenomena: an introduction to the renormalization group*. Oxford University Press, 1992.
- [12] H. W. J. Blöte and M. P. Nightingale. Critical behaviour of the two-dimensional potts model with a continuous number of states; a finite size scaling analysis. *Physica A: Statistical and Theoretical Physics*, 112(3):405–465, 1982.
- [13] Stephen Blundell and Katherine M. Blundell. *Concepts in thermal physics*. Oxford University Press, 2006.
- [14] Richard Brauer and Hermann Weyl. Spinors in n dimensions. *American Journal of Mathematics*, 57:425–449, April 1935.

- [15] S. G. Brush. History of the Lenz-Ising Model. *Rev. Mod. Phys.*, 39:883–893, 1962.
- [16] H. B. Callen. *Thermodynamics and an Introduction to Thermostatistics, 2nd Edition*. John Wiley & Sons, August 1985.
- [17] P. Chaikin and T. Lubensky. *Principles of condensed matter physics*. Cambridge University Press, 2000.
- [18] Gary Chartrand. *Introductory graph theory*. Courier Dover Publications, 1985.
- [19] Chi-Ning Chen, Chin-Kun Hu, and F. Y. Wu. Partition function zeros of the square lattice potts model. *Phys. Rev. Lett.*, 76(2):169–172, Jan 1996.
- [20] Debashish Chowdhury and Dietrich Stauffer. *Principles of equilibrium statistical mechanics*. Wiley-VCH, 2000.
- [21] Barry A. Cipra. An introduction to the ising model. *The American Mathematical Monthly*, 64(10):937–959, Dec 1987.
- [22] C. R. J. Clapham. *Introduction to mathematical analysis*. Routledge, 1973.
- [23] Youjin Deng, Wenan Guo, Jouke R. Heringa, Henk W.J. Blöte, and Bernard Nienhuis. Phase transitions in self-dual generalizations of the baxter-wu model. *Nuclear Physics B*, 827(3):406–425, 2010.
- [24] H. T. Diep. *Frustrated spin systems*. World Scientific, 2004.
- [25] Reinhard Diestel. *Graph Theory*, volume 173. Springer-Verlag, Heidelberg, 4th edition, July 2010.
- [26] Cyril Domb. *The critical point: a historical introduction to the modern theory of critical phenomena*. Taylor & Francis, 1996.
- [27] Cyril Domb and Melville S. Green. *Phase transitions and critical phenomena*, volume 1. Academic Press, 1972.
- [28] Christian Ebert. *The Mathematics of Language: 10th and 11th Biennial Conference*. Springer, 2010. Page 257.
- [29] Sabino Jose Ferreira and Alan Sokal. Antiferromagnetic potts models on the square lattice: A high-precision monte carlo study. *Journal of Statistical Physics*, 96(3):461–530, August 1999.
- [30] M. E. Fisher. *Lecture Notes in Theoretical Physics*, volume 7c. University of Colorado Press, Boulder, 1965.
- [31] Paul R. Gerber and Michael E. Fisher. Critical temperatures of classical n -vector models on hypercubic lattices. *Phys. Rev. B*, 10(11):4697–4703, Dec 1974.

- [32] R G Ghulghazaryan and N S Ananikian. Partition function zeros of the one-dimensional potts model: the recursive method. *Journal of Physics A: Mathematical and General*, 36:6297, 2003.
- [33] Nigel Goldenfeld. *Lectures on phase transitions and the renormalization group*. Westview Press, 1992.
- [34] U. Grimm and M. Baake. Aperiodicity and disorder - does it matter? In K.-H. Hoffmann and M. Schreiber, editors, *Computational Statistical Physics - From billiards to Monte Carlo*, chapter 12, pages 199–237. Springer Berlin, 2001.
- [35] A J Guttmann and I G Enting. Series studies of the Potts model. I. The simple cubic Ising model. *Journal of Physics A: Mathematical and General*, 26(4):807, 1993.
- [36] Morton Hamermesh. *Group theory and its application to physical problems*. Courier Dover Publications, 1989.
- [37] John Harris, Walter Benenson, and Horst Stöcker. *Handbook of physics*. Springer, 2002.
- [38] A. Hintermann, H. Kunz, and F. Y. Wu. Exact results for the potts model in two dimensions. *Journal of Statistical Physics*, 19:623–632, 1978. 10.1007/BF01011773.
- [39] Stephen Holloway and Neville V. Richardson. *Handbook of surface science, Volume 1*. Elsevier, 1996.
- [40] Kerson Huang. *Statistical Mechanics*. John Wiley & Sons, 1987.
- [41] E. Ising. *Beitrag zur Theorie des Ferro- und Paramagnetismus*. PhD thesis, Hamburgischen Universitt, 1924.
- [42] E. Ising. Beitrag zur theorie des ferromagnetismus. *Zeitschrift für Physik*, 31:253–258, 1925.
- [43] C. Itzykson, R. B. Pearson, and J. B. Zuber. Distribution of zeros in ising and gauge models. *Nuclear Physics B*, 220(4):415–433, 1983.
- [44] E. Atlee Jackson. *Equilibrium Statistical Mechanics*. Courier Dover Publications, 2000.
- [45] Nathan Jacobson. *Basic Algebra*. W. H. Freeman and Company, 2nd edition, 2009.
- [46] Surender Kumar Jain and Dinesh Khurana. *Noncommutative rings, group rings, diagram algebras, and their applications*. American Mathematical Society, 2008.
- [47] Shigetoshi Katsura. Distribution of roots of the partition function in the complex temperature plane. *Progress of Theoretical Physics*, 38(6):1415–1417, 1967.
- [48] Bruria Kaufman and Lars Onsager. Crystal statistics. iii. short-range order in a binary ising lattice. *Phys. Rev.*, 76(8):1244–1252, Oct 1949.
- [49] Charles Kittel. *Introduction to solid state physics*. John Wiley & Sons, 1996.

- [50] John B. Kogut. An introduction to lattice gauge theory and spin systems. *Rev. Mod. Phys.*, 51(4):659–713, Oct 1979.
- [51] H. A. Kramers and G. H. Wannier. Statistics of the two-dimensional ferromagnet. part i. *Phys. Rev.*, 60(3):252–262, Aug 1941.
- [52] D. Landau and K. Binder. *A Guide to Monte Carlo Simulations in Statistical Physics*. Cambridge University Press, 2009.
- [53] O. L. De Lange and John Pierrus. *Solved problems in classical mechanics: analytical and numerical solutions with comments*. Oxford University Press, 2010.
- [54] David Anthony Lavis and George Macdonald Bel. *Statistical Mechanics of Lattice Systems: Exact, series, and renormalization group methods*. Springer, 1999.
- [55] W Lenz. Beiträge zum verständnis der magnetischen eigenschaften in festen körpern. *Physikalische Zeitschrift*, 21:613–615, 1920.
- [56] Laurent-Patrick Lévy. *Magnetism and superconductivity*. Springer, 2000.
- [57] Chuang Liu. Explaining the emergence of cooperative phenomena. *Philosophy of Science*, 1999.
- [58] J M Maillard and R Rammal. Some analytical consequences of the inverse relation for the potts model. *Journal of Physics A*, 16:353, 1983.
- [59] P. P. Martin. Private communications.
- [60] P. P. Martin. Finite lattice $z(3)$ models in two and three dimensions. *Nuclear Physics B*, B225:497–504, 1983.
- [61] P. P. Martin. Ising lattice gauge theory in three dimensions. *Nuclear Physics B*, 220(4):366–382, 1983.
- [62] P. P. Martin. Potts models and dichromatic polynomials. In Giacomo M. D’Ariano and Mario Rasetti, editors, *Integrable Systems in Statistical Mechanics*, pages 129–142. World Scientific, 1985.
- [63] P. P. Martin. Exact finite lattice results for z_n symmetric spin models. *J. Phys. A: Math. Gen.*, 21:4415–4421, 1988.
- [64] P. P. Martin. *Potts Models and Related Problems in Statistical Mechanics*, volume 5. World Scientific, 1991.
- [65] P. P. Martin. The partition algebra and the potts model transfer matrix spectrum in high dimensions. *J. Phys. A: Math. Gen.*, 33:3669–3695, 2000.
- [66] P. P. Martin and J M Maillard. Zeros of the partition function for the triangular lattice three-state potts model. *J. Phys. A: Math. Gen.*, 19:L547–L551, 1986.

- [67] D.C. Mattis and R.H. Swendsen. *Statistical mechanics made simple*. World Scientific, 2008.
- [68] Victor Matveev and Robert Shrock. Complex-temperature singularities in potts models on the square lattice. *Phys. Rev. E*, 54(6):6174, December 1996.
- [69] Gene Mazenko. *Nonequilibrium statistical mechanics*. Wiley-VCH, 2006.
- [70] B. M. McCoy and T. T. Wu. *The Two-Dimensional Ising Model*. Harvard University Press, Cambridge, Mass., 1973.
- [71] Duncan McKie & Christine McKie. *Crystalline solids*. Wiley, 1974.
- [72] N. Metropolis, A.W. Rosenbluth, M.N. Rosenbluth, A.H. Teller, and E. Teller. Equations of state calculations by fast computing machines. *Journal of Chemical Physics*, 21(6):1087–1092, 1953.
- [73] Carl Dean Meyer. *Matrix analysis and applied linear algebra*, volume 1. SIAM, 2000.
- [74] G. Mussardo. *Statistical field theory: an introduction to exactly solved models in statistical physics*. Oxford University Press, 2009.
- [75] Gordon F. Newell and Elliott W. Montroll. On the theory of the ising model of ferromagnetism. *Rev. Mod. Phys.*, 25(2):353–389, Apr 1953.
- [76] F Ninio. A simple proof of the perron-frobenius theorem for positive symmetric matrices. *Journal of Physics A: Mathematical and General*, 9(8):1281, 1976.
- [77] S. Ono, Y. Karaki, M. Suzuki, and C. Kawabata. Statistical mechanics of three - dimensional finite Ising model. *Physics Letters A*, 24(12):703–704, 1967.
- [78] Lars Onsager. Crystal Statistics. I. A Two-Dimensional Model with an Order-Disorder Transition. *Phys. Rev.*, 65(3-4):117–149, Feb 1944.
- [79] Pierre Papon, Jacques Leblond, and Paul Herman Ernst Meijer. *The physics of phase transitions: concepts and applications*. Springer, 2006.
- [80] Athanasios Papoulis. *Probability, random variables, and stochastic processes*. McGraw-Hill, 1998.
- [81] Robert B. Pearson. Partition function of the ising model on the periodic $4 \times 4 \times 4$ lattice. *Phys. Rev. B*, 26(11):6285–6290, Dec 1982.
- [82] R. Peierls. On ising’s model of ferromagnetism. *Mathematical Proceedings of the Cambridge Philosophical Society*, 32(03):477–481, 1936.
- [83] R. B. Potts. Some generalized order-disorder transformations. *Mathematical Proceedings of the Cambridge Philosophical Society*, 48(01):106–109, 1952.

- [84] Sartaj Sahni. *Data Structure, Algorithms and Application in C++*. University Press (India) Private Limited, 2005.
- [85] Jess Salas and Alan D. Sokal. Transfer matrices and partition-function zeros for antiferromagnetic potts models. i. general theory and square-lattice chromatic polynomial. *Journal of Statistical Physics*, 104:609–699, 2001. 10.1023/A:1010376605067.
- [86] Robert Savit. Duality in field theory and statistical systems. *Rev. Mod. Phys.*, 52(2):453–487, Apr 1980.
- [87] Hans Schneider and George Philip Barker. *Matrices And Linear Algebra*. Holt, Rinehart and Winston, Inc, 1968.
- [88] T. D. Schultz, D. C. Mattis, and E. H. Lieb. Two-dimensional ising model as a soluble problem of many fermions. *Rev. Mod. Phys.*, 36(3):856–871, Jul 1964.
- [89] H. E. Stanley. *Introduction to phase transitions and critical phenomena*. Oxford University Press, Inc., 1971.
- [90] J Stephenson. On the density of partition function temperature zeros. *Journal of Physics A*, 13:4513, 1987.
- [91] Keith S. Stowe. *An introduction to thermodynamics and statistical mechanics*. Cambridge University Press, 2007.
- [92] A L Talapov and H W J Blöte. The magnetization of the 3d ising model. *Journal of Physics A: Mathematical and General*, 29(17):5727, 1996.
- [93] Yogendra Valani. Exact partition function results. <http://www.priyena.com>.
- [94] W. D. Wallis. *A beginner's guide to graph theory*. Birkhuser, 2007.
- [95] Whittaker; Watson. *A Course of Modern Analysis*. Cambridge Mathematical Library. Cambridge University Press, 4th edition, September 1996.
- [96] Ulrich Weiss. *Quantum dissipative systems*. World Scientific, 2008.
- [97] Hassler Whitney. Congruent graphs and the connectivity of graphs. *American Journal of Mathematics*, 54(1):pp. 150–168, 1932.
- [98] Francis Wright. *Computing with Maple*. Chapman Hall, 2001.
- [99] F. Y. Wu. The potts model. *Rev. Mod. Phys.*, 54(1):235–268, Jan 1982.
- [100] F. Y. Wu. Potts model of magnetism (invited). *Journal of Applied Physics*, 55(6):2421–2425, 1984.
- [101] F. Y. Wu. Potts model and graph theory. *Journal of Statistical Physics*, 52:99–112, 1988. 10.1007/BF01016406.
- [102] F. Zwicky. On Cooperative Phenomena. *Phys. Rev.*, 43(4):270–278, Feb 1933.